Methyl-coenzyme M reductase: Elucidating the process of activation and study of the effect of the methanogenesis inhibitor 3-nitrooxypropanol

by

Divya Prakash

A dissertation submitted to the Graduate Faculty of
Auburn University
in partial fulfillment of the
requirements for the Degree of
Doctor of Philosophy

Auburn, Alabama
December 13, 2014

Methyl-Coenzyme M Reductase, Activation, Methane, Iron-Sulfur Flavoprotein, McrC, 3-Nitrooxypropanol

Approved by

Evert Duin, Chair, Associate Professor of Chemistry and Biochemistry
Sang-Jin Suh, Associate Professor of Biological Sciences
Doug Goodwin, Associate Professor of Chemistry and Biochemistry
Holly Ellis, Associate Professor of Chemistry and Biochemistry
Paul A. Cobine, Associate Professor of Biological Sciences

Abstract

To use methane as a biocatalyst, it is important to establish a cell free system to convert the inactive form of methane forming enzyme i.e Methyl-coenzyme M reductase (MCR) to the active form. MCR catalyzes the reversible reduction of methyl-coenzymeM (CH_3-S-CoM) and coenzyme B (HS-CoB) to methane and heterodisulfide CoM-S-S-CoB (HDS). It contains the hydroporphinoid nickel complex coenzyme F430 in its active site, and the Ni center has to be in its Ni(I) valence state for the enzyme to be active. Until now, no in vitro method that fully converted the inactive MCRsilent-Ni(II) form to the active MCRred1-Ni(I) form has been described. With the potential use of recombinant MCR in the production of biofuels and the need to better understand this enzyme and its activation process, we studied its activation under nonturnover conditions and achieved full MCR activation in the presence of dithiothreitol and protein components A2, an ATP carrier, and A3a. It was found that the presence of HDS promotes the inactivation of MCRred1, which makes it essential that the activation process is isolated from the methane formation assay, which tends to result in minimal activation rates. Component A3a is a multienzyme complex that includes the mcrC gene product, an Fe-protein homolog, an iron-sulfur flavoprotein, CODH/ACS complex and protein components involved in electron bifurcation. According to our postulated model of activation, electrons from polyferredoxin or an artificial electron source with a potential close to that of polyferredoxin ($E^{o'}$ ~ -500 mV at pH 7 vs. SHE) can reduce the Fe-S cluster in PISF and concomitant hydrolysis of ATP by the A2 protein/Fe protein homolog will lower the potential of this cluster allowing

reduction of the Ni centers on MCR. Activation studies were performed in the presence of the artificial electron sources dithionite ($E^{o'}$ ~ -420 mV at pH 7 vs. SHE) or Ti (III) citrate ($E^{o'}$ ~ -500 mV at pH 7 vs. SHE). The rate of methane formation increased almost two fold in the presence of McrC, PISF, the Fe-protein homolog, the A2 protein, and Ti(III) citrate as an artificial electron source. There was no activation observed when dithionite was used instead of Ti(III) citrate. The fact that activation is only observed in the presence of Ti(III)citrate which has a midpoint potential close to that of polyferredoxin ($E^{o'}$ ~ -500 mV at pH 7 vs. SHE), would be in line with our proposal that polyferredoxin is the direct electron donor and possible A3a protein would be McrC, Iron Sufur Flavoprotein and Fe-Protein Homolog.

On the other hand, Methane is an important greenhouse gas and it has a global warming potential 21 times more than that of carbon dioxide. Digestive processes of ruminants contribute a significant amount of methane. It has been estimated that cattle alone are responsible for emission of around 11-17% of methane globally. Additionally, between 2-12% of ingested gross energy of ruminants is lost due to the formation of methane. This loss of energy could be potentially used by the animal. Hence, controlling methane formation is important from the perspective of both environmental impact and animal productivity. 3-Nitrooxypropanol (3-NOP) has been identified and shown to be effective at inhibiting methane production both *in vitro* and *in vivo* with no signs of animal toxicity. 3-NOP is speculated to inhibit the key enzyme of methanogenesis, i.e. MCR, however, no studies describing the effect of 3-NOP against MCR have been reported in the literature to date. Considering this fact effect of 3-NOP on MCR was

studied and it was found that 3-NOP quenches the active form of MCR via a radical type mechanism in which nitrite is released as a byproduct of this reaction.

Acknowledgments

First and foremost I thank God for the wisdom and perseverance that he has bestowed upon me during this research project, and indeed, throughout my life. The contributions of many different people, in their different ways, have made this dissertation possible. At the end of my thesis, it is a pleasant task to express my thanks to all those who contributed in many ways to the success of this study and made it an unforgettable experience for me.

My deepest gratitude is to my advisor, Dr. Duin for his support, guidance and belief in my capabilities. This project was bold and ambitious from the start and your courage for exploring the unknown has been very inspiring. Your patience and support helped me overcome many crisis situations and finish this dissertation. I have learnt a lot from you for which I am very grateful to you.

I must offer my profound deep and sincere gratitude to my other committee members: Dr. Sang, Dr. Goodwin, Dr. Ellis and Dr. Cobin, for their valuable comments and instructive suggestions to my research and dissertation.

I must express my deep and sincere gratitude to Dr. Sang for his guidance at every stage of this research. Above all and the most needed, he provided me unflinching encouragement and support in various ways. He was always there for each and every problem of mine whether official or personal and to solve my queries by providing her fine thoughts about the subject that helped me to bring this dissertation to its conclusion

I am highly grateful to Drs. Goodwin and Ellis for their insightful comments and constructive criticisms and invaluable suggestions at different stages of my research and they helped me focus my ideas.

I am also thankful to Dr. Cobin for reading my reports, commenting on my views and helping me understand and enrich my ideas.

I honestly thank Drs Mansoorbadi, Ada and Kyle WIilian for theirs help and support.

I sincerely owe thanks to my lamates, Selam, Xiao, Weiya, Mi Wand, Jospeh, Bryan and Dr. Sang students: Zho, Bingu, Cichi and Yu.

Above and beyond all, my heartfelt gratitude to my family: for unconditional love, support and encouragement to pursue my interests. I express my special appreciation to my beloved wife Dr. Shikha Singh Chauhan for her loving support, and endless patience. I truly thank her for believing in me, for sticking by my side and motivating me when I was depressed, for helping me and sharing her research experience with me. Without my family, it would have been nearly impossible for me to give my work the present silhouette.

Finally, I would like to thank everybody who was important to the successful realization of thesis, as well as expressing my apology that I could not mention personally one by one.

I am also grateful to the Department of Chemistry and Biochemistry at Auburn University, Malone-Zallen fellowhip and CMB-EPSCoR Graduate Research Award for their financial support during the course of this work.

Table of Contents

List of Tables

List of Figures

List of Abbreviations

MCR	Methyl coenzyme-M reductase
McrC	Methyl coenzyme M reductase I, operon protein C
MtrC	Methyl coenzyme M reductase II, operon protein C
PISF	Predicted Iron Sulfur Flavoprotein
CC	Cluster Carrier (Fe-Protein Homolog)
HDR	Heterodisulfide reductase
HDS	Heterodisulfide
MCoM	Methyl Coenzyme M
CoB	Coenzyme B
CW	Continuous wave
IPTG	Isopropyl-β-D-thiogalactoside
EPR	Electron paramagnetic resonance spectroscopy
SDS-PAGE	Sodium dodecyl sulfate-polyacrylamide gel electrophoresis
E. coli	*Escherichia coli*
WT	Wild-Type
3-NOP	3-Nitrooxypropanol
2-BES	2-Bromoethanesulfonate
ANME	anaerobic methanotrophs

CHAPTER ONE: INTRODUCTION

1.1 Methanogenesis and Methane

1.1.1 Methanogenic and Methanotrophic Archaea:

Methanogenic archaea produce biological methane in anaerobic environments like swamps, paddy fields, landfills, the intestinal tract of ruminants and termites, as well as deeper layers of marine and freshwater sediments. The methanogenic environments contain flora of anaerobic bacteria, protozoa, fungi and methanogenic archaea (methanogens). In methanogenic environments, biomass such as glucose from cellulose is completely decomposed to CO_2 and CH_4.

Glucose $\longrightarrow$ 3 CO_2 + 3 CH_4, $\Delta G^{\circ'}$ = -418.1 kJ mol^{-1}

The above reaction is made possible by syntrophic associations of microorganisms. Glucose is first fermented to either acetate, formate or CO_2 and H_2 by anaerobic bacteria and/or protozoa. The products of glucose fermentation are then converted to methane by methanogens with a high rate of conversion that keeps the concentrations of acetate (< 1mM), formate (<0.1 mM) and H_2 (< 1 µM) very low in the anaerobic sediments (1) .

$CH_3COO^- + H^+ \longrightarrow CO_2 + CH_4$, $\Delta G^{\circ'}$ = -36 kJ mol^{-1}

$4\ H_2 + CO_2 \longrightarrow CH_4 + 2\ H_2O$, $\Delta G^{\circ'}$= -131 kJ mol^{-1}

$4\ HCOO^- + 4\ H^+ \longrightarrow 3\ CO_2 + CH_4 + 2\ H_2O$, $\Delta G^{\circ'}$ = -144.5 kJ mol^{-1}

Methanogens are highly specialized in substrate utilization and can only use C1-compounds (CO_2, formate, dimethyl sulfide, methanethiol, methanol, methylamines) and acetate as energy substrates. Despite the high specialization, methanogens are not phylogenetically closely related. This is reflected, for instance, in differences in cell wall composition (2,3) and growth conditions.

They can have very different optimal growth conditions from below 20°C to or near the temperature of boiling water (4).

All Methanogens taxonomically belong to the archaeal kingdom of *Euryarchaeota.* They are classified in five orders Methanobacteriales, Methanococcales, Methanomicrobiales, Methanopyrales and Methanosarcinales. Of these, only the Methanosarcinales can ferment acetate to CO_2 and CH_4, and grow on methanol, methylthiols or methylamines as sole energy source. In turn, hyperthermophilic species are only found among the Methanobacteriales, Methanococcales and Methanopyrales (4). A sixth order, Methanocellales, was recently proposed based on an isolate from a rice paddy soil, *Methanocella paludicola*, that obtains energy for growth only by the reduction of CO_2 with H_2 or formate (5).

Methanotrophic *Euryarchaeota* (ANME) are responsible for the anaerobic oxidation of methane (AOM). AOM is mediated by microbial consortia of methanotrophic *Euryarchaeota* (ANME) and sulfate-reducing bacteria (SRB) in a proposed syntrophy (6,7). ANME is hypothesized to oxidize methane, passing reducing equivalents via an unknown intermediate to the SRB, which use these to reduce sulfate (8-10). The enzyme activating methane in methanotrophic archaea has tentatively been identified as a homologue of methyl-coenzyme M reductase (MCR) that catalyzes the methane forming step in methanogenic archaea (11,12). Presently, three clades of Archaea are known to be involved in AOM with sulfate: ANME-1 (6), ANME-2 (13) and ANME-3 (14). The archaea belonging to these clades exhibit distinct characteristics. ANME-1 is only distantly related to the orders Methanosarcinales and Methanomicrobiales, whereas ANME-2 and ANME-3 belong to the *Methanosarcinales* (8).

1.1.2 The global methane cycle:

Approximately 140 Gt of biomass is annually formed from fixation of 70 Gt carbon via Oxygenic photosynthesis. Out of this, around 2-3 % is fixed to methane in anaerobic environments that are not only deprived of O_2 but also deficient in other electron acceptors with high redox potential, such as nitrate, manganese(IV), Iron(III), and sulfate (15). Most of the global methane is produced by methanogens. In addition, Methane is also generated geochemically and thermogenically which can be distinguished by the relative depletion of ^{13}C (16). Over millions of years, methane has built up to large deposits. The quantities trapped in the form of methane hydrates are estimated to be close to 10000 Gt (**Fig. 1.1**). Presently, the atmosphere comprises 1.8 ppm (by volume) methane, a significant increase relative to the values of 250 years ago (0.7 ppm) (17), which is mainly due to human agricultural activity (rice fields and animal farming) (18). Methane has been proposed to have a large impact on climate-change because it is considered to be 21 times more active as a greenhouse gas than CO_2 (17).

A small portion of the formed methane is oxidized back to CO_2 in the atmosphere and anoxic environments by ANME and aerobic bacteria. In the atmosphere, the major source of methane oxidation to CO_2 is photochemical oxidation by UV light (19). However, a part of the methane is oxidized in anoxic environments by ANME before it is released to the atmosphere. This biological methane degradation is carried out at about 0.6 Gt per year by aerobic bacteria and to a slightly lesser extent by anaerobic methanotrophs (ANME) (15).

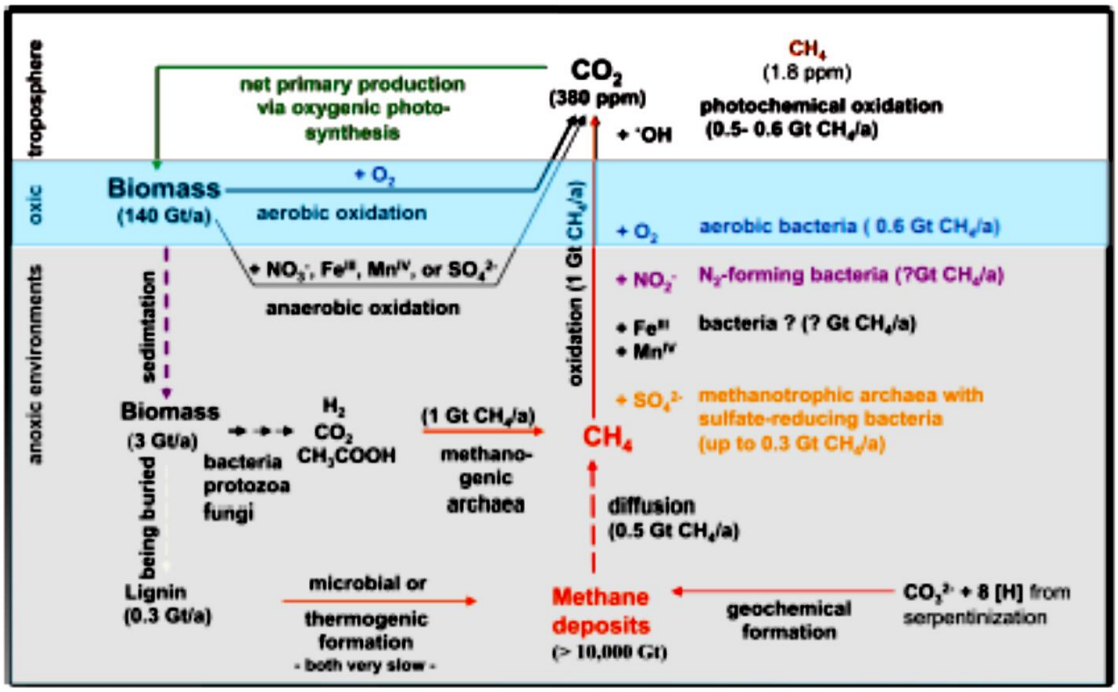

Figure 1.1: Processes of the global methane cycle (with permission (18,20)).

1.1.3 Biochemistry of Methanogenesis:

On the basis of the starting substrate, there are three pathways reported for methanogenesis; the hydrogenogenic pathway (CO_2/H_2 or formate), the acetoclastic pathway (acetate CH_3COO^-) and the methylotrophic pathway (Methanol or Methylamine). *Methanothermobacter marburgensis* utilizes the hydrogenotrophic pathway, where the carbon atom of CO_2 undergoes an 8-electron reduction to finally give methane (**Fig. 1.2**). The activation of CO_2 to CH_4 proceeds via coenzyme-bound C1 intermediates, methanofuran, tetrahydromethanopterin and Coenyzme M. The first step, conversion of CO_2 into a formyl group is catalyzed by the formylmethanofuran dehydrogenase (21).The formyl group is then transferred to tetrahydromethanopterin (H_4MPT) (22) at which, after cyclisation to methenyl-H_4MPT (23), two reduction steps occur to yield a *N*-methyl group (24). This nitrogen-bound methyl group is transferred by coenzyme M methyl-transferase (25) to the thiol group of coenzyme M to form methyl-coenzyme M which is subsequently converted into methane.

The activation of CO_2 in the first step of the hydrogenotrophic pathway is endergonic by 16 kJ mol^{-1}. ATP formation in this pathway via Na^+ gradients (0.5 ATP/CH_4) is not enough to overcome the energy requirement for the first step (26,27). In order to overcome this first endergonic step, a coupling to the exergonic reduction of the heterodisulfide was proposed (28-30). A protein complex containing all required enzymes together was identified recently which supports this hypothesis (28,30) where The Heterodilsulfide/Hydrogenase (HDR/H_2ase) complex couples the endergonic reduction of ferredoxin with H_2 to the exergonic reduction of CoM-S-S-CoB with H_2 via the mechanism of flavin-based electron bifurcation. The reduced ferredoxin in

turn is utilized for the reduction of CO_2 in the first step. The bifurcation complex removes the need for additional Na^+ pumping and/or ATP synthesis. In addition, the exergonic reaction of the methyl transferase ($\Delta G^{\circ'} = -30$ kJ mol^{-1}) is coupled to a sophisticated energy- accumulating system that is also linked with the heterodisulfide reductase used for ATP production (20). It was speculated by Rouvière and Wolfe (31) that methane formation from H_2 and CO_2 by methanogenic archaea could be a cyclical process. With the recent discovery of an electron bifurcation complex in methanogens it has been concluded that the hydrogenotrophic pathway is cyclic and is now being called the Wolfe cycle (28-30).

All metabolic pathways use the same last step in which the methyl-coenzyme M reductase (MCR) reduces the sulfur-bound methyl group to methane with the thiol coenzyme B as the reductant and the heterodisulfide of coenzymes M and B as the second product (32). Hence, MCR is the central protein in the process of methanogenesis and it represents almost 10% of the total amount of protein in the cell (12). During methogenesis, methane is produced as a waste product. The heterodisulfide is the desired product that is used to make ATP indirectly or is used directly to make low potential electrons that can be used in important cellular processes.

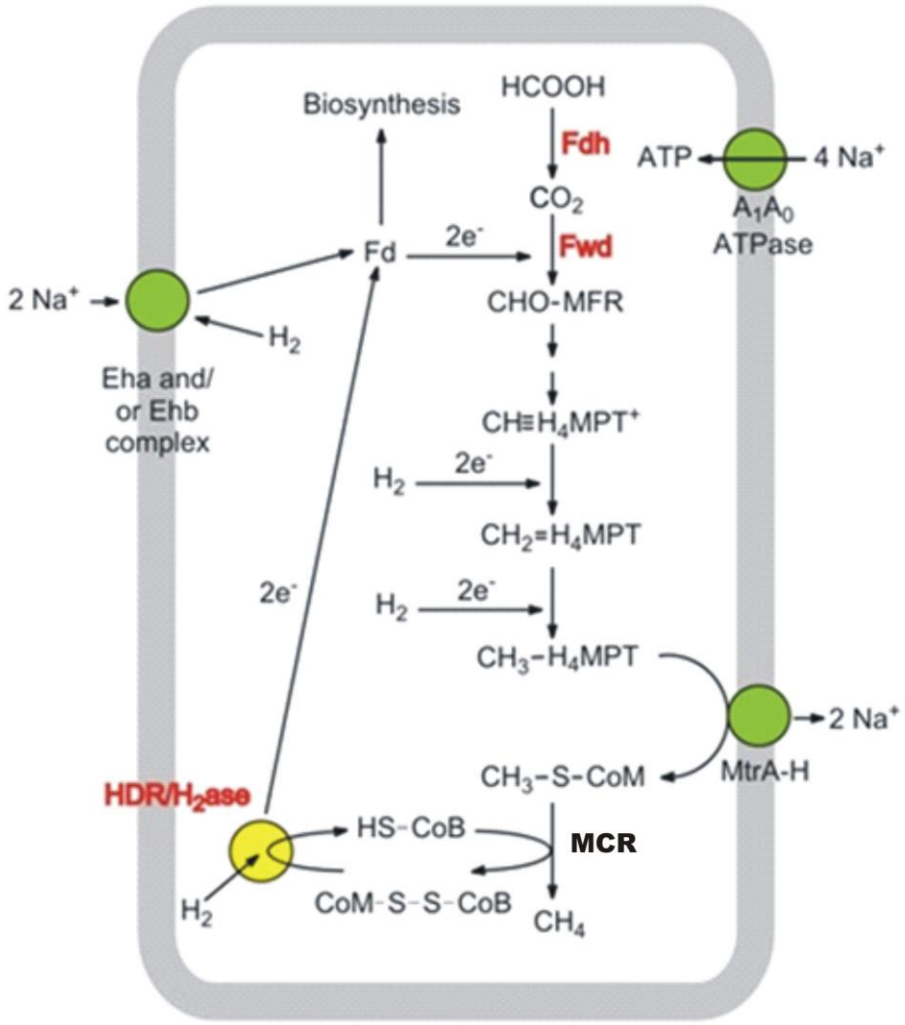

Figure 1.2: The eight electron reduction pathway from carbon dioxide to methane. Abbreviations:CHO-MFR,formylmethanofuran**;$CH{\equiv}H_4MPT^+$,** methenyltetrahydromethanopterin**;** **CH_2==H_4MPT,** methylenetetrahydromethanopterin**;** **CH_3-H_4MPT,** methyltetrahydromethanopterin**; CoB-SH,** coenzyme B with its thiol group**; CoM-SH, CoM-S-S-CoB,** heterodisulfide**; EchA-F, EhaA-T, and EhbA-Q,** energy-converting [NiFe]-hydrogenases**;** **Fd,** ferredoxin**;** **Fwd:** Formyl methanofuran dehydrogenase, **Fdh:** Formate dehydrogenase, **HDR/H_2ase:** Heterodisulfide reductase / Hydrogenase complex, **MCR:** Methyl Coenzyme M reductase.

1.2 Methyl-Coenzyme M Reductase (MCR)

1.2.1 MCR reaction and its isoenzyme:

Methyl-coenzyme M reductase (MCR, EC 2.8.4.1) catalyzes the reduction of methyl-coenzyme M (CH_3-S-CoM) with Coenzyme B (HS-CoB) to methane and the heterodisulfide CoM-S-S-CoB as shown in more detail in **Fig. (1.3)** (33,34). The reaction catalyzed by MCR involves the cleavage of the C-S bond and the S-H bond in the substrates and the formation of the S-S bond and a C-H bond in the products. Formally, the two involved sulfur atoms are oxidized to the disulfide and the methyl group is reduced from the –II to the –IV oxidation state in the product methane. The enzyme has recently been proposed to be involved also in the anaerobic oxidation of methane (AOM) (35,36) and therefore the reaction is shown as reversible.

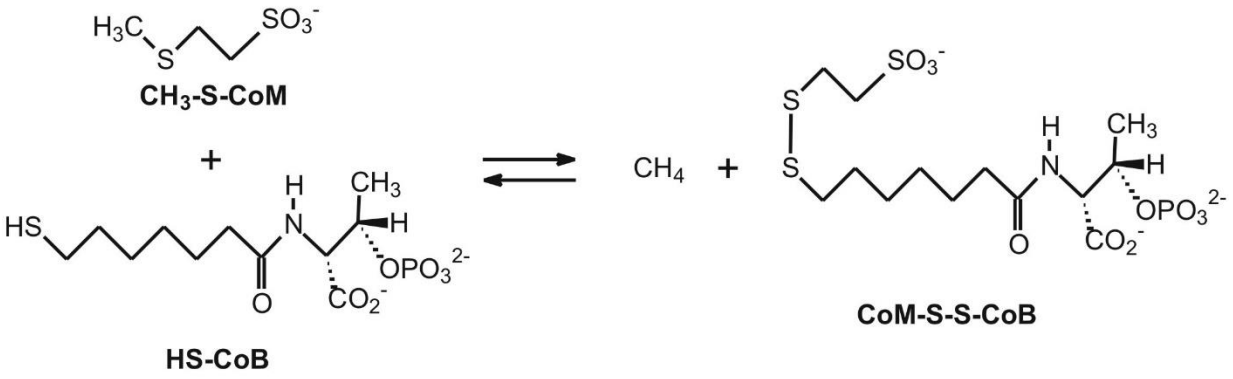

Figure 1.3: Reaction catalyzed by methyl-coenzyme M reductase (MCR). CH_3-S-CoM, methyl-coenzyme M (2-(methylthio) ethanesulfonate); HS-CoB, coenzyme B (*N*-7-mercaptoheptanoyl-*O*-phospho-L-threonine); CoM-S-S-CoB, heterodisulfide of coenzyme M (2-mercaptoethanesulfonate) and coenzyme B.

Most of the members of the Methanobacteriales and Methanococcales lik*e* *Methanobacterium marburgenesis, Methanobacterium thermoautotrophicum, Methanothermus feruidus* and *Methanococcus jannaschii* have been shown to contain, besides MCR, a genetically distinct isoenzyme of methyl-coenzyme M reductase designated as MRT (37-41). The expression of the two isoenzymes is differentially regulated by the growth conditions (32,42-44). The genes encoding the three subunits of the isoenzyme I (MCR) form a transcription unit (*mcrBDCGA*) which additionally contains two open reading frames encoding two polypeptides, McrC and McrD, of molecular masses of approximately 20 kDa (45-47). These two proteins can be detected in cell extracts (47,48) but are not part of the active form of the enzyme (49-52). The genes encoding the three subunits of the isoenzyme II (MRT) also form a transcription unit *(mrtBDGA)* which contains only one extra open reading frame encoding a protein with sequence similarity to McrD (41). The gene similar to McrC, MrtC, is coded elsewhere in the genome. The function of the *mcrC, mcrD, mrtC* and *mrtD* gene products is not known (43). Recently, however, we found that the *mcrC* and *mrtC* gene products are part of an activating complex involved in the activation of MCR (47). The McrD was found to be a part of recombinant *Methanothermococcus okinawensis* MCR when overexpressed in a *Methanococcus maripaludis* host (unpublished data). Since MCR I is the major isoenzyme in *Methanobacterium marburgensis,* the activation of MCR I was studied for this dissertation.

1.2.2 Coenzyme F_{430} and its chemistry:

Coenzyme F_{430} has only been found in methanogenic archaea. It is non-covalently bound in the active site of MCR and can be liberated by denaturing the enzyme with dilute perchloric acid (53,54). The π chromophore of F_{430} extends only over three of the four nitrogen ligands, making F_{430}, the most reduced tetrapyrrole found in nature (**Fig. 1.4**). The high degree of saturation in the coenzyme F_{430} ligand is required for a metal-centered oxidation and reduction of Ni (II). F_{430} is a tetrahydrocorphin type of tetrapyrrole in which the carbon framework of a porphin is combined with the linear chromophore typical for corrins. Two additional rings are found in F_{430}, a lactam ring fused to ring B and a 6-membered carbocycle formed through intramolecular acylation of C_{15} by the propionic acid side chain at ring D (33,55).

F_{430} is both thermally and oxidatively unstable. Due to thermal unstability acid side chains at β-carbon positions 12 and 13 of pyrrole ring C epimerize to form 12,13-diepimer. This form of F_{430} is slowly oxidized in air to 12, 13-didehydro-F_{430}, which is termed F_{560} since it shows an absorption maximum at 560 nm in electronic absorption spectroscopy. A pentamethylester form of F_{430} ($F_{430}M$) can be made by methylation of the five carboxy groups to generate a more stable form that is soluble in organic solvents and has been studied intensively.

Both Ni(II)F_{430} and Ni(II)$F_{430}M$ can be reduced to Ni(I) (56-58). Oxidation of Ni(II)$F_{430}M$ in acetonitrile leads to Ni(III)$F_{430}M$ (57). The midpoint potential (E_m°') of the Ni(II)F_{430}/Ni(I)F_{430} couple has been determined to be below −0.6 V. The Em°' for the Ni(II/III) couple is more than +1.21 V (35,56,59).

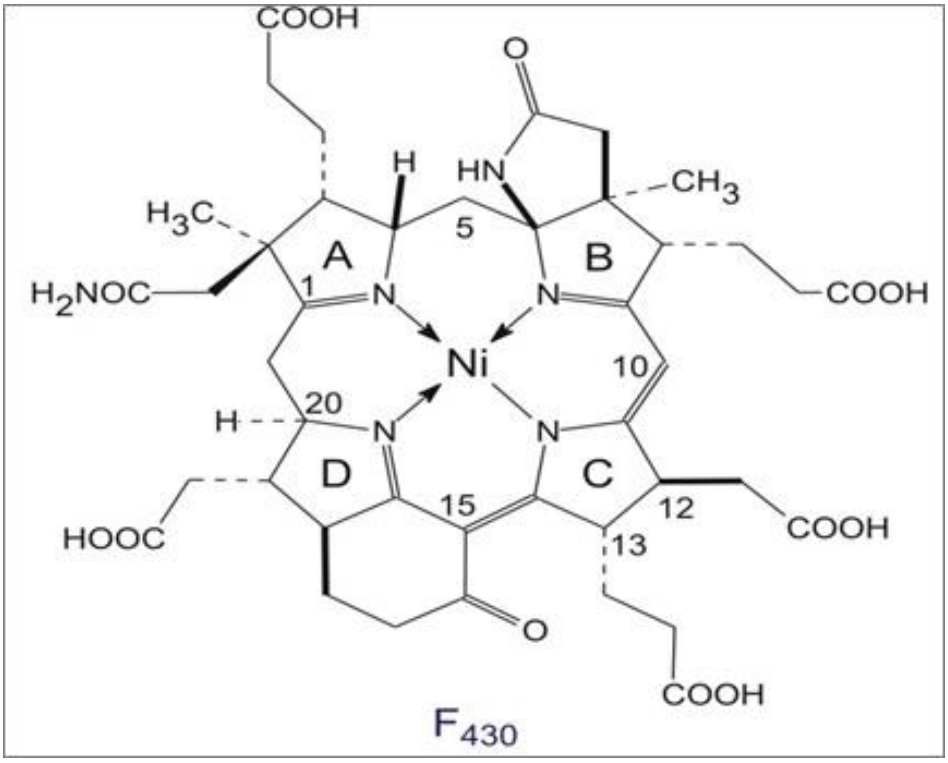

Figure 1.4: Structure of coenzyme F_{430}

1.2.3 Activity of MCR in forward and reverse reaction:

It is well established that the MCR_{red1}-Ni(I) form is the only active form while the other two major forms MCR_{ox1}-Ni(III) and MCR_{silent}-Ni(II), that can be detected in purified enzyme and whole cells, are inactive (52,60-63). Methane formation from methyl-coenzyme M and coenzyme B can be determined under anaerobic conditions using stoppered serum vials (51,52). The formation of CH_4 is measured by taking samples of the gas phase and analyzing these by gas chromatography with flame ionization detection (GC-FID). For optimal activity measurements, aquacobalamin and the reductant titanium(III) citrate are added (20,47,50,52). The cobalamin reduces the formed heterodisulfide back to the single thiols, coenzyme M and coenzyme B. This is important since heterodisulfide inhibits the reaction. With this method, the specific activity for the *M. marburgensis* isoenzyme I is 70–100 μmol min^{-1} mg^{-1} calculated for 1 spin per mol F_{430}. (In this case a spin of 1 means that all nickel in MCR is present as MCR_{red1}). MCR is very particular when it comes to substrates. The only other substrates for MCR are ethyl-coenzyme M (CH_3CH_2–S–CoM), seleno-methyl-coenzyme M (CH_3–Se–CoM), fluoro-methyl-coenzyme M (CFH_2–S–CoM), difluoro-methyl-coenzyme M (CF_2H–S–CoM), and C_6-coenzyme B (one methylene group shorter than coenzyme B).

Most of the steps in the hydrogenotrophic pathway (conversion of CO_2 into CH_4) have always been considered reversible, except for the reaction catalyzed by MCR. The formation and consumption of methane is favored under standard conditions (20,35). Under equilibrium conditions, MCR from *M. marburgensis* can indeed catalyze the conversion of methane into methyl-coenzyme M with a specific activity of 11.4 nmol min^{-1} mg^{-1} (11). Initially, it was proposed that the oxidation of methane by consortia of ANME/sulfate reducer was performed by a new enzyme. MCR, however, was shown to be present in the consortia ANME archaea. These consortia

were isolated from biomats that grow on top of methane hydrates at the bottom of the black sea. The high methane concentration in this environment would make the reversible reaction a possibility.

1.2.4 Structure of methyl-coenzyme M reductase (MCR):

MCR has been crystalized in the catalytically inactive Ni(II) state from *Methanothermobacter marburgensis, Methanosarcina barkeri* and *Methanopyrus kandleri* (54,64,65). The 280–kDa enzyme is composed of three different subunits, α, β and γ, forming an $(\alpha\beta\gamma)_2$ heterohexamer (64). Each molecule of MCR contains two molecules of the cofactor F_{430}, as prosthetic group (66-68). The binding sites of two coenzymes F_{430} are roughly 50 Å apart, forming two separated structurally identical active sites as shown in **Fig.1.5**.

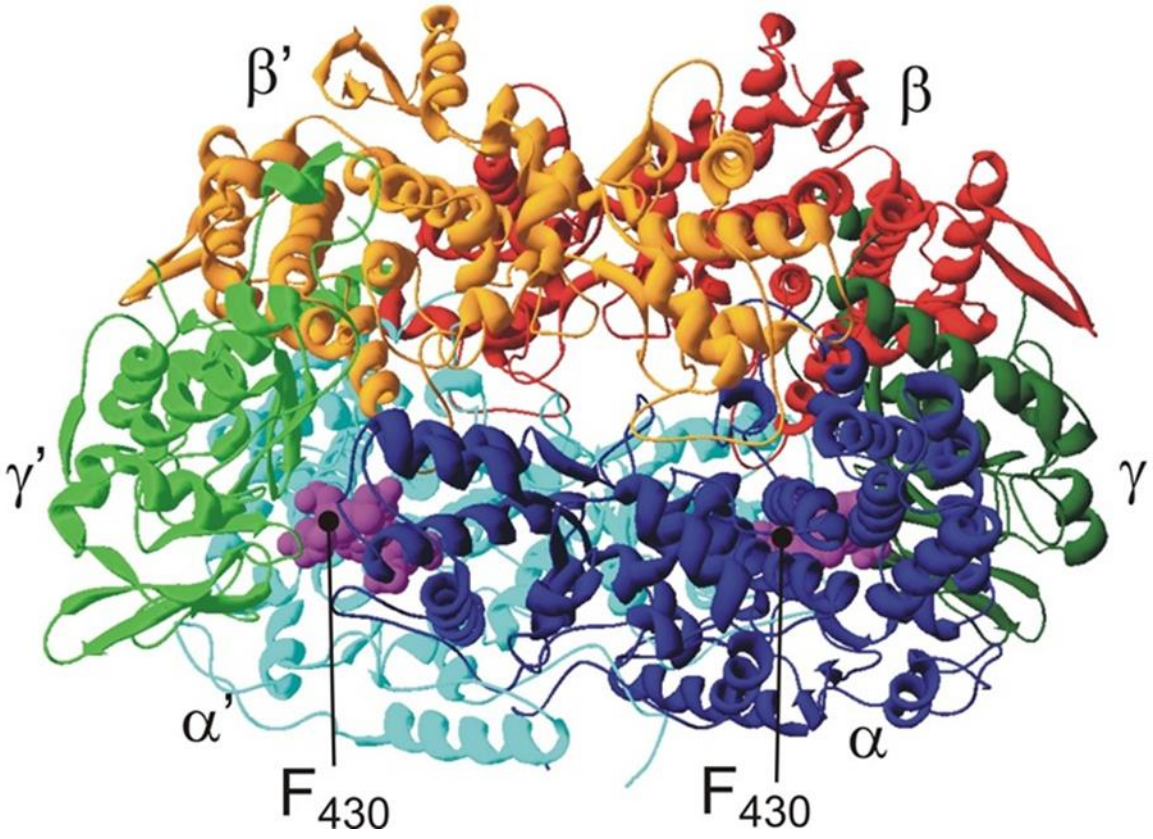

Figure 1.5: The crystal structure of MCR(64).

The active site consists of a 40 Å long channel leading from the enzyme surface towards the proximal face of F_{430} **(Figs. 1.6 and 1.7).** The channel is polar and wider near the surface and becomes very narrow and hydrophobic near the entrance into a cavity above the macrocycle of F_{430}. This section of the channel is coated by five annular arranged aromatic residues (3 Phe and 2 Tyr) to generate the hydrophobic environment. The active channels are lined with the amino acid chains of either subunits α, α', β and γ or subunits α', α, β' and γ'. In addition, as shown in Figure 1.7, the active site region contains five post translationally modified (PTM) amino acids (64,69,70) comprising 1-N-methyl-Hisα^{257}, S-methyl-Cysα^{452}, 5-methyl-Argα^{71} and 2-methyl-Glnα^{400} and thio-Glyα^{445}. The methylations are the result of posttranslational modification (69,70). The role of these modifications is not known. However, it has been speculated by some that the thioglycine is involved in the catalytic cycle of MCR (69,71,72).

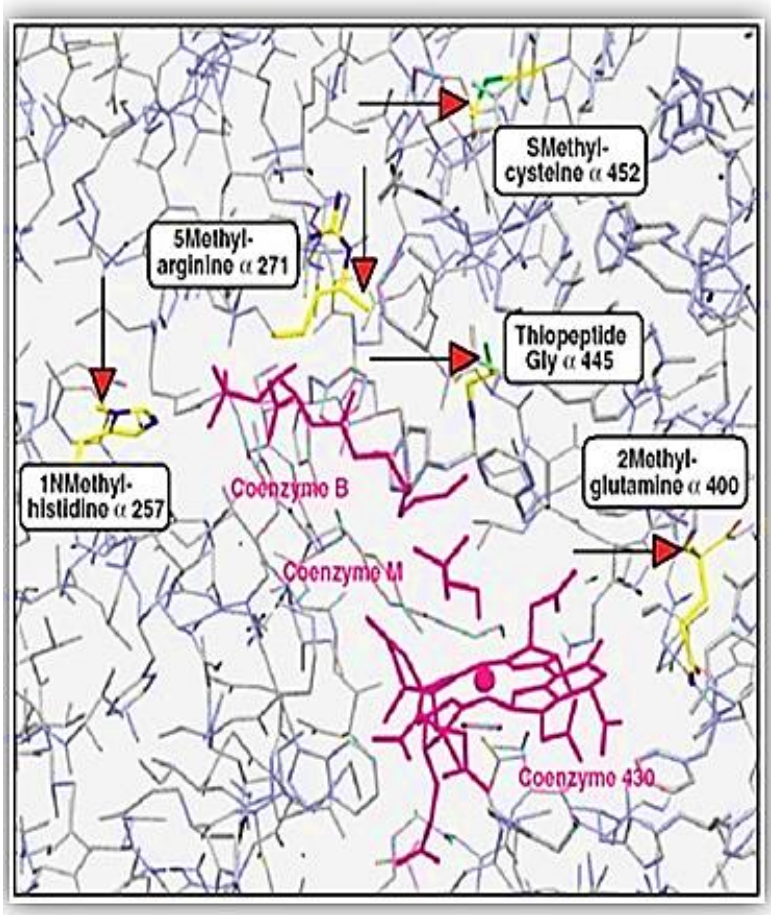

Figure 1.6: Active site region of $MCR_{ox-\ Silent}$.

In the crystal structure of the $MCR_{ox1\text{-}silent}$ form **(Fig. 1.7)**, coenzyme M and coenzyme B are bound in the channel, showing that the active site of MCR extends from the nickel of cofactor F_{430} via the thioether group of CH_3–SCoM to the sulfhydryl group of HS–CoB. In the case of MCR_{silent}, the heterodisulfide is bound to the channel while HS-CoM is present around 4 Å from Ni center in $MCR_{\text{-}red1\text{-}silent}$ form. A less well-resolved X-ray structure of MCR without substrates or inhibitors bound shows a wider and less ordered channel structure (73). Although no crystal structures with only methyl-coenzyme M bound are available, it is reasonable to assume that the binding of the first substrate at the active enzyme leads to an ordering of the protein chains forming the channel. Such ordering can increase the affinity towards the second substrate (coenzyme B), which binds in the channel, and would explain the kinetically observed ordered substrate binding (74).

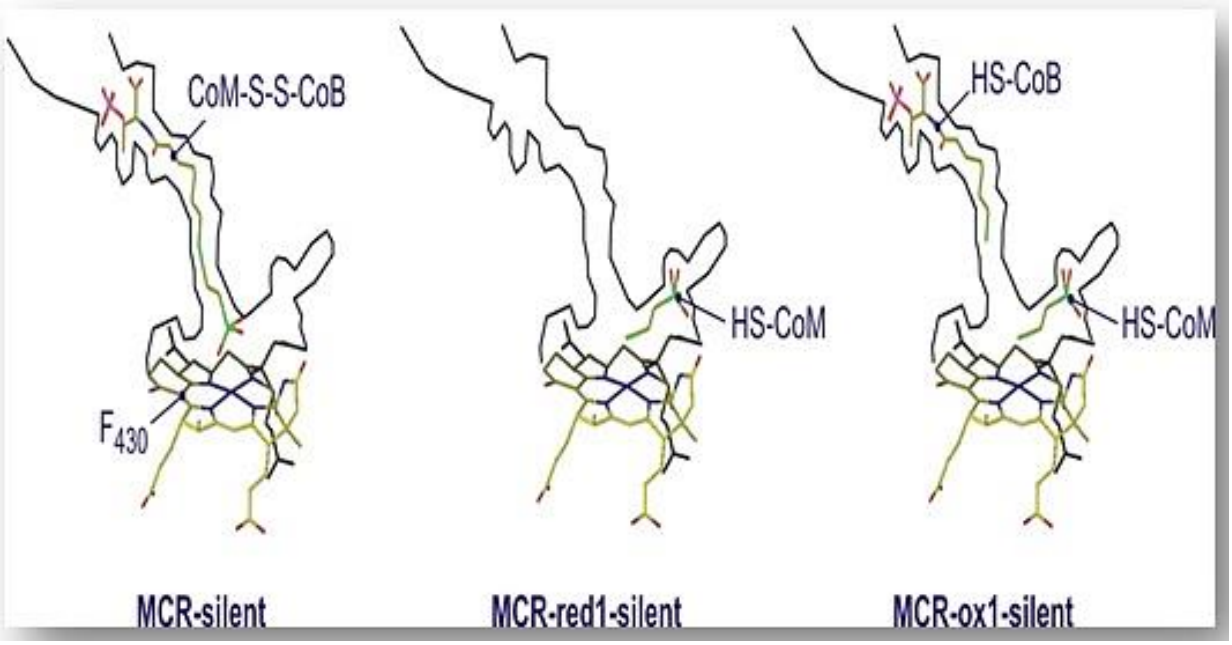

Figure 1.7: Crystal–structure based models of active–site region of the different silent forms.

1.3 The Electron paramagnetic resonance:

1.3.1 Introduction:

Electron Paramagnetic Resonance (EPR) spectroscopy is a technique that measures the absorption of microwave radiation between energy levels of an unpaired electron when it is placed in a strong magnetic field. It characterizes the properties and probes the environment of this paramagnetic center (*79*). A more noteworthy application area of EPR spectroscopy is the biological systems that encompass paramagnetic species like metal ions, substrate radicals, and redox-active centers in proteins (*80*). Transition ions are usually open–shell system, i.e. they contain partially filled *d* or *f* shells, and they have one (S = 1/2) or more (S > 1/2) unpaired electrons in at least one of their common oxidation states. Thus, BIOMOLECULAR spectroscopy is predominately a means to study the structure and functioning of active sites of enzymes containing cofactors (75,76). MCR contain the Ni-containing cofactor F_{430} in its active site and different forms of MCR can be easily distinguished and quantified by EPR. Therefore, the basic principles of EPR are explained in this chapter.

1.3.2 Basic Principles:

Spectroscopy is the measurement and interpretation of the energy differences between the atomic or molecular states and, with knowledge of these energy differences (ΔE), the identity, structure, and dynamics of the sample. According to Planck's law, electromagnetic radiation will be absorbed if:

$$\Delta E = h\nu, \tag{1}$$

Where h is Planck's constant and ν is the frequency of the radiation. In EPR spectra one does not vary the frequency (ν) of the radiation due to electronic constraints but the magnetic field is swept.

The most commonly used frequency is in the range of 9-10 GHz (the X-band). The unit of energy used in EPR is wavenumber (cm^{-1}). A frequency of 9.5 GHz means an energy $h\nu \sim 0.3\ cm^{-1}$.

Due to charge and angular momentum, an isolated electron acts like a bar magnet with a magnetic moment ($\bar{\mu}$). The energy differences we study in EPR spectroscopy are predominately due to the interaction of unpaired electrons in the sample with a magnetic field (B_0) produced by an external magnet. This effect is called the *Zeeman Effect*. The magnetic field, B_0, produces two energy levels for the magnetic moment, $\bar{\mu}$, of the electron with highest and lowest energy state depending on alignment of B_0 along or against $\bar{\mu}$ as shown in equation 2 and 3. For an electron $\mu = g_e \beta m_s$, where β is a conversion constant called the Bohr magneton and g_e is the spectroscopic g factor of the free electron and equals 2.0023192778 (≈ 2.00). Therefore, the energies for an electron with $m_s = +½$ and $m_s = -½$ are, respectively

$$E_{1/2} = ½\ g_e \beta B_0 \qquad (2)$$

and

$$E_{-1/2} = -\ ½\ g_e \beta B_0 \qquad (3)$$

As a result there are two energy levels for the electron in a magnetic field shown as in **Fig. 1.8**.

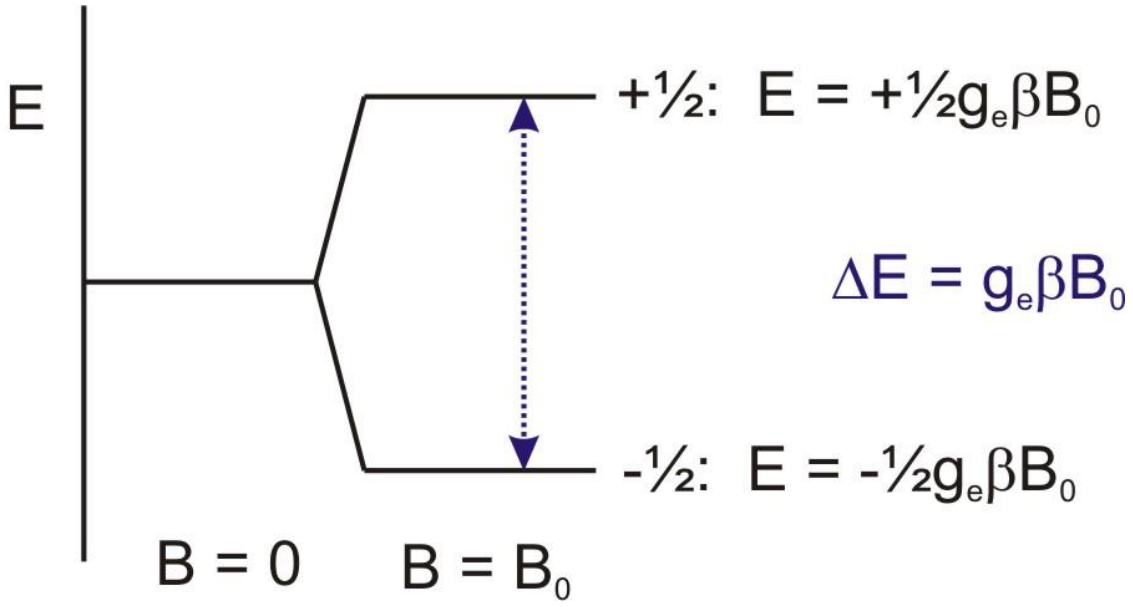

Figure 1.8: Induction of the spin state energies as a function of the magnetic field B_0.

Absorption of energies will occur when the condition in (4) is satisfied

$$\Delta E = g\beta B_0 = h\nu \tag{4}$$

The value of g can then be calculated from ν (in GHz) and B_0 (in gauss) using,

$$\mathrm{g} = \frac{h\nu}{\beta B_0} \tag{5}$$

or

$$\mathrm{g} = 714.484\frac{\nu}{B_0} \tag{6}$$

($h = 6.626 \cdot 10^{-34}$ J·s; $\beta = 9.274 \cdot 10^{-28}$ J·G^{-1})

When we take an electron in space with no outside forces on it and place it on to a molecule, its total angular momentum changes because, in addition to the intrinsic spin angular momentum ($\bar{S}$), it now also possesses some orbital angular momentum ($\bar{L}$). These two magnetic moments interact, and the energy of this spin-orbit interaction depends on their relative orientations.

Electron in space

$$\bar{\mu} \propto g_e\bar{S} \tag{7}$$

Electron in a molecule

$$\bar{\mu} \propto g_e\bar{S} + \bar{L} \tag{8}$$

Spin-orbit coupling term is proportional to $\bar{S}$ that allows to combine both terms on the right and change the value of g_e to g, or

$$\bar{\mu} \propto g\bar{S} \tag{9}$$

and

$$h\nu = (g_e + \delta g)\beta B = g\beta B \quad (10)$$

The quantity '$g_e + \delta g$' contains the chemical information on the nature of the bond between the electron and the molecule, the electronic structure of the molecule. The value of $g = g_e + \delta g$ can be taken as a fingerprint of the molecule.

1.3.3 Line shape:

Because orbitals are oriented in the molecule, the magnitude of mixing of spin angular momentum to orbital angular momentum is direction dependent, or **anisotropic**. For every paramagnetic molecule, there exists a unique axis system called the **principal axis system**. The *g* factors measured along these axes are called the principal *g* factors and are labeled g_x, g_y and g_z. **Fig.1.9** represents the absorption and first-derivative spectra for three different classes of anisotropy. In the first class, called **isotropic**, all of the principal *g* factors are the same. In the second class, called **axial**, there is a unique axis that differs from the other two ($g_x = g_y \neq g_z$). The *g* factor along the unique axis is said to be parallel with it, $g_z = g_{/\!/}$ while the remaining two axes are perpendicular to it, $g_{x,y} = g_{\perp}$. The last class, called **rhombic**, occurs when all the *g* factors differ. For electronic and practical reasons, the first derivative instead of the true absorption is recorded. Most EPR spectra of biological transition metals are recorded on frozen solution samples to fix the molecules in all possible orientations. Therefore the spectrum of a frozen sample represents the summation of all possible orientations and is called a powder spectrum.

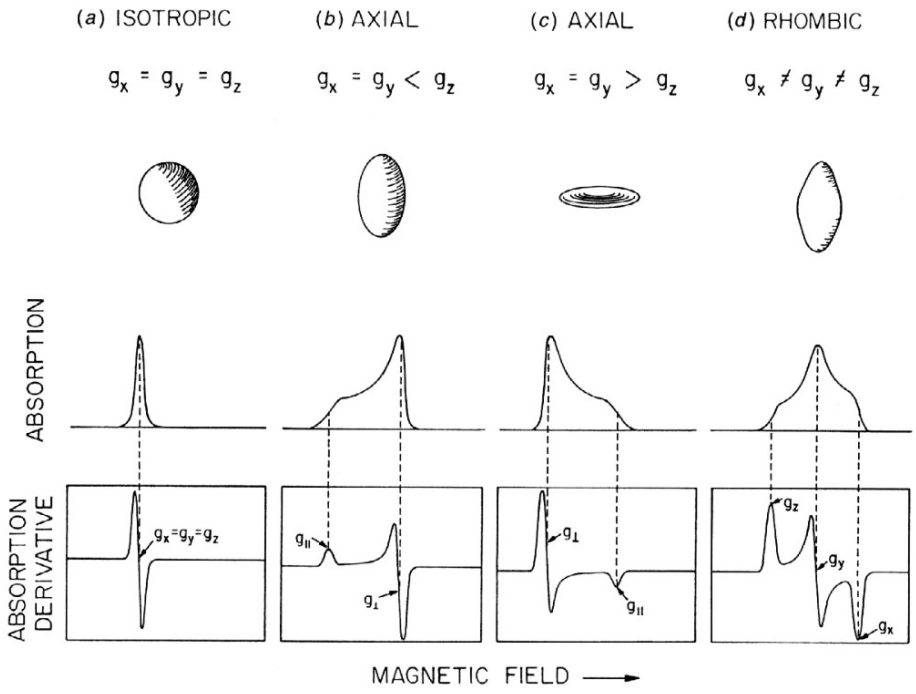

Figure 1.9: Schematic representation of the *g* tensor and the consequential EPR spectra. The upper solid bodies show the shapes associated with isotropic, axial and rhombic magnetic moments. Underneath are shown the absorption curves. The corresponding EPR derivative curves are shown on the bottom (with permission (77)).

1.3.4 Hyperfine and superhyperfine interaction, the effect of nuclear spin:

In EPR there are three types of interaction that can occur. The first two types are due to the interaction between an unpaired electron and a magnetic nucleus. Interaction of unpaired electron with nuclear magnetic moment is termed ***nuclear hyperfine interaction***. It is called ***hyperfine*** when the unpaired electron originates from the nucleus and ***superhyperfine*** when it is from a neighboring nucleus. The third type is the interaction between two unpaired electrons on different atoms normally within a molecule and it is termed ***spin-spin interaction***.

Table 1.1: Lists of the nuclei that are important in biology. Indicated are isotopes present (natural abundance), isotopes with a nuclear spin and the respective spin.

Atom	Isotope	Spin (abundance)
H	***1***, ***2***	^{1}H, $\mathbf{1/2}$ (99.985); ^{2}H, 1 (0.015)
C	12, ***13***	$\mathbf{1/2}$ (1.07)
N	***14***, ***15***	^{14}N, 1 (99.632); ^{15}N, $\mathbf{1/2}$ (0.368)
O	16, ***17***, 18	$\mathbf{5/2}$ (0.038)
F	***19***	$\mathbf{1/2}$
P	***31***	$\mathbf{1/2}$
S	32, ***33***, 34	$\mathbf{3/2}$ (0.76)
Cl	***35***, ***37***	^{35}Cl, $\mathbf{3/2}$ (75.78); ^{37}Cl, $\mathbf{3/2}$ (24.22)
As	***75***	$\mathbf{3/2}$
Se	76, ***77***, 78, 80, 82	$\mathbf{1/2}$ (7.63)
Br	***79***, ***81***	^{79}Br, $\mathbf{3/2}$ (50.69); ^{81}Br, $\mathbf{3/2}$ (49.31)
I	***127***	$\mathbf{5/2}$
V	***50***, ***51***	^{50}V, 6 (0.25); ^{51}V, $\mathbf{7/2}$ (99.75)
Mn	***55***	$\mathbf{5/2}$
Fe	54, 56, ***57***, 58	$\mathbf{1/2}$ (2.119)
Co	***59***	$\mathbf{7/2}$
Ni	58, 60, ***61***, 62	$\mathbf{3/2}$ (1.14)
Cu	***63***, ***65***	^{63}Cu, $\mathbf{3/2}$ (69.17); ^{65}Cu, $\mathbf{3/2}$ (30.83)
Mo	92, 94, ***95***, 96, ***97***, 98, 100	^{95}Mo, $\mathbf{5/2}$ (15.92); ^{97}Mo, $\mathbf{5/2}$ (9.55)
W	180, 182, ***183***, 184, 186	$\mathbf{1/2}$ (14.3)

The effect of hyperfine interaction is to add a term to the energy expression for an EPR transition

$$\Delta E = h\nu = g\beta B_0 + hA_{mI} \quad (11)$$

Where A is the Hyperfine Coupling Constant (measured in cm^{-1} or MHz but also expressed in G) and m_I is the magnetic quantum number for the nucleus. Since there are $2I + 1$ possible values of m_I, the hyperfine interaction terms splits the Zeeman transition into $2I + 1$ lines of equal intensity. For example, interaction of the electron with a nucleus with $I = ½$ (for example a proton) will yield an EPR spectrum containing two lines. The local field of the nucleus either adds or subtracts from the applied B_0 field. As a result the energy levels are split in two (**Fig. 1.10**). In the EPR experiment we detect now two lines instead of one (**Fig. 1.11**). The hyperfine interaction can make an EPR spectrum look very complex.

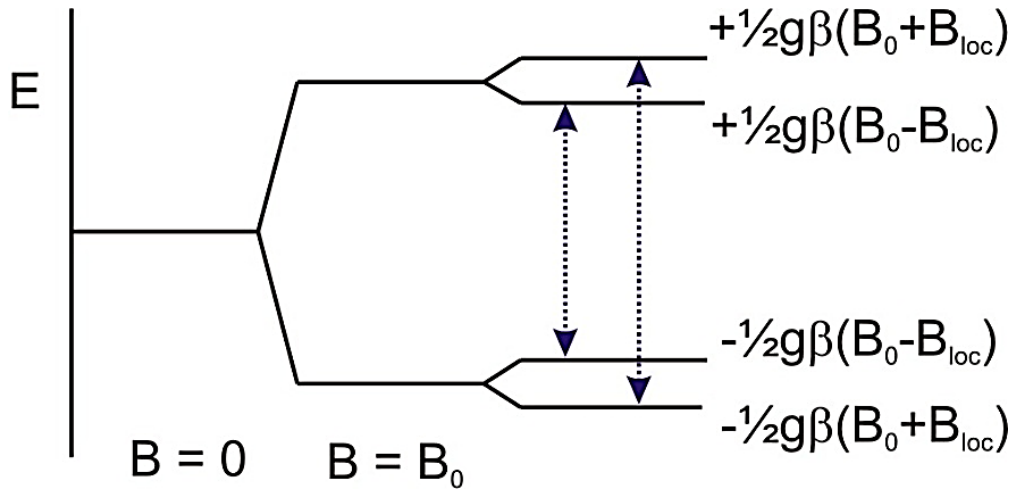

Figure 1.10: Permanent local fields arising from the magnetic moments of magnetic nuclei

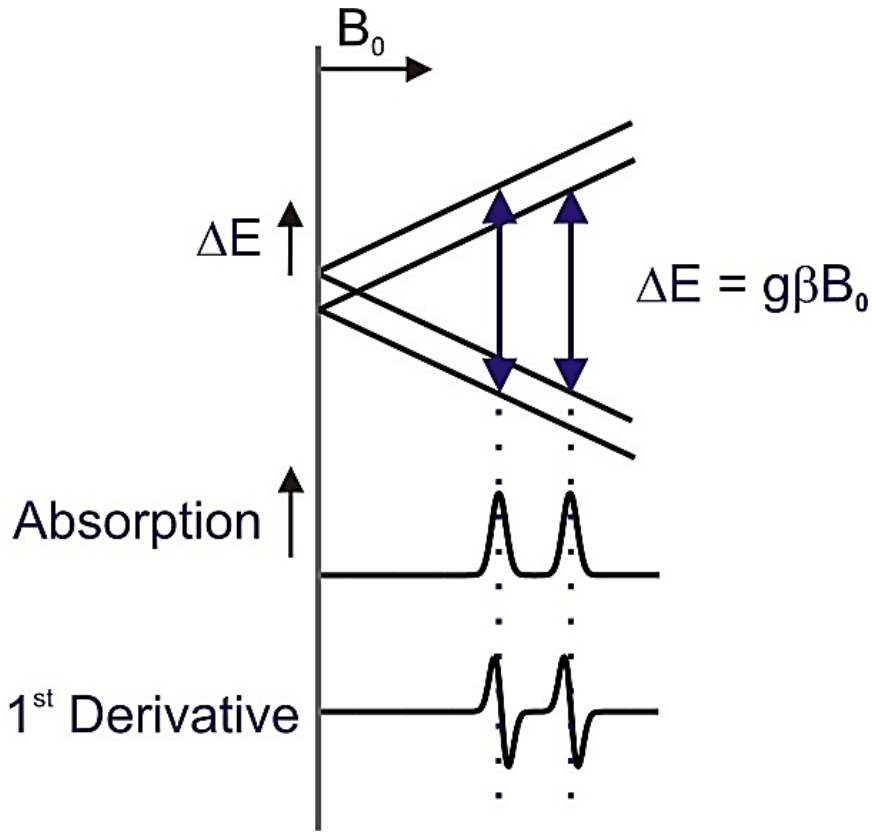

Figure 1.11: EPR experiment for a single electron interacting with a magnetic nucleus with nuclear spin $I = ½$.

1.3.5 Ni^{1+} in methyl-coenzyme-M reductase:

In methyl-coenzyme M reductase, four nitrogen atoms from the tetrapyrrole F_{430} coordinate the nickel (**Fig. 1.4**). This is an example of superhyperfine interaction. The paramagnetic Ni^{1+} (d^9) is coordinated by four nitrogen atoms of which the nuclei have a nuclear spin 1. **Fig. 1.12** shows two spectra. The top spectrum shows the methyl-coenzyme M in the red1 state. The superhyperfine lines due to the four nitrogen ligands can clearly be detected on the $g_{\perp}$ peak. The resolution of the hyperfine structure on the $g_{/\!/}$ peak is less but still detectable. In an effort to prove that the signals that were detected in this enzyme were due to nickel, the enzyme was enriched in ^{61}Ni, which has a nuclear spin 3/2. The bottom spectrum in **Fig. 1.12** shows the resulting spectrum. In addition to the superhyperfine structure from nitrogen we also detect hyperfine structure due to the nickel. The $g_{/\!/}$ peak is now split into four lines. The splitting on the $g_{\perp}$ peak is only detectable as a line broadening since the hyperfine splitting is less than the line width of the peak.

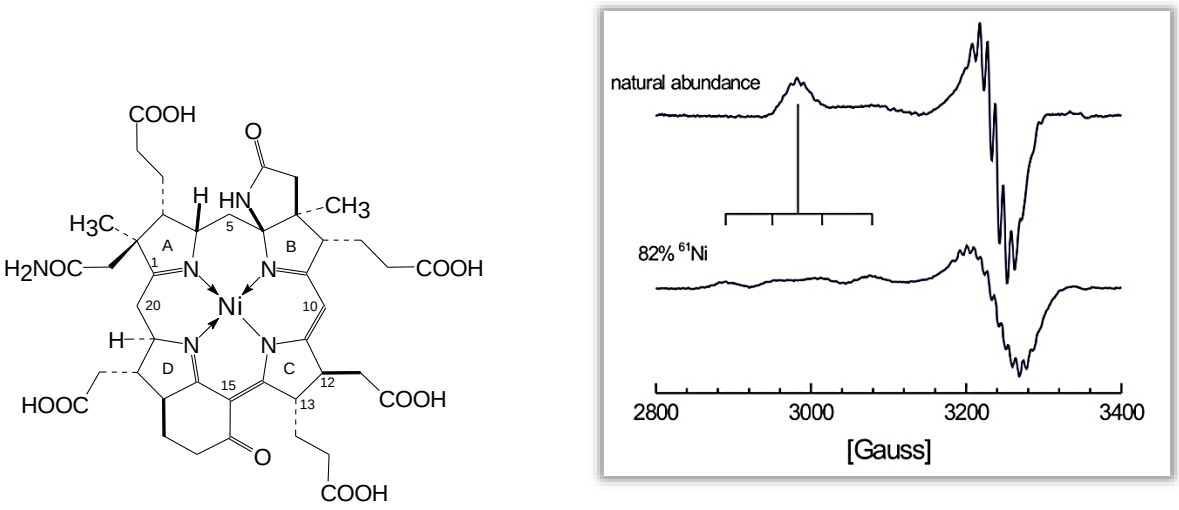

Figure 1.12: EPR spectra of methyl-coenzyme M from *Methanothemobacter marburgensis* in the red1 state. The top spectrum shows the spectrum obtained after growing cells with natural abundance nickel isotopes. The bottom spectrum shows the spectrum obtained after growing cells on ^{61}Ni (I = 3/2). The structure of cofactor 430 (F_{430}) is shown on the right.

1.3.6 Different forms of F_{430}:

Different forms of F_{430} can be distinguished by the EPR spectra as shown in **Fig. 1.13** for F_{430} M in the Ni(I), Ni(II) and Ni(III) forms. In the Ni(III) state, the unpaired electron is in the dz^2 orbital that points to the loosely bound axial ligands, in this example two molecule of propionitrile. This ligand also contains a nitrogen atom, which coordinates to the nickel causing the superhyperfine structure detectable on the g_z peak. In the Ni(I) state the unpaired electron is in the $d_{x^2-y^2}$ orbital that point towards the nitrogen ligands of F_{430}. In this case, the hyperfine splitting because of N is of the same magnitude as the line width of the signal. As hyperfine structure can only be detected when the hyperfine splitting is bigger than the line width, therefore, in case of Ni(I) hyperfine splitting is not recognizable.

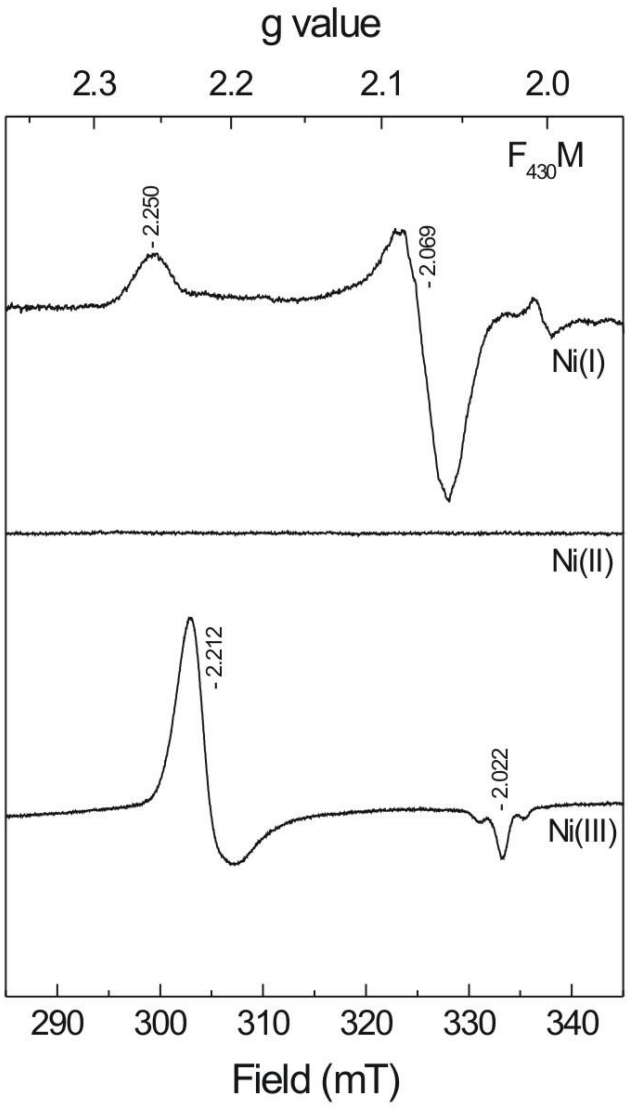

Figure 1.13: EPR spectra of from F_{430} pentamethylester (F_{430} M) (33)

1.4 Different MCR Forms:

The naming of all relevant MCR forms are based on the conditions used to induce these forms (52,78). Some of the forms were first discovered in whole cell experiments (52,60,61). There are three major forms of MCR: MCR_{red} (Ni^{I+}, d^9), MCR_{ox} (Ni^{3+}, d^7) and MCR_{silent} (Ni^{2+}, d^8). For a cell using the hydrogenotrophic pathway, H_2, through hydrogenases, is a reductant and the substrate CO_2 can be considered an oxidant. Therefore the signals that were induced by gassing with H_2 were dubbed "red" and the number indicated the order in which they were discovered. In the same way, the signals, which were detected upon incubation with a mixture of N_2 and CO_2, were called "ox" signals. Both the MCR_{red1} (Ni^{1+}, d^9) and the MCR_{ox1} (Ni^{3+}, d^7) forms are paramagnetic and are detectable in EPR spectroscopy. The Ni^{2+} (d^8) from is diamagnetic (S =1) and is not detectable in EPR spectroscopy. This form is also referred as "EPR silent". These forms can be distinguished by EPR and UV-VIS spectroscopies as shown in **Fig. 1.14 A** and **B,** respectively. With EPR spectroscopy, the intensity of MCR signals can be measured by using a double integration method. Therefore in this dissertation, EPR is used to compare the percentage of species presented in different samples (47).

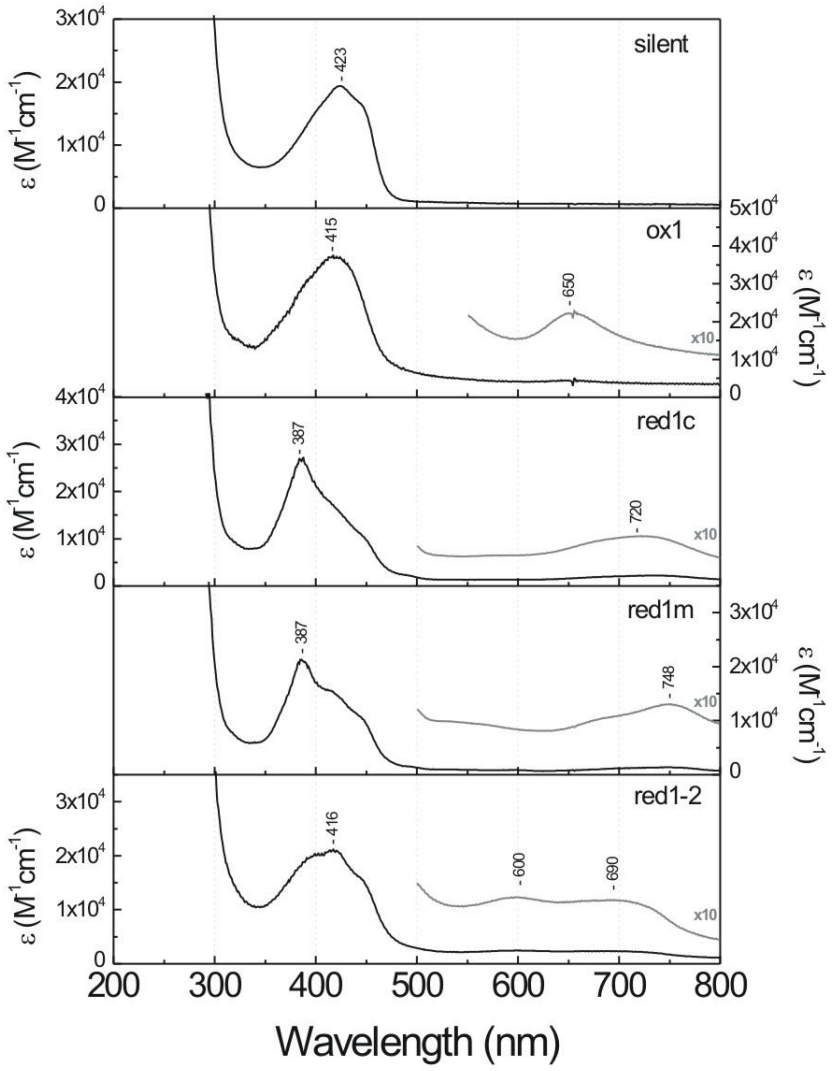

Figure 1.14 A: Uv-Vis spectra of methyl-coenzyme M reductase in different forms.

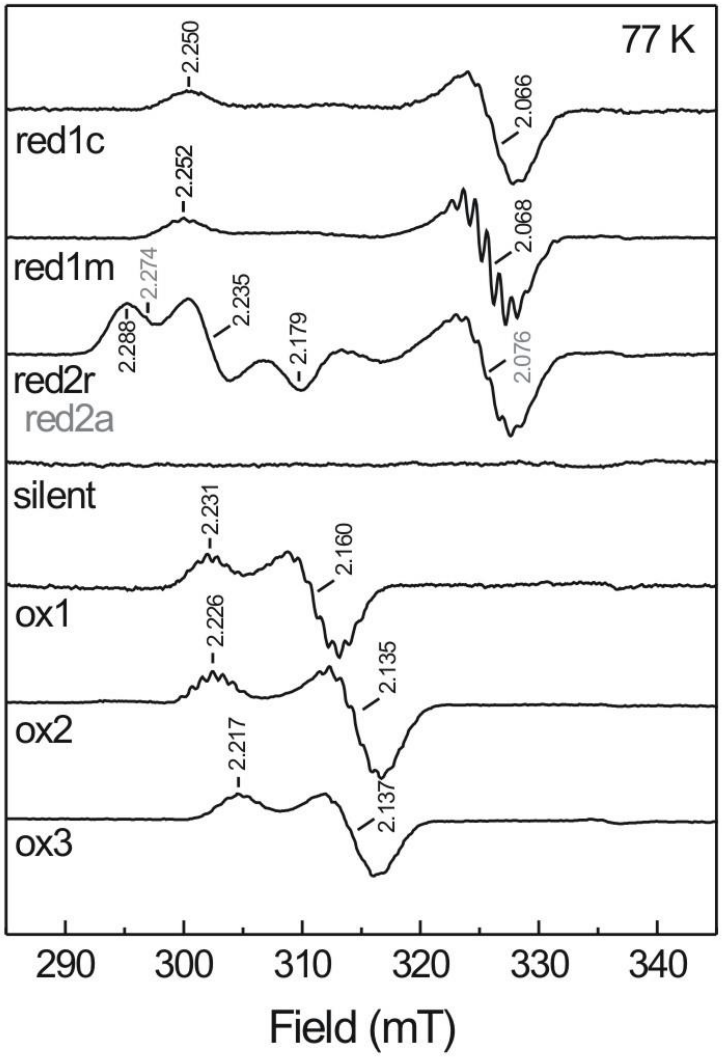

Figure 1.14 B: EPR spectra of methyl-coenzyme M reductase in different forms.

The addition of either the substrate methyl coenzyme M or coenzyme M will stabilize MCR. MCR_{red1c} is the form in the presence of coenzyme M. MCR_{red1m} is the form in the presence of methyl coenzyme M. The MCR_{red1m} EPR spectrum shows a more resolved hyperfine-splitting pattern due to the four nitrogen ligand from F_{430} to the nickel. Electron nuclear double resonance (ENDOR) measurements with labeled methyl-coenzyme M showed that in this from there is a weak interaction between the Ni(I) center and the thioether sulfur atom of methyl-coenzyme M, which is at a Ni-S distance of 3.94 Å. Removal of methyl coenzyme M and/or coenzyme M results in the very unstable MCR_{red1a} form ("a" for absence). **Fig. 1.15** depicts the in vitro interconversion of different forms of MCR. MCR_{red1c} can be converted into MCR_{red2} by the addition of coenzyme B (78). Two forms are induced, MCR_{red2a} ("a" for axial) and MCR_{red2r} ("r" for rhombic) based on their differences in EPR signals (79,80).

MCR_{red2} can be converted into several oxidized forms: Adding of polysulfide will convert it into MCR_{ox1}, addition of sulfite will convert it into the MCR_{ox2} form, and exposure to oxygen will convert it into MCR_{ox3} (81). Both MCR_{ox1} and MCR_{ox3} can be converted back into the active MCR_{red1m} form upon incubation with the reductant Ti(III) citrate. Three of the MCR forms, MCR_{red2}, MCR_{ox2}, and MCR_{ox3} are light sensitive (78) as indicated with an asterisk in **Fig. 1.15**. The first step is the rate limiting step in the reaction mechanism of MCR. Therefore, even with rapid quench/rapid detection techniques, it was not possible to detect any reaction intermediates. Instead, substrate analogs and inhibitors were used to study the MCR reaction. Three of the most commonly used inhibitors are bromopropane sulfonate (BPS), bromoethane sulfonate (BES) and bromomethane (BrMe) (27,82). All forms will eventually become EPR-silent due to inherent instability of the protein. Not all silent forms are therefore the same. Exposure to oxygen will also

turn most forms into an EPR-silent form, including the MCR_{ox} forms, although very slowly. The only exception to this is MCR_{red2}.

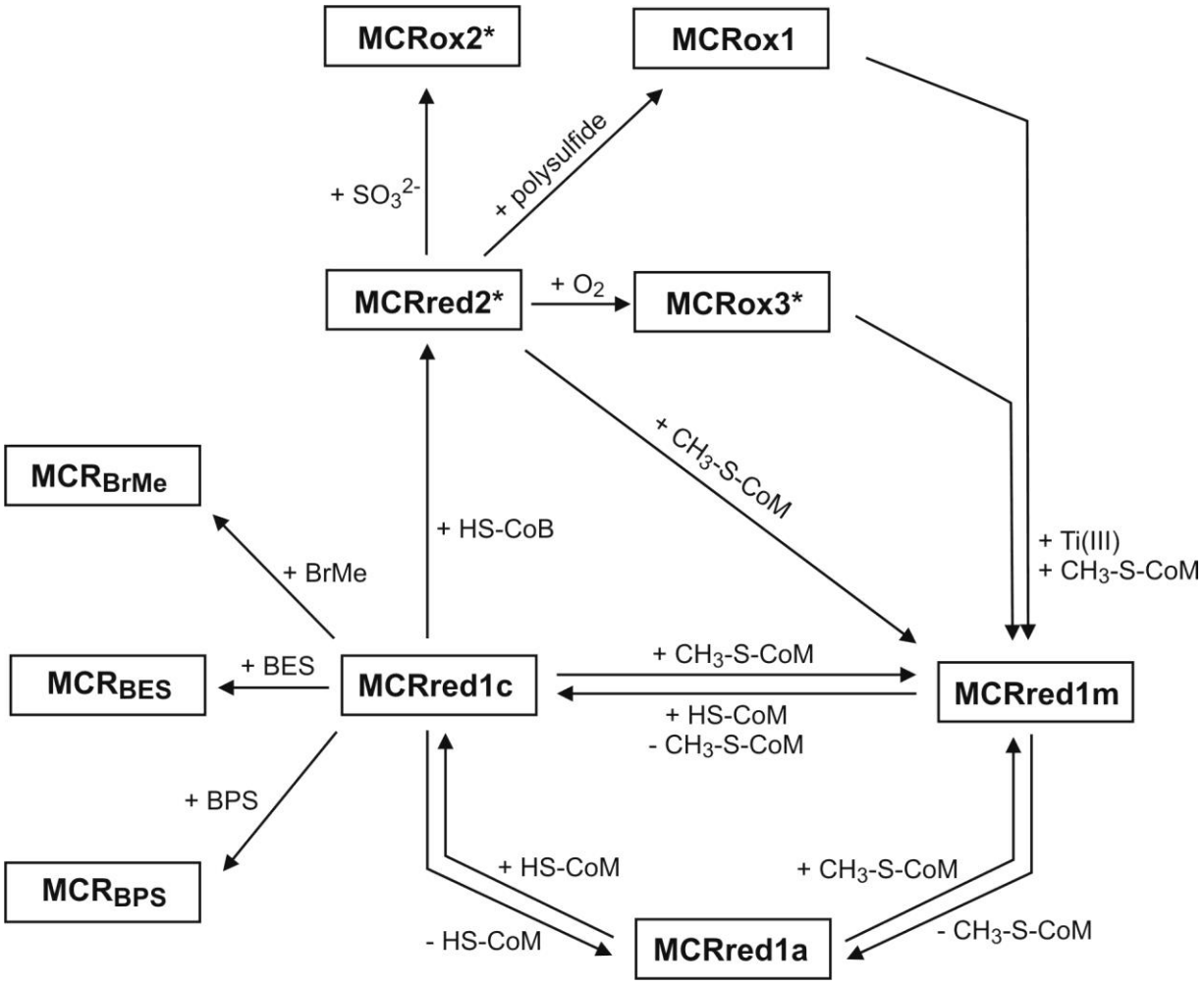

Figure 1.15 : In vitro conversion of different forms of MCR (52)

1.5 Possible mechanisms of MCR:

The reaction mechanism of MCR is not well understood because the first step is the rate limiting step when MCR_{red1} reacts with the native substrates either separately or together. Therefore most of our knowledge on the mechanism is based on crystallization and kinetic studies with substrate analogs and inhibitor compounds (57,64,65,73,83-87). The distance of Coenzyme B from Ni center in the active site channel of the $MCR_{ox1silent}$ form **(Fig. 1.16)** indicates the requirement of conformational change in the MCR for the reaction to occur. If we assume methyl-coenzyme M in the structure, this would represent a possible starting point of the catalytic cycle. However, the position of the coenzyme B thiolate is too far (8Å) from the nickel to be directly involved in the reaction. Moreover, Coenzyme B is anchored to the protein by salt bridges between the negatively charged threonine phosphate moiety and five positively charged amino acids that would also not allow the coenzyme B to move closer to the nickel ion without a conformational change in the channel. Further, conformational change in the enzyme is supported by ENDOR studies on the MCR_{red2} form. In the MCR_{red2a} form, the thiolate sulfur of coenzyme M is bound to the nickel, while in the MCR_{red2a} form, a hydride species is present. Unlike all MCR forms, in the MCR_{red2r} form the electron-nuclear spin coupling constants with the four nitrogen ligands to the nickel ion are not equal and, at least one nitrogen ligand shows a much weaker coupling constant. This indicates a change in the F_{430} electronic structure which is probably correlated to a conformational change in the ring structure. At the same time, labeling studies showed that coenzyme B moves about 2Å closer to the nickel in this form. The binding of CoB is believed to induce a conformational change in the active-site channel that allows the thiolate sulfur of coenzyme B to move within 6 Å of the nickel and concurrently pushes methyl-coenzyme M closer to the nickel. A very short lived ternary complex is formed upon binding of coenzyme B. However,

no one has been able to trap this short lived ternary complex intermediate until now. A theoretical mechanism that includes these steps was proposed by Duin and McKee (88).

Alkylation of free or enzyme bound cofactor F_{430} is possible by alkylating agents like bromopropane sulfonate (BPS) or bromomethane (BrMe). Addition of BPS to MCR_{red1} results in a new EPR signal which is due to a Ni(III) species with the propane sulfonate moiety attached to the nickel via the C3 carbon (MCR–BPS or MCR–PS). With bromomethane a relative stable Ni(III)-methyl species is induced (MCR–BrMe). When MCR-BrMe is incubated with coenzyme M, methyl-coenzyme M is formed. As a result the Ni(III)–CH_3 species has been proposed to play an important role in the reaction mechanisms for both methane production and methane oxidation. However, density function theory (DFT) calculations ruled out this possibility because the methyl-Ni(F_{430}) formation is predicted to be endothermic by 98.4 kJ/mol (89). Some inhibitors like bromoethane sulfonate (BES) also introduce radical species in MCR. The relative stability of these radical species indicates that the active-site channel provides a suitable environment for such species to survive for a longer time period suggesting that MCR could make use of a radical-based mechanism.

A distinctive approach to avoid the rate limitation of the first reaction step is to use substrate analogs that change the energy profile of the reaction and cause other steps to become rate limiting. Studies have been performed with ethyl-coenzyme M that slows down the reaction by a factor 10, and C_6-coenzyme B that slows down the reaction by a factor 100–1,000. Using this method the formation of a transient Ni-alkyl species and a transient radical species was detected when MCR_{red1} was mixed with methyl-coenzyme M and C_6-coenzyme B (84). The radical has properties indicative of a sulfur–based radical and can be allocated to either coenzyme M or coenzyme B or even the nearby thioglycine residue. Additional labeling studies are needed to distinguish between

these possibilities. Based on these studies the hypothetical mechanism in **Fig. 1.16** was proposed. In the first step (step 1), a nucleophilic attack of Ni(I) on the methyl group of methyl-SCoM takes place to form methyl-Ni(III) and $^{-}$S–CoB. This is followed by reduction of the methyl-Ni (III) species to methyl-Ni(II) (step 2) and subsequent proton transfer from the HSCoM thiol to generate methane and a CoMS radical (step 3). Equilibration between the CoMS radical and $CoBS^{-}$ generates a CoBS thiyl radical (step 4), and condensation of the CoBS radical with the thiolate of-SCoM forms a disulfide anion-radical intermediate (step 5). Electron transfer from the disulfide anion radical to Ni(II) completes the catalytic cycle by regenerating active Ni(I)-MCR_{red1} (step 6). This step would not work in reverse direction because we recently found that addition of HDS to red1 gives MCR_{ox1} (47). To date, no radical species have been determined.

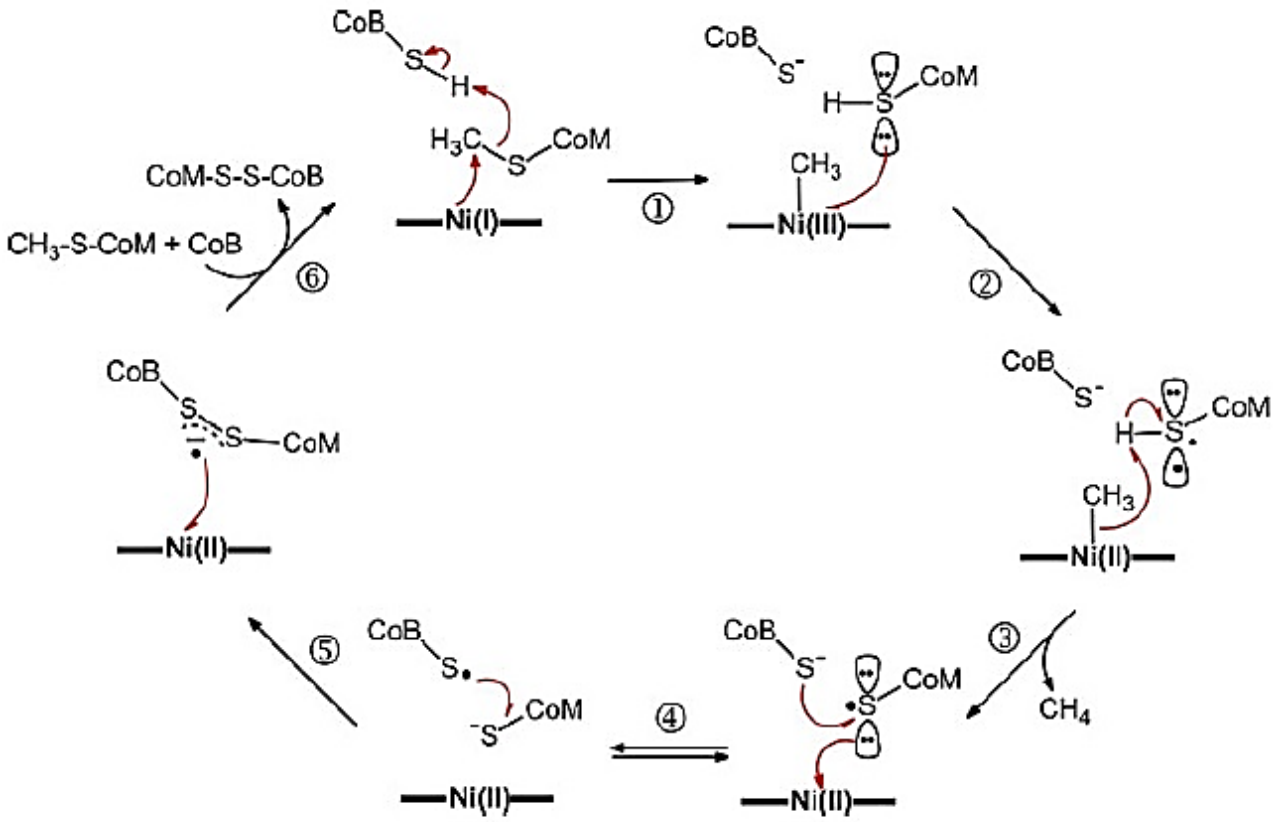

Figure 1.16: Hypothetical reaction mechanism I (with permission (84))

However, in addition to the theoretical objections to a Ni(III)–CH_3 species (89), a radical based mechanism is unable to explain the reversibility of the reaction as recently revealed for MCR (11,90). Also, based on the reverse reaction of methane into methyl-coenzyme M and ethane into ethyl-coenzyme M (11,90), an alternative mechanism was proposed based upon kinetic isotopic effects. **Fig. 1.17** displays the mechanism for the ethyl-coenzyme M/ethane exchange reaction. In this model, the conformational change in the F_{430} ring is proposed to open up the possibility to form both a hydride-nickel species like MCR_{red2a} and an S-alkane-nickel complex.

Although, we have a better understanding about the role and the reaction mechanism of this enzyme, an essential piece of the puzzle is still missing, as indicated by the question mark in **Fig. 1.17**. A strategy to solve this would be to crystalize the MCR_{red2a} form of the enzyme because this would allow detection of all of the conformational changes induced by the binding of coenzyme B.

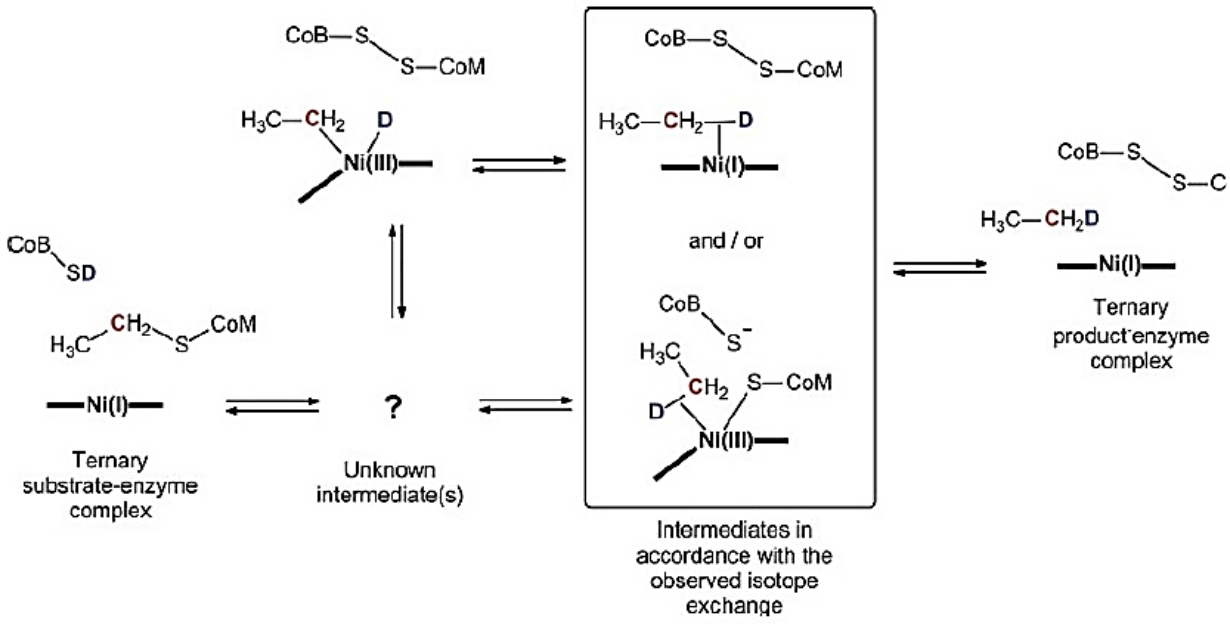

Figure 1.17: Hypothetical reaction mechanism II(with permission (90)

Chapter Two: Isolation and characterization of protein components required for activation of methyl-coenzyme M reductase

2.1 INTRODUCTION:

The highest heat of combustion per mass unit (55.7 kJ/g) among all the hydrocarbons makes methane an important source of clean renewable energy (91). At the same time it is also a potent greenhouse gas with surplus methane production in the geological cycle leading to a slow increase in atmospheric methane concentrations. Understanding the mechanism of methane formation and activation is important for controlling methane emission and improvement of the production of alternative fuels in the form of natural gas. MCR is the central enzyme in biological methane formation by methanogenic archaea and consumption by anaerobic methanotrophs (12,92,93). For the methane production, it catalyzes the exergonic conversion of methyl coenzyme M (CH_3-S-CoM) and coenzyme B (HS-CoB) into methane and the heterodisulfide of coenzyme B and coenzyme M (CoB-S-S-CoM; HDS):

$$CH_3\text{-S-CoM} + \text{H-S-CoB} \rightleftarrows CH_4 + \text{CoM-S-S-CoB}, \qquad \Delta G^{\circ\prime} = -30\ \text{kJ}\cdot\text{mol}^{-1}$$

MCR is composed of three different subunits, α, β and γ, forming an $(\alpha\beta\gamma)_2$ heterohexamer (64). Each molecule of MCR contains two molecules of the cofactor F_{430}, a Ni-porphinoid, as prosthetic group (66-68). The binding sites of two coenzymes F_{430} are roughly 50 Å apart and form two separated structurally identical active sites. The active site region of MCR contains five post-translationally modified (PTM) amino acids (64,70) comprising 1-N-methyl-Hisα^{257}, S-methyl-Cysα^{452}, 5-methyl-Argα^{71} and 2-methyl-Glnα^{400} and thio-Glyα^{445}. The role of these modifications

is not known. In addition, MCR has been subjected to numerous spectroscopic and crystallographic studies. Despite this the details of the catalytic mechanism are still not clear (33,94-96).

It is well established that the MCR_{red1}-Ni(I) form is active while the other two major forms MCR_{ox1}-Ni(III) and MCR_{silent}-Ni(II), that can be detected in purified enzyme and whole cells, are inactive (52,60-63). The MCR_{red1} form can be obtained by incubating *Methanothermobacter marburgensis* cells either with H_2 or CO (60,97). However, it is extremely O_2 sensitive due to the low mid-point potential of the Ni(II)/Ni(I) couple in F_{430} which is estimated to be around -650 mv (vs. hydrogen electrode, pH 7) (98). Moreover, the MCR_{ox1} form can be converted to the MCR_{red1} form by incubating it with the reductant Ti(III) citrate (62). In order to study the reaction mechanism or to explore the role of the PTMs, it is important to develop a cell free system capable of activating inactive MCR. No cell free system has been reported to date that can fully convert MCR_{silent} to MCR_{red1}. Theoretically, the reduction of the Ni center in MCR should be possible with electrons having a potential lower than the mid-point potential of the Ni(II)/Ni(I) couple. It was postulated that activation of MCR could work similar to the Nitrogenase system. The nitrogenase enzyme is composed of two distinct components: the Fe Protein and the MoFe protein. The Fe protein is a homodimer of γ-subunits containing two MgATP binding sites and a single 4Fe-4S cluster. The nucleotide binding sites are about 20Å away from the edge of the 4Fe-4S cluster (99). It implies that ATP hydrolysis and electron transfer are not directly coupled but are mediated by allosteric effects. When MgATP binds to the Fe protein, the resulting conformational change allows the Fe Protein to form a complex with the MoFe protein. The complex formation causes a further substantial decrease in the reduction potential of the Fe proteins cluster allowing electron transfer to take place. Unexpectedly it was recently proven that the electron transfer from the Fe protein to the MoFe protein occurs before ATP hydrolysis on the Fe protein (100).

In a similar process to nitrogenase, it was shown that MCR can be partially activated in the presence of A2, an ATP binding protein, and semi purified A3a protein that probably contains Fe-S clusters and an ATP hydrolysis site. **Fig. 2.1** depicts the postulated model to generate the low potential electron to reduce the Ni (II) center in MCR to the Ni (I) form. In this model of activation, Component A2 donates ATP to component A3a. ATP hydrolysis occurring on A3a would change the midpoint potential of the cluster enabling it to bridge the potential gap between the cluster and the Ni center of F_{430}.

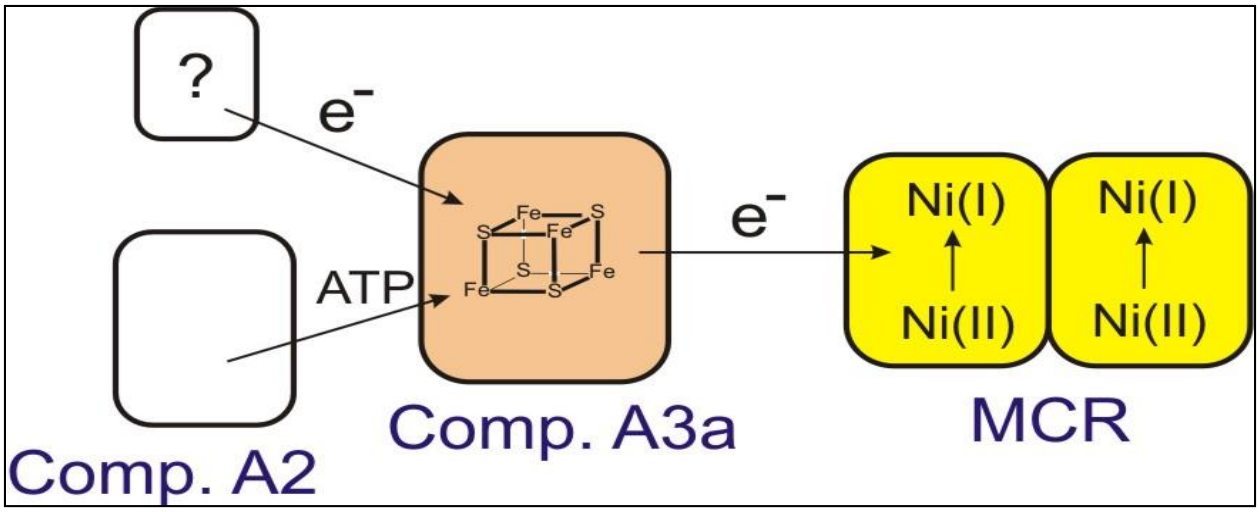

Figure 2.1: Schematic illustration of the postulated system for activation of MCR_{silent}

Very low amounts of activation were reported using cellular components purified directly from cell free extract using column chromatography (101,102). In the first fractionation step, three fractions were discovered: A, an unknown fraction; B, which turned out to be HS-CoB; and C, MCR itself. Fraction A was further fractionated and contained: A1, an F_{420}-reducing hydrogenase; A2, an ATP-binding protein; A3a, an uncharacterized iron-containing protein; and A3b, a methyl-viologen-reducing (F_{420}-non reducing) hydrogenase. The activation of MCR was measured by detecting methane formation in the head space of a closed bottle containing a solution with Ti(III) citrate, component A2, MCR, the column fraction containing A3a, ATP, CH_3-S-CoM, and HS-CoB. A maximum activity of ~0.1 μmol min^{-1} mg^{-1} was obtained (101-103).

The need to further develop this system disappeared when methods were discovered that preserve the active form of MCR during cell harvesting, preparation of cell extract and subsequent protein purification procedures (52,60-63). In this case enzyme can be obtained with a specific activity of up to 100 μmol min^{-1} mg^{-1} (62). The low activity obtained upon activation makes it clear that the activation process is not well understood. It is possible that the low amount of activation was due to the presence of traces of MCR_{ox1} that can be activated in the presence of Ti(III) citrate. It is also possible that not all essential components were present. Most importantly we desired to characterize the role of A3a. Herein, we report the complete activation of MCR_{ox1} and 65% activation of MCR_{silent} under non-turnover condition in the presence of dithiothreitol (DTT, E_m = -320 mV) with components A2 and A3a. This is the first time activation of the silent form was achieved with an electron source with a midpoint potential higher than that of the H_2/H^+ couple which is estimated to be -414 mV under growth conditions.

As shown in **Fig. 2.2**, Component A2 contains two ATP binding sites and it belongs to the ABC_ATPase superfamily. ABC transporters are a large family of proteins involved in the

transport of a wide variety of different compounds including sugars, ions, peptides, and more complex organic molecules. The nucleotide-binding domain shows the highest similarity between all members of the family. ABC transporters are a subset of nucleotide hydrolases that contain a signature motif, Q-loop, and H-loop/switch region, in addition to the Walker A motif (GxxxxGK[S/T], where x is any residue), and the Walker B motif (hhhh[D/E], where h is a hydrophobic residue motif commonly found in a number of ATP- and GTP-binding and hydrolyzing proteins. The Walker A and B motifs bind the beta-gamma phosphate moiety of the bound nucleotide (typically ATP or GTP) and the Mg^{2+} cation, respectively. Component A2 is cytosolic and facilitates transfer of electrons from A3a to Ni center in MCR. These characteristics are inconsistent with a protein belonging to the ABC transport model in that electrons have not been shown to be substrates for ABC transporters. Hence although A2 protein to the ABC transporter family, it is not expected to be a transporter. In this dissertation, we used *M. marburgensis* as the model organism that possesses two 2 proteins, A2 and A2 homolog. Pairwise sequence alignment of A2 and A2 homolog shows only 32.1% identity and 49.8% similarity. In addition to two A2 proteins, *M. marburgensis* expresses two MCRs (MCRI and MCRII) during its growth. Thus, it is possible that the two A2 proteins are required for the activation of MCR I and II, respectively. Since the MCRI is the major isoenzyme in *M. marburgensis*, we focused on the activation of this enzyme.

We found that component A3a is a multi-enzyme complex that includes the *mcrC* gene product, a Fe-protein homolog, iron-sulfur flavoprotein, and protein components involved in electron bifurcation. On the basis of these protein components a model is presented on how all the components could work together to provide the low-potential electrons needed to reduce the active-site nickel ions in MCR.

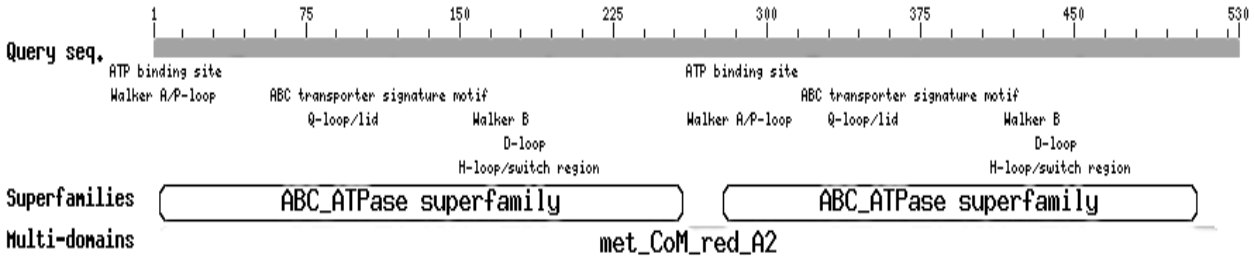

Figure 2.2: Sequence analysis of A2 Protein

2.2 Materials and Methods:

2.2.1 Reagents:

Thermostable DNA polymerase *Pfu* was purchased from Agilent Technologies (Clara, CA). The pQE-80L vector, universal T5-promoter primer, plasmid isolation kit and gel extraction kit were purchased from Qiagen (Valencia, CA). The primers were purchased from Integrated DNA Technologies (San Jose, CA) and the restriction enzymes were purchased from New England Biolabs (Ipswich, MA). 3-[(3-cholamidopropyl)-dimethyl-ammonio]-1-propanesulfonate (CHAPS) was purchased from AMRESCO (Solon, OH). Coenzyme M was from Merck. 7-Bromoheptanoic acid was from Karl Industries Inc. All other chemicals were from either Fisher Biotech (Pittsburg, PA) or Sigma-Aldrich (St. Louis, MO) and were purchased with the appropriate purity needed for the experiments. Diethyl amino ethyl (DEAE) sepharose, Q-sepharose, S-300 Sephacryl, Phenol Sepharose and PD-10 columns were purchased from GE Healthcare. Centricon ultrafiltration units were from Millipore (Bedford, MA).

Anaerobic buffers were used for all purifications and experiments. The buffers were filtered (0.22 μm), boiled under constant flow of nitrogen gas and stirred under vacuum for a period of 2-4 h. The buffers could then be used or stored under argon with 0.3-0.5 atmospheric overpressure applied to the head space of the bottle.

A 200 mM Ti(III) citrate solution was prepared by dissolving Ti(III) chloride powder in 250 mM sodium citrate under strictly anoxic conditions (104). After stirring at RT for 20 min the solution was neutralized by slow addition of solid $KHCO_3$ until gas formation stopped and a pH of 6-7 was reached.

2.2.2 Synthesis of 2-Methylthioethane Sulfonate (Methyl-coenzyme M):

Methyl-coenzyme M was synthesized from coenzyme M (2-mercaptoethanesulfonate) by methylation with methyl iodide as described in the literature (105). Coenzyme M (3 mmol) was incubated for 12h with 6 mmol of methyliodide in 5 ml of a 33% aqueous ammonia solution under a 100% N_2 atmosphere. After incubation for 12h at room temperature the reaction mixture was evaporated to almost dryness and lyophilized. The dry yellow residue was dissolved in 10 ml distilled water. Aliquots of the solution of 5-ml were loaded on a Q-Sepharose column (volume 30 ml) and a linear gradient of 0 to 1 M ammonium carbonate was applied for elution. Ammonium carbonate was used instead of hydrochloric acid to elute methyl-coenzyme M from the Q-Sepharose column since methyl-coenzyme M in the non-dissociated sulfonic acid form and water produce an azeotropic mixture. Methyl-coenzyme M generally eluted from the column between 250-350 mM ammonium carbonate. Fractions containing methyl-coenzyme M were combined and lyophilized to remove the ammonium carbonate. Subsequently, the lyophilized powder was heated to 60°C to remove remaining traces of iodine. Eluate was collected and tested for methyl-coenzyme M by thin layer chromatography (TLC) on Kieselgel 60 F_{254} with butanol/acetic acid/water (2:1:1) as the mobile phase. TLC plate was further develop with 1% $KMnO_4$ and Na_2CO_3. In the presence of developer, the whole plate turned purple with yellow band indicating the position of methyl-coenzyme M. Generally 1.5 g of a dry white powder was obtained at the end of the procedure.

2.2.3 Synthesis of [(+)-(2S,3R)-N-[7-Mercaptoheptanoyl]-O-phospho-L-threonine (Coenzyme B):

Coenzyme B was synthesized by the following steps (106):

7, 7'-Dithioheptanoic acid:

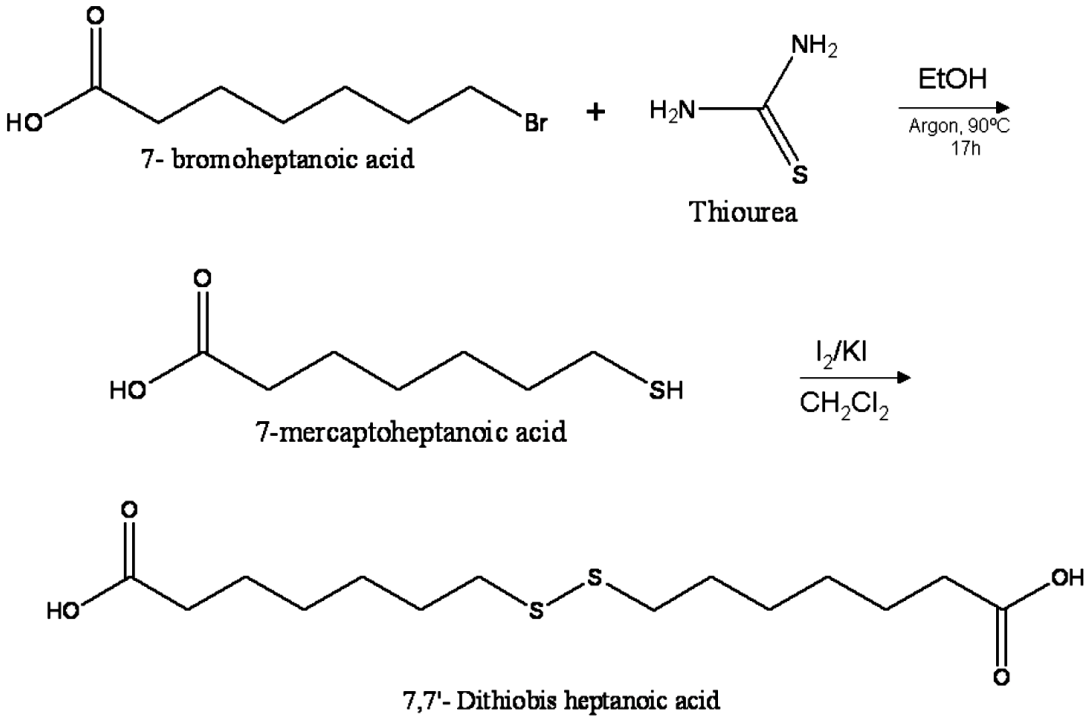

7-Mercaptoheptanoic acid was synthesized by dissolving 17.4 g (228 mmol) of thiourea in a stirred solution of 7-bromoheptanoic acid (9.6 g, 46.6 mmol) in 110 ml of ethanol. This mixture was refluxed under argon at 90°C for 17 h, cooled to room temperature, and 25 ml of a 60% aqueous solution (w/v) of sodium hydroxide was added. The mixture was refluxed under argon for an additional 2 hours and cooled to room temperature. The yellow/white solution was concentrated. A 100 ml aqueous solution of 1M HCl was added followed by 20 ml concentrated HCl. The thiol was extracted 3 times with 100 ml dichloromethane. The dichloromethane phase

was extracted 3 times with 150 ml of an aqueous solution of 1M sodium bicarbonate. The aqueous extract was acidified with HCl to a pH of 1-2, and extracted 3 times with 200 ml dichloromethane. The organic phase was filtered over cotton and concentrated to 70 ml. The thiol was oxidized to a disulfide by mixing the dichloromethane phase with an aqueous solution of 10% (w/v) iodine and 20% (w/v) potassium iodide until the brown color persisted. The aqueous phase was removed and the dichloromethane phase was washed 3 times each with an aqueous solution of 1M sodium thiosulfate and water. The organic phase was filtered over cotton, dried over anhydrous magnesium sulfate, and concentrated under vacuum. The product was crystallized twice from benzene (or toluene) and dried for two days under high-vacuum to yield 3.3 g (46%) of white crystals. Mp is 70ºC.

7, 7'-Dithiobis (succinimido-oxyheptanoate):

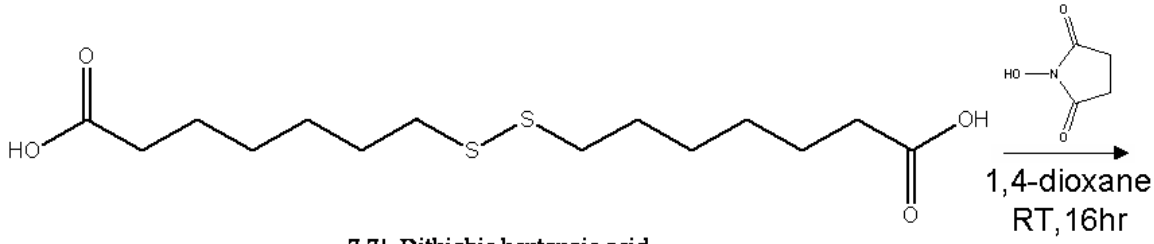

7,7'- Dithiobis heptanoic acid

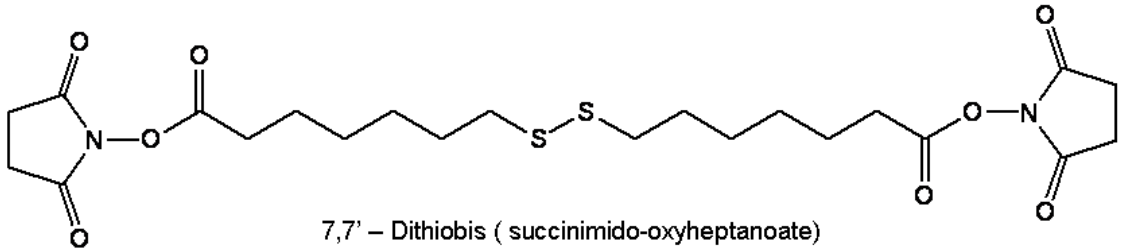

7,7' – Dithiobis (succinimido-oxyheptanoate)

7,7'-Dithiodiheptanoic acid (388 mg, 1.2 mmol) was dissolved in 8 ml of 1,4-dioxane at room temperature. Subsequently, 290 mg (2.5 mmol) of N-hydroxysuccinimide was added under stirring. A solution of 505 mg (2.4 mmol) dicyclohexylcarbodiimide in 3 ml 1,4-dioxane was added drop-wise and the resulting solution was stirred for 16 h at room temperature. The

precipitated dicyclohexylurea was removed by filtration over a glass filter and the filtrate was washed 2 times with 5 ml 1,4-dioxane, and dried (to a clear oil) under vacuum. The product was recrystallized twice from boiling 2-propanol, and dried for 1 day under high vacuum to give 384 mg (62%) of white crystals. Mp is 105-106ºC.

(+)-N,N'-(7,7'-Dithio-diheptanyl) bis (O-phospho-L-threonine) :

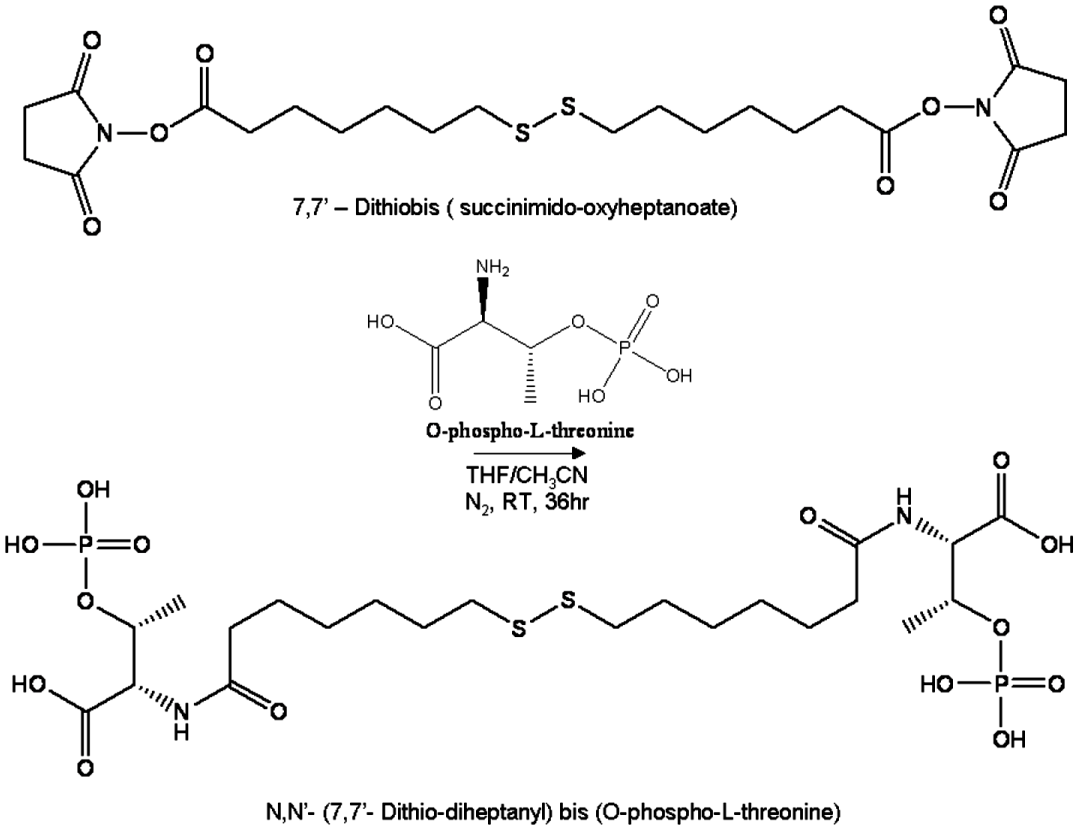

A solution of O-phospho-L-threonine (400 mg, 2 mmol) and triethylamine (0.56 ml, 4 mmol) in 4 ml water was added under stirring to a solution of 7,7'-dithiobis(succinimido-oxyheptanoate) (362 mg, 0.7 mmol l) in 18 ml tetrahydrofuran and 4 ml acetonitrile. After stirring at room temperature under argon for 36 h, the solvents were removed under vacuum at 30°C. The resulting white residue was dissolved in 1M HCl (25 ml) and washed three times with dichloromethane (3 × 8 ml). Traces of dichloromethane were removed from the aqueous phase

under vacuum. The aqueous phase was applied to a 2 × 13 cm column of polystyrene XAD-2, (Serva Serdolit Pad II) column equilibrated with 1M HCI. The column was washed with 100 ml of 1M HCI, followed by 150 ml H_2O. The product was eluted with a methanol gradient (80 ml H_2O/MeOH, 4:1; 120 ml H_2O/MeOH, 1:1; 80 ml H_2O/MeOH, 1:4, 100 ml MeOH). TLC analysis (solvent system: n-butanol/acetic acid/H2O, 2:1:1) of the collected fractions (10 ml each) showed that CoB-S-S-CoB (Rf = 0.35) had been completely separated from O-phosphothreonine (Rf = 0.24) and less polar products (Rf > 0.6). The combined fractions containing pure CoB-S-S-CoB were concentrated under vacuum (50°C) to 1/10 of the original volume, 2 ml 2 M ammonia was added to obtain the ammonium salt. After lyophilization, 112 mg (20%) (+)-N,N'-(7,7'-dithiodiheptanoyl)bis(O-phospho-L-threonine) of a white solid was obtained. Mp is 105-106ºC.

(+)-(2S,3R)-N-[7-Mercaptoheptanoyl]-O-phospho-L-threonine :

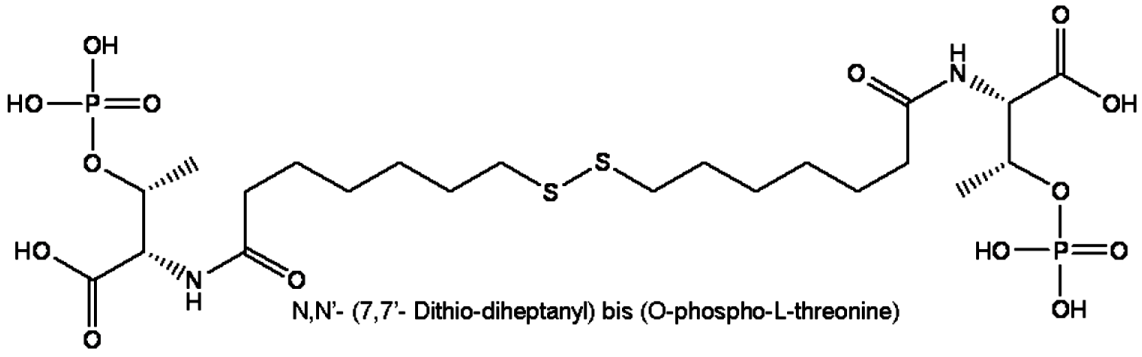

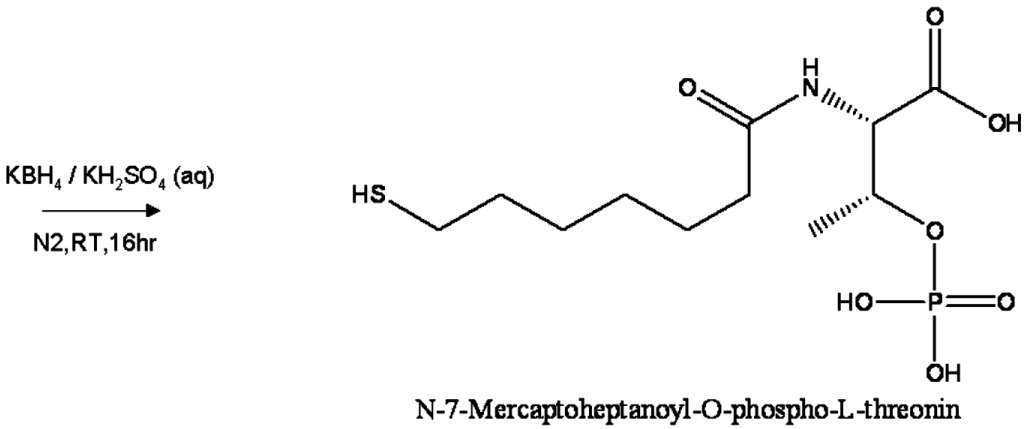

25 mg (32 μmol) CoB-S-S-CoB (Ammonium salt) was dissolved in 0.5 ml anoxic 50 mM potassium phosphate buffer, pH 7.0, under a nitrogen atmosphere. Subsequently, 2 ml of an anoxic KBH_4-solution (10% in 50 mM potassium phosphate buffer, pH 7.0) was added and the solution was stirred for 16 h under nitrogen atmosphere at RT. Excess KBH_4 was removed by addition of 0.5 ml 25% HCl (aq) and the acid solution (pH 0) was loaded on a Amberlite XAD-2 column (1 cm x 10 cm) equilibrated with anoxic 1 M HCl (aq). The column was washed with anoxic water and the HS-CoB was eluted with anoxic water/methanol (70:30; v/v). The collected HS-CoB fractions were lyophilized, and the powder was dissolved in anoxic 50 mM Tris/HCl buffer (pH 7,6). The pH was adjusted to 7.0 with a 2 M NaOH solution. The HS-CoB concentration was determined indirectly by determining the thiol concentration with Ellman's Reagent (5,5'-dithiobis-(2-nitrobenzoic acid) and ^{1}H-NMR. Approximately, 17 mg (70% yield) of coenzyme B was obtained.

Ellman's reagent or DTNB is an important reagent for quantization of thiols (107,108). In the disulfide exchange reaction one half of the DTNB molecule, 5-mercapto-2-nitrobenzoic acid, is released as a bright yellow-colored chromophore (absorption maximum 410 nm, ε = 13,600 $cm^{-1}M^{-1}$ (107,109).

^{1}H-NMR (600 MHz, D_2O, dioxane = 3.700 ppm): 4.65 (*dqd*, *J* = 7.50, 6.48, 3.54, 1 H, C***H***OPO_3 2-); 4.21 (*dd*, *J* = 3.42, 1.92, 1 H, C***H***NC=O); 2.49 (*t*, *J* = 7.17, 2 H, C***H₂***S); 2.34 (*dt*, *J* = 14.16, 7.65, 1 H, C***H₂***C=O); 2.29 (*dt*, *J* = 14.16, 7.35, 1 H, C***H₂***C=O); 1.58 (*quint*, *J* = 7.47, 2 H, CH_2); 1.55 (*quint*, *J* = 7.38, 2 H, CH_2); 1.35 (*quintetoid*, *Jobs* = 7.5, 2 H, CH_2); 1.29 (*quartetoid*, *Jobs* = 7.0, 2 H, CH_2); 1.25 (*d*, *J* = 6.42, 3 H, C***H₃***).

2.2.4 Synthesis of Heterodisulfide (CoM-S-S-CoB; HDS):

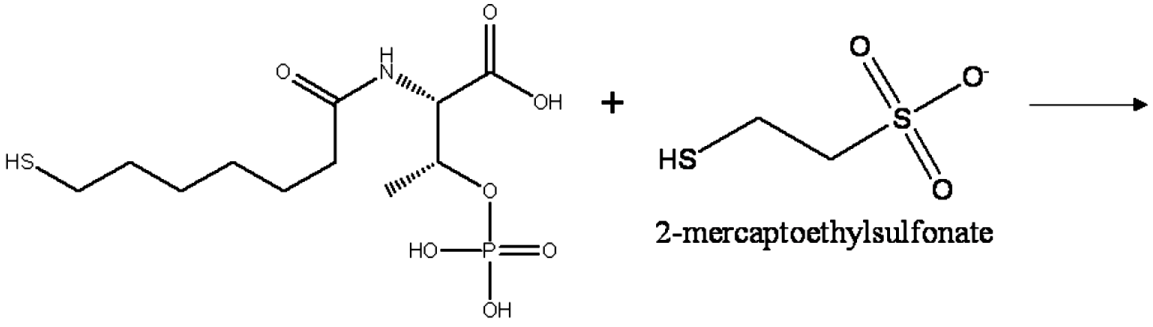

N-7-Mercaptoheptanoyl-O-phospho-L-threonin

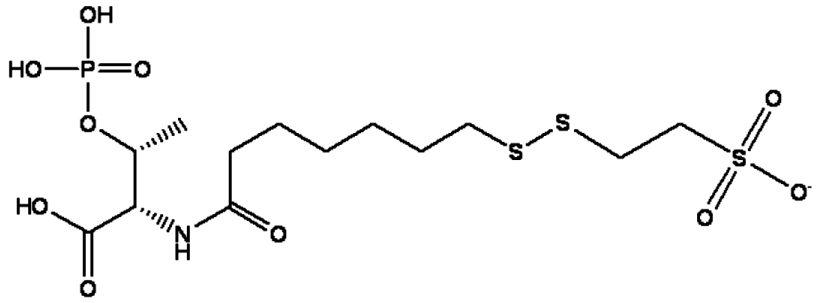

73 mg of Coenzyme B disulfide tetraammonium salt and 330 mg of coenzyme M sodium salt (330 mg, 2.0 mmol) were dissolved in water (5 ml) and NH_3 (conc., 0.50 ml). After stirring for one hour KI_3 (0.5 M in water) was added drop wise until the brown color faded away slowly. The solution was acidified with HCl (20%) to pH = 0 and loaded on an XAD-2 column conditioned as described for the purification of coenzyme B disulfide but equilibrated in 20% HCl overnight. The column was washed with HCl (aq., 1 M, 0.5 M, 0.2 M, 0.1 M and finally 0.025 M) until all coenzyme M homodisulfide had eluted (UV: λmax ca. 240 nm). The product was eluted with water followed by methanol in water (10%, 25% and 50%). The product containing fractions (UV: λmax = 245 nm) were checked for purity (^{1}H-NMR), combined, and the pH adjusted to 5. Fractions containing HDS were lyophilized (80 mg, 80%).

2.2.5 Cloning of component A2 (AtwA):

The gene coding for AtwA was generated by amplifying the *atwA* gene directly from lysed *M. marburgensis* cells by PCR using the forward primer CATGGATCCATGTCT TTCATAAAGCTGGAAAACG containing a *Bam*HI (underlined) site and the reverse primer CATAAGCTTGGTTAT TCCCTGAGCATCCCCC containing a *Hin*dIII (underlined) site with the high fidelity thermostable DNA polymerase *Pfu*. The primers were purchased from Integrated DNA Technologies (San Jose, CA) and the restriction enzymes were purchased from New England Biolabs. The resulting PCR product was digested with *Bam*HI and *Hin*dIII and ligated into a *Bam*HI-*Hin*dIII-digested pQE-80L vector. The ligation mix was electroporated into *Escherichia coli* strain DH10B and recombinant plasmid was selected. The integrity of the recombinant plasmid was confirmed by restriction endonuclease digestions and sequencing of the *atwA* insert with a universal T5-promoter primer. Expression of the cloned fragment produces a protein that is tagged at the N-terminus with six histidine residues.

2.2.6 Expression and purification of component A2 (AtwA):

E. coli DH10B cells harboring a pQE-80L-*atwA* plasmid were grown in the LB medium supplemented with Ampicillin (100 µg/ml) at 37°C with shaking (at 250 rpm) to an A_{600} of 0.5. Then isopropyl-β-D-thiogalactopyranoside (IPTG) was added to a final concentration of 1 mM to induce expression of the cloned gene from the T5 promoter. The cells were incubated for a further 5 hours before being lysed to purify recombinant A2. The A2 protein was purified by immobilized metal affinity chromatography using a 5 ml Ni-Sepharose column (GE Healthcare) connected to an Äkta fast protein liquid chromatography (FPLC) system. The cell pellet from a 1 L *E. coli* DH10B culture harboring the pQE-80L-*atwA* plasmid was resuspended in 80 ml 50 mM Tris-HCl

buffer, pH 8, with 100 mM NaCl (buffer A). Cells were lysed by sonication followed by centrifugation at 20,000 g x 30 min at 4°C to collect cell free extract (CFE). The supernatant containing the A2 protein was filtered using a 0.22 μm filter and loaded on the Ni-Sepharose column. The protein was then eluted using a linear imidazole gradient from 0% to 100% buffer B containing 50 mM Tris HCl, pH 8, 100 mM NaCl, and 500 mM imidazole. The fractions containing the pure A2 protein were pooled. Imidazole was removed by repeated concentration and dilution steps (3x) with buffer A using a Centricon centrifugal filter unit (Millipore) with a cutoff of 10 kDa. The protein concentration was determined by the Bradford assay and the purity was determined by SDS-PAGE and sequencing.

2.2.7 Purification of the A3a protein:

Purification was performed under strictly anoxic conditions at 4°C except for the chromatographic steps which were performed at room temperature. Cell extracts were routinely prepared from ~60 g (wet mass) of *M. marburgensis* cells that had been freshly harvested under anoxic conditions without special pretreatment of the cell culture. The cells were suspended in ~80 mL 50 mM TrisHCl, pH 7.6 (buffer A). Cells were lysed by sonication followed by centrifugation at 35,000 g x 30 min to collect CFE. The supernatant was concentrated to 10 ml with an Amicon ultrafiltration unit with a 100 kD cut-off filter and loaded on a Sephacryl S-300 column equilibrated with buffer A containing 0.1 mM NaCl (buffer B). The protein was eluted with buffer B. The activation of MCR was only observed with the dark brown colored high molecular weight pool. These fractions where pooled and applied to a Phenyl-Sepharose column, followed by elution with a decreasing step gradient of 1.0 mM, 0.8 mM, 0.6 mM, and 0.5 mM NaCl in Buffer A. A3a activity was observed in the peak eluted with 0.8 mM NaCl. The fractions

with A3a activity were combined, concentrated, and applied to a MonoQ column followed by elution with an increasing salt gradient from 0 to 1 M NaCl in Buffer A. The A3a activity was observed in fractions eluted between 0.50-0.55 M NaCl. MonoQ fractions with A3a activity were further purified by using a Superdex 200 column equilibrated with buffer B. The A3a protein comes down as a single isolated peak from the Superdex 200 column. The concentration of the A3a protein in the different experiments is expressed in g/l since an exact molecular weight was not obtained for the multi-protein complex.

2.2.8 Purification of MC_{Rred1}, MCR_{OX1} and MCR_{silent} forms:

The protein from *M. marburgensis* was purified as described (52). *M. marburgensis* cells were grown at 65°C in a 13 L glass fermenter (New Brunswick) containing 10 L of growth medium. The growth medium (52,110) contained 65 mM KH_2PO_4, 50 mM NH_4Cl, 30 mM Na_2CO_3, trace elements (0.5 mM nitrilotriacetic acid, 2 mM $MgCl_2$, 50 μM $FeCl_2$, 1 μM $CoCl_2$, 1 μM Na_2MoO_4, 5 μM $NiCl_2$) and 20 μM resazurin. For growth, the cell culture had to be gassed with the 80% H_2/20% CO_2 mixture with ~1% of H_2S. The resazurin was added to the medium to indicate when sufficient anoxic conditions were reached. After 2 h of equilibration, the medium was inoculated with 200-300 ml of fresh cell culture. In the beginning, the cells grew exponentially with approximate doubling time of 2h. After 15h of growth, cell density reached OD_{578} nm of ~6. Cells were harvested after 15h.

To get MCR in the MCR_{silent} state no special treatment before harvesting was necessary. In order to induce the red1 form, the gas was switched to pure hydrogen while for the MCR_{ox1} form the gas supply was switched to 80% N_2/20% CO_2 for 20 min before harvesting. The cell culture was cooled down over a 10 min period to 10°C under continuous gas flow and the cells were

subsequently harvested anoxically by centrifugation using a flow-through centrifuge (Hettich, contifuge 17 RS). Approximately 60 g of wet cells were usually obtained using this procedure. All the following steps were performed in an anaerobic chamber (Coy Instruments) filled with 95% N_2/5% H_2.

After the cells were collected by centrifugation, the rotor was brought into the anaerobic chamber. The cell pellet was resuspended in 50 ml 10 mM Tris-HCl buffer, pH 7.6, and sonicated 3 times for 7 min each at 80% power on ice, followed by ultra-centrifugation at 350,000 x *g* for 20 min at 4°C. For the ox1 purification, cell pellet was dissolved in 150 mM KPP buffer (22.550 g K_2P, 2.794 g KH_2). To stabilize the red1 and ox1 signal, all of the purification buffers contained 10 mM CoM or 10 mM MCoM, respectively. The supernatant was subjected to a 70% ammonium sulfate precipitation step by addition of the appropriate amount of a saturated ammonium sulfate solution. MCR stays in solution under these conditions. Precipitated protein was removed by ultra-centrifugation at 350,000 x *g* for 20 min at 4°C. The supernatant was subsequently subjected to a 100% ammonium sulfate precipitation step by addition of the appropriate amount of solid ammonium sulfate. The 100% precipitation step separates MCR from small cofactors present in the cell extract of methanogens. After the 100% precipitation step, the protein pellet was resuspended in 100 ml 10 mM Tris-HCl pH 7.6 and subsequently loaded on a Q-Sepharose column equilibrated with 50 mM Tris-HCl pH 7.6. The column was developed with a step gradient using the same buffer containing 2 M NaCl. MCR eluted at about 0.52 M NaCl. The protein concentration was determined with the Bradford assay (111) with bovine serum albumin (Serva) as a standard or by measuring the absorbance of oxidized enzyme (MCRsilent) at 420 nm using ε = 44,000 M^{-1} cm^{-1} for a molecular mass of 280 KD. The method generally yielded approximately 150 mg of protein.

2.2.9 Determination of methyl-coenzyme-M reductase activity:

Activity of MCR was determined as described (62). Methane formation was detected by withdrawing a gas sample from the headspace of a closed off bottle containing 400 µl assay solution. The solution contained 500 mM Mops/NaOH, pH 7.2, 10 mM methyl-coenzyme M, 1 mM coenzyme B, 0.3 mM aquocobalamin, 30 mM Ti(III) citrate, and purified enzymatic components. Samples were kept on ice. The assay was started by increasing the temperature to 65°C. The assays in Table 2 contained 11.2 µg MCR (0.1 µM), and when indicated 0.48 µg A2 (0.02 µM), and 2.08 µg A3a.

2.2.10 Activation of methyl-coenzyme-M reductase:

100 µM MCR was incubated for 15 min and 60 min at 60°C in the presence of 20 µM component A2, 5.2 mg/ml component A3a, 10 mM MgATP, 5 mM dithiothreitol and 10 mM methyl-coenzyme.

2.2.11 Mass Spectrometry:

For protein identification, in-gel tryptic digestion was performed according to the literature (112). Digested peptides were analyzed using an Acquity UPLC system coupled to a quadrupole-time-of-flight mass spectrometer (Q-Tof premier, Waters) using electrospray ionization (ESI) in the positive ion mode operated by Masslynx software (V4.1). Digested peptides were constituted in injection solution (50% methanol and 0.1% formic acid) and eluted off a C-18 reverse phase column (ACQUITY UPLC® BEH C18, 1.7 µm, 2.1 x 50 mm, Waters) using a 2–40% acetonitrile gradient. Each peptide was registered for the retention time, intensity, m/z, and MS/MS ions. The instrument was calibrated at the time of data acquisition in addition to real time calibration by the

lockmass. Mass accuracy at 5 ppm or less was the key for assuring the presence of target molecules. Ion source parameters such as the source temperature (gas and sample cone), mobile phase flow rate, and cone voltage were optimized and fixed throughout the study.

De novo sequencing of the registered peptide ion was performed using the data dependent acquisition method (DDA, Waters). Acquired MS/MS fragmentation spectra were interpreted using Proteinlynx software (Proteinlynx Global Servers 2.1, Waters). Protein databases searched were SwissProt, None-Redundant (NCBI), and Marburgensis UniProt, downloaded from UniProt in the FASTA format. The questionable sequence call was checked occasionally using Biolynx software (Waters).

2.2.12 EPR Spectroscopy:

CW EPR spectra were measured at X-band (9 GHz) frequency on a Bruker EMX spectrometer, fitted with the ER-4119-HS high sensitivity perpendicular-mode cavity. The Oxford Instrument ESR 900 flow cryostat in combination with the ITC4 temperature controller was used for measurements in the 4 K to 300 K range using a helium flow. Measurements at 77 K were performed by fitting the cavity with a liquid nitrogen finger Dewar. All spectra were recorded with a field modulation frequency of 100 kHz, modulation amplitude of 0.6 mT, and a frequency of 9.386 GHz. Sample specific conditions are indicated in the figure legends.

The EPR signal intensities were determined by measuring the respective EPR-active species under nonsaturating conditions. Since the signals represent the first derivative of the absorption-type signal, the spectra were double integrated and the surface area of each signal, corrected for the presence of two nickel sites per MCR, and compared with that of a 10 mM copper

perchlorate standard (10 mM CuSO4; 2 M $NaClO_4$; 10 mM HCl). The values obtained this way were compared to the known enzyme concentration which was set to 100%. When more than one signal was present, each signal was simulated, the compound spectrum was reproduced, and the double integration value of each individual component was obtained. The BioEPR package developed by Fred Hagen was used for spectral simulation and double integration of the signals (113). Only the intensities of the paramagnetic species (red1 and ox1) could be determined as described. The amount of the EPR-inactive form, MCR_{silent}, was assigned as the difference between the concentrations of MCR present minus the concentration of paramagnetic species.

2.3 RESULTS:

2.3.1 Synthesis of 2-Methylthioethane Sulfonate (Methyl-coenzyme M):

After separation on the Q-sepharose column, MCoM was detected by thin layer chromatography (TLC) plates Silica Gel 60 with butanol/acetic acid/water (2:1:1). TLC plates were developed with 1% $KMnO_4/Na_2CO_3$. Fractions containing MCoM were lyophilized and further analyzed by ^1H NMR (**Fig. 2.3**).The purity of MCoM was measured as compared to an internal standard, 1,4,-dioxane.

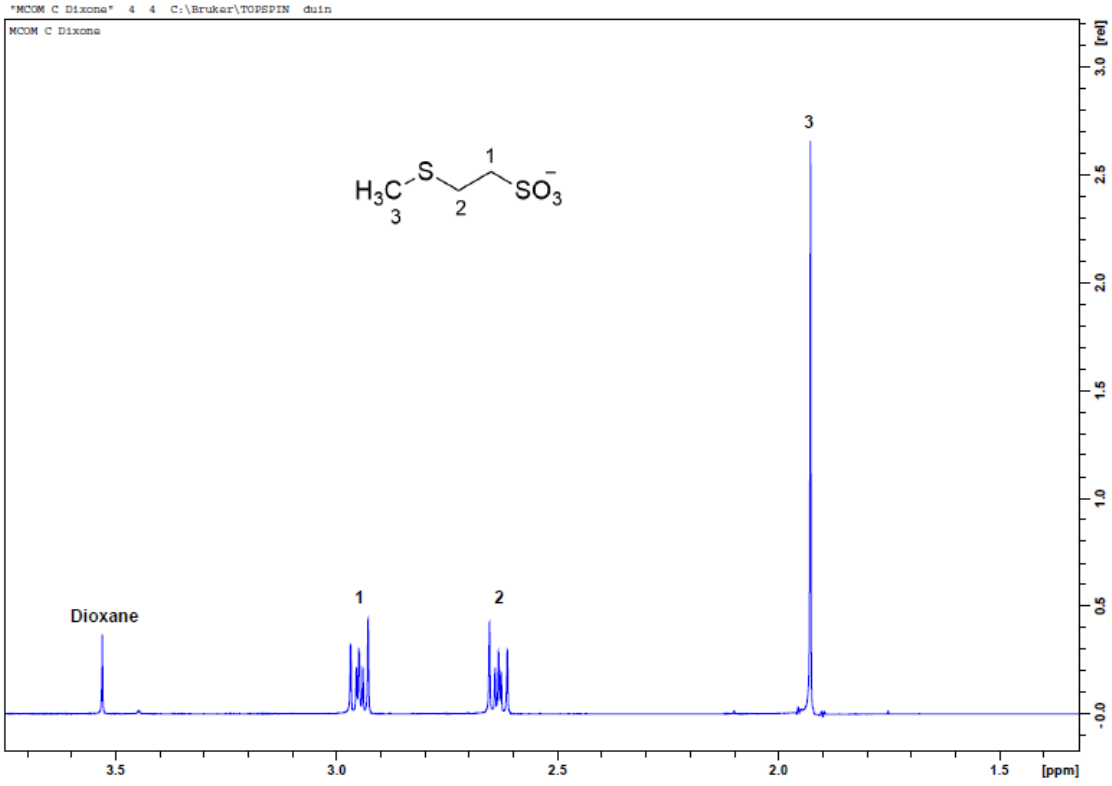

Figure 2.3: ^{1}H NMR of Methyl-coenzyme M

2.3.2. Synthesis of [(+)-(2S,3R)-N-[7-Mercaptoheptanoyl]-O-phospho-L-threonine (Coenzyme B):

After the XAD-2 column steps, fractions were tested for the presence of CoB by Ellman's reagents. Fractions containing CoB were collected and lyophilized and further analyzed by ^{1}H NMR **(Fig. 2.4)**. 1,4,-dioxane was used as internal standard to measure the percentage purity of the product.

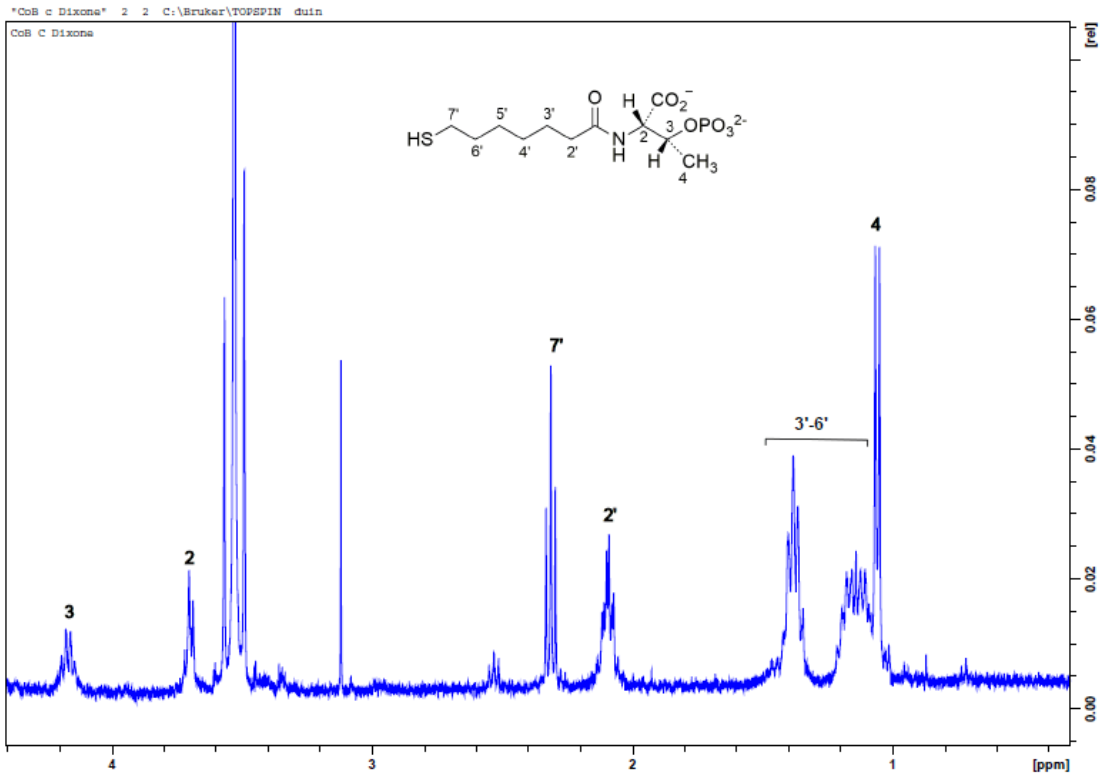

Figure 2.4: ^{1}H NMR of Coenzyme B.

2.3.3 Synthesis of Heterodisulfide of CoM-S-S-CoB:

The product containing fractions (UV: λmax = 245 nm) were collected and lyophilized. The Purity of sample was detected by ^{1}H-NMR in the presence of an internal standard **(Fig. 2.5).**

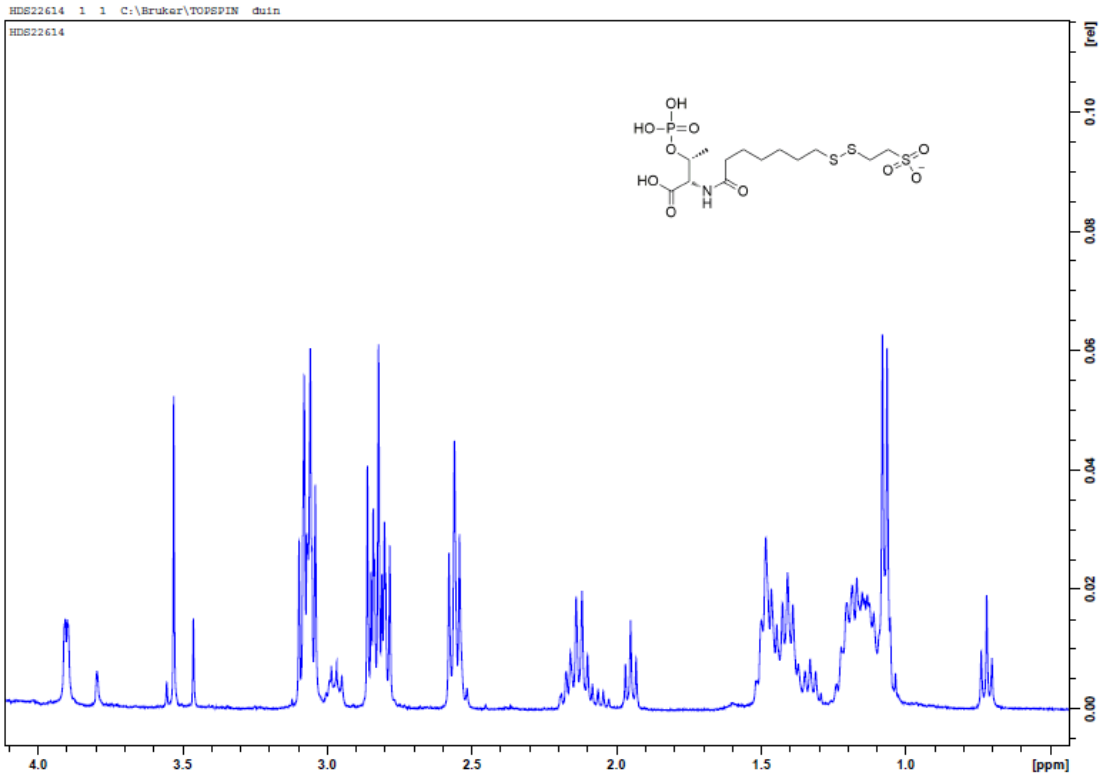

Figure 2.5: ^{1}H NMR of Heterodisulfide of CoM-S-S-CoB.

2.3.4 Cloning of component A2 (AtwA):

The ORF encoding for AtwA was amplified from lysed *M. marburgensis* cells by PCR using the forward primer CATGGATCCATGTCT TTCATAAAGCTGGAAAACG containing a *Bam*HI (underlined) site and the reverse primer CATAAGCTTGGTTAT TCCCTGAGCATCCCCC containing a *Hin*dIII (underlined) site with the high fidelity thermostable DNA polymerase *Pfu*. The amplified DNA fragment was analyzed on a 1% agarose gel as a single fragment of ~1.6 kb (**Fig. 2.6, panel A)** corresponding to the size of the *atwA* gene**.** The PCR product was double digested with *Bam*HI and *Hin*dIII and ligated into a *Bam*HI-*Hin*dIII-digested pQE-80L vector (**Fig. 2.6, panel B**) to generate a AtwA protein that is tagged at the N-terminus with six histidine residues. Integrity of the recovered plasmid was confirmed by restriction endonuclease digestion and sequencing of the *atwA* insert using a universal T5-promoter primer of pQE-80L. Restriction endonuclease digestion profile shows the presence of the vector pQE-80L at around 4.8 Kb and the insert *atwA* (**Fig. 2.6, panel C)** after digesting the putative clone pQE-80L-atwA with *Bam*H1 and *Hin*dIII.

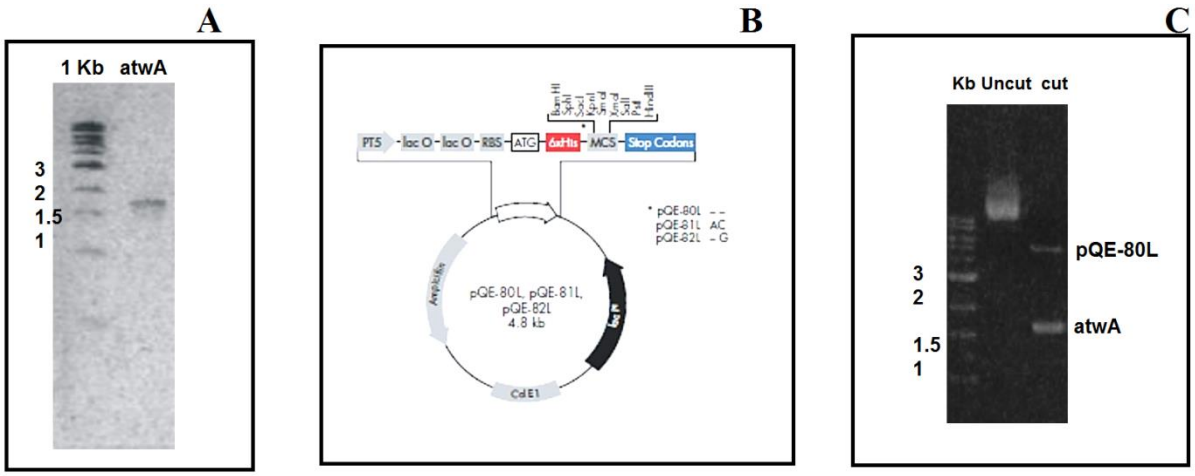

Figure 2.6: Cloning of atwA gene: Panel A shows the 1% agarose gel profile of the amplified *atwA* gene, Panel B, show the 4.8 kb pQE-80l vector containing *Bam*H1 and *Hin*dIII restriction site and 6x His tag on the N-terminal, Panel C shows the restriction digestion profile of the construct after digestion with *Bam*H1 and *Hin*dIII.

2.3.5 Purification of component A2:

The A2 protein was overexpressed in *E. coli* and purified from the cell extract using a Ni-sepharose column. The purity of the protein was determined by SDS-PAGE which showed a single band at around the expected weight of the protein, 60 kDa (**Fig. 2.7**). The protein concentration was determined by the Bradford assay and the extinction coefficient for (A_{280}) for the A2 protein (44,725 $M^{-1}cm^{-1}$).

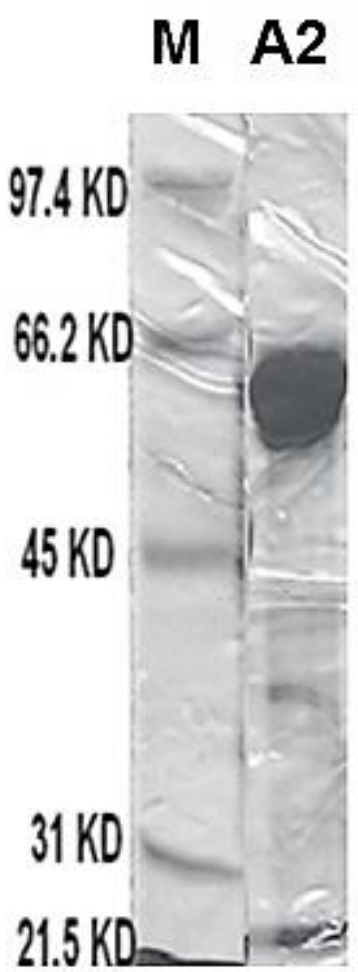

Figure 2.7: SDS-PAGE analysis of the A2 purification. A2 protein after separation on a column were denatured in sample buffer at 95°C for 5 min and loaded onto a 12 % polyacrylamide gel. The gel was stained using Coomassie brilliant Blue R-250 I (Bio-Rad).

2.3.6 Purification of different forms of Methyl Coenzyme- M reductase (MCR):

All three major forms of MCR (MCR_{red1}, MCR_{silent} and MCR_{ox1}) were purified and characterized by absorption **(Fig. 2.8)** and EPR spectroscopy **(Fig. 2.9**).The 10 mM copper perchlorate standard was used to measure the signal percentage of different signals present in the purified MCR. The purity of purified protein was established by SDS-PAGE (**Fig. 2.10**). Three bands were observed on SDS-PAGE corresponding to subunit α (66 kDa), β (46 kDa) and γ (38 kDa).

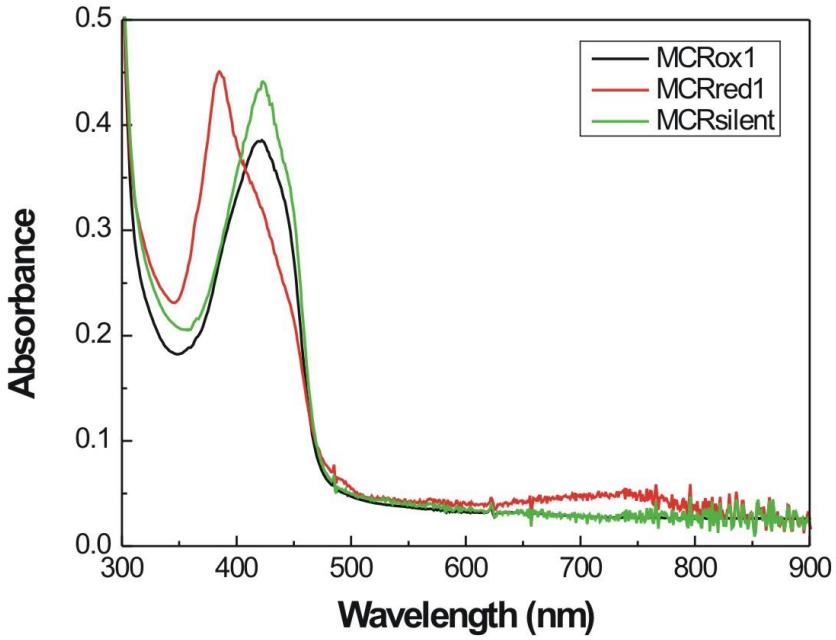

Figure 2.8: UV-Vis of different forms of purified MCR

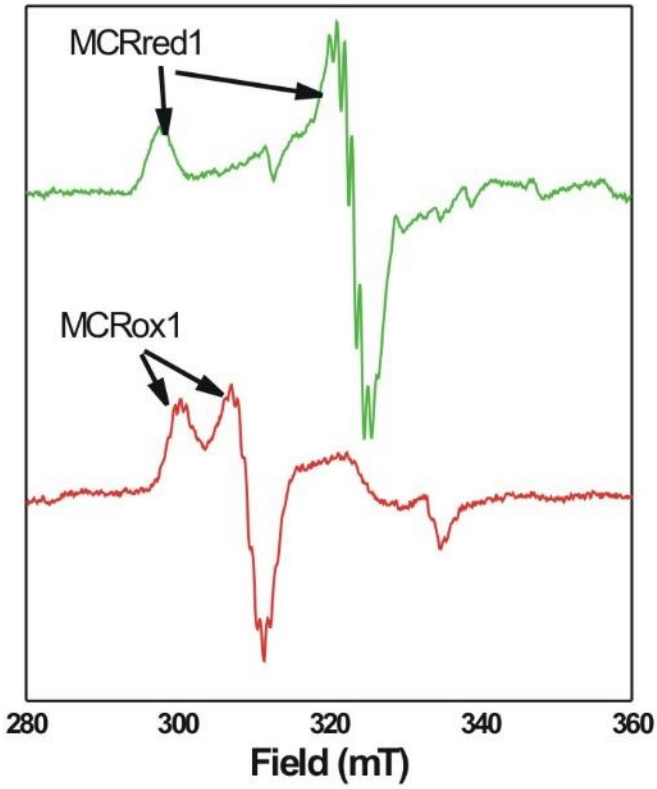

Figure 2.9: EPR spectra of the purified forms of MCR_{red1} and MCR_{ox1}. The MCR_{silent} form does not have an EPR signal.

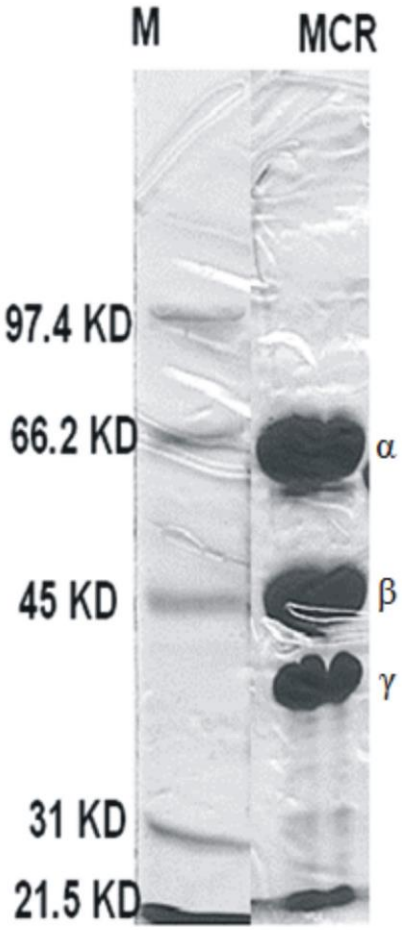

Figure 2.10: SDS-PAGE analysis of the MCR purification. Fractions containing MCR protein after the Q-sepharose column step was denatured in SDS reducing sample buffer at 95°C for 5 min and loaded onto a 12 % polyacrylamide gel. The gel was stained using Coomassie brilliant Blue R-250 I (Bio-Rad). α (66 kDa), β (46 kDa) and γ (38 kDa) bands are corresponding to three subunits of MCR.

2.3.7 Optimization of activation conditions:

Since the amount of activity achieved in a cell free system with the A2/A3a protein complex reported was almost 1000 times less than the activity of purified MCR, activation condition were analyzed and optimized to enhance the activation.

2.3.7.1 Activation study with *M. marburgensis* cells:

MCR makes up 10% of the total protein content in methanogens. Therefore, it can be readily detected by EPR spectroscopy in whole cells and cell extracts. Activation of MCR in whole cells is a relatively rapid process. As depicted in **Fig. 2.11**, cells that show minimal amounts of the MCR_{red1} EPR signal showed a large increase in this signal when they were incubated for 5 to 15 min in the presence of H_2 at 65°C. This is in agreement with previous studies where an increase in the red1 signal was reported in the presence of 80% H_2/20% CO_2 at 65°C (52,61).

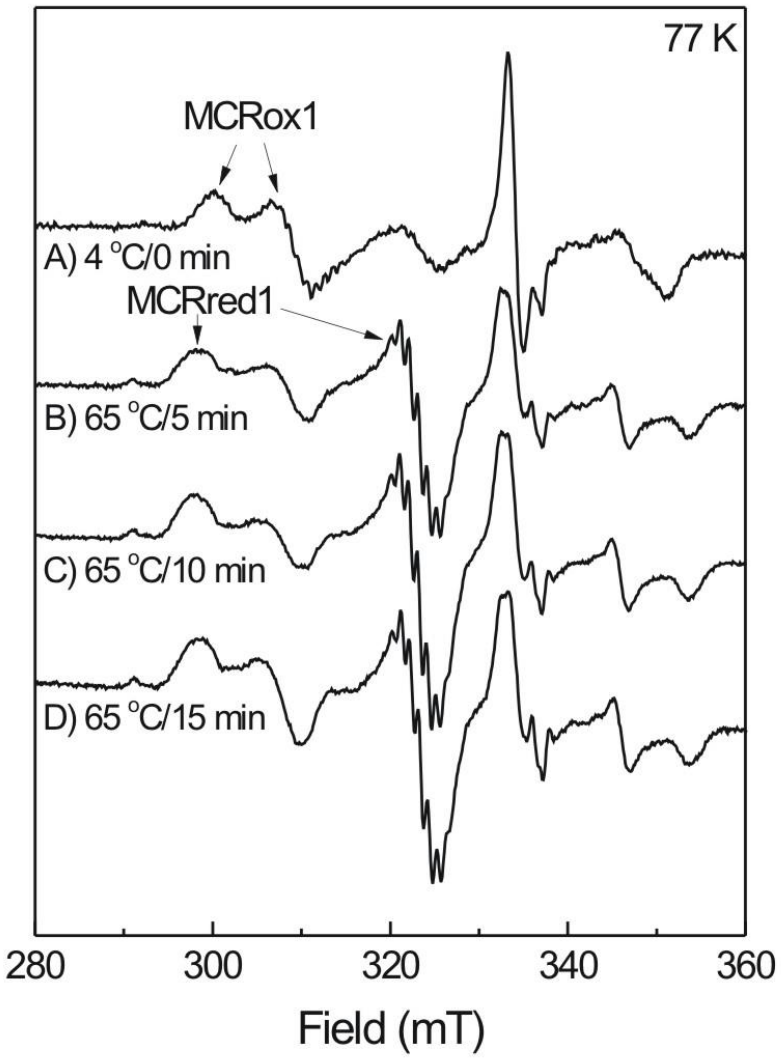

Figure 2.11: EPR Spectra for activation of MCR in whole cells. Activation of the cell suspension was done at 65°C under 100% H_2 for 5, 10 and 15 min after which the sample was transferred under exclusion of oxygen to an EPR tube, frozen, and stored in liquid nitrogen. The peaks at around 335 mT are due to the formylmethanofuran dehydrogenase and/or heterodisulfide reductase. EPR conditions: Microwave power to the cavity 2 mW.

2.3.7.2 Activation study with *M. marburgensis* Cell Extracts:

Similar studies performed with cell extracts allowed the evaluation of compounds that could enhance the activation of MCR. During growth (80% H_2/20% CO_2 at 65 °C), the EPR signal of both MCR_{red1} and MCR_{ox1} can be detected in whole cells with EPR spectroscopy (52). Upon breaking the cells most of the MCR_{red1} signal is lost. Fresh cell free extract kept at 4°C can be reactivated by bubbling with 100% H_2 gas at 60°C. Higher amounts of activation are found when HS-CoM and additional ATP is added (**Fig. 2.12, traces A, B, C, and D**). This is in line with earlier studies that showed that MCR_{red1} can be stabilized by the addition of either coenzyme M or methyl- coenzyme M (114), and that the activation was ATP dependent (102). CH_3-S-CoM could also be added with the same effect as observed for coenzyme M (not shown). The addition of HS-CoB, however, consistently, resulted in much lower amounts of activation (**Fig. 2.12, trace E**). In the presence of both HS-CoB and CH_3-S-CoM, HDS will be formed which is known to inhibit MCR activity (115). Some of this could be removed, however, by the effect of the heterodisulfide reductase reaction. The effect of HDS on MCR activity was discovered in activity assays (115).

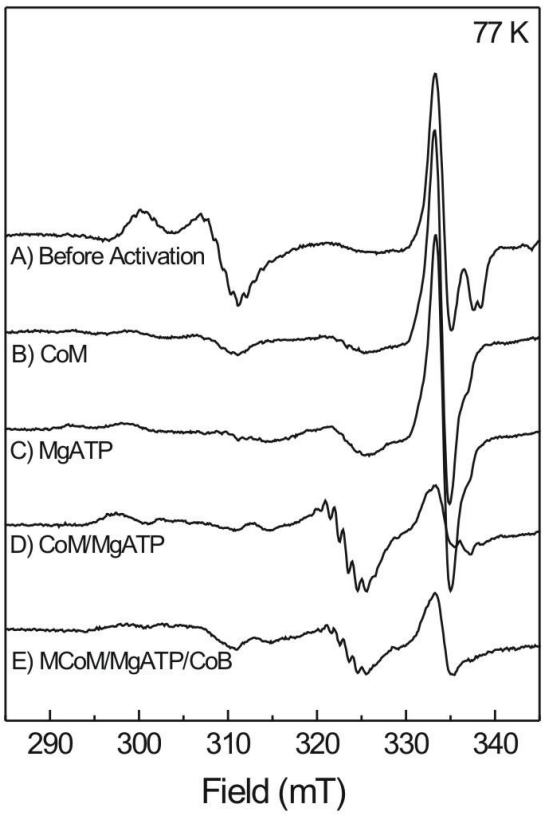

Figure 2.12: Activation of methyl-coenzyme M reductase (MCR) in cell extracts. Activation of the cell extract was done at 65°C under 80% H_2/20% CO_2 for 15 min after which the sample was transferred under exclusion of oxygen to an EPR tube, frozen and stored in liquid nitrogen. A: EPR spectrum of the cell extract kept at 4°C under an atmosphere of 100% N_2. Of the MCR forms only the MCR_{ox1} signal is detectable. B: Activation in the presence of coenzyme M (CoM). C: In the presence of 10 mM MgATP. D: In the presence of both CoM and MgATP. E: In the presence of 10 mM methyl-coenzyme M (MCoM), 10 mM MgATP, and 5 mM coenzyme B (CoB). Trace A shows mainly the MCR_{ox1} signal, main peak at 310 mT, while all other traces show different amounts of the MCRred1 signal, main peak at 325 mT. The peaks at around 335 mT are due to the formylmethanofuran dehydrogenase and/or heterodisulfide reductase. EPR conditions: Microwave power to the cavity 2 mW.

2.3.7.3 Effect of heterodisulfide under turn-over condition:

In the methane formation assay, cobalamin and Ti(III) citrate were added to reduce HDS to the two thiols, coenzyme M and coenzyme B, to prevent the accumulation of HDS. When fully active MCR in the red1 state was allowed to turn over in the presence of excess CH_3-S-CoM and HS-CoB, the red1 state rapidly disappeared (**Fig. 2.13**). At the same time there was a less rapid formation of the MCR_{ox1} form. From the intensities of the EPR signal it could be calculated that approximately 50% of the red1 form was converted into the ox1 form while the other half was converted into silent forms. It was not possible to repeat this experiment in the presence of Ti(III) citrate due to its EPR signal.

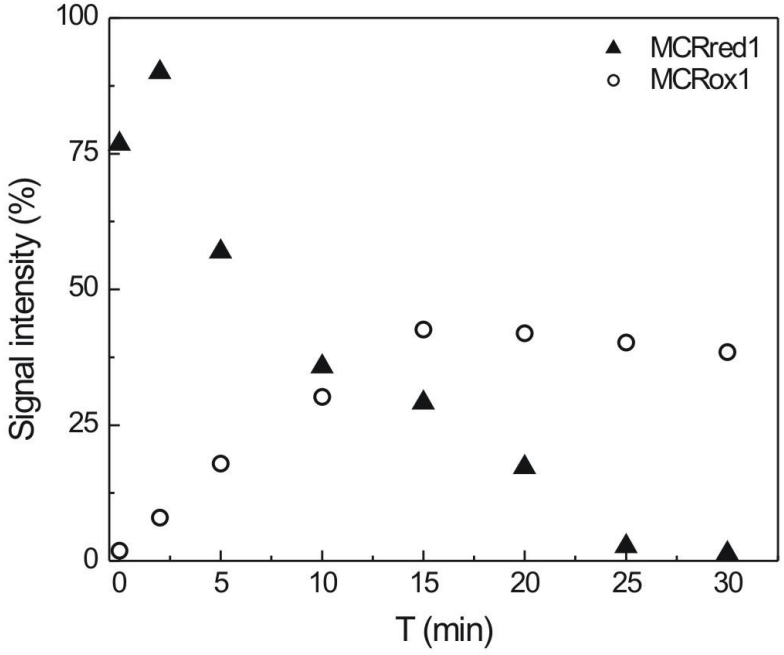

Figure 2.13: Changes in EPR signal intensities detected in methyl-coenzyme M reductase (MCR) under turn-over conditions. Reaction conditions: 100 μM MCR, 10 mM methyl-coenzyme M, 5 mM coenzyme B, 50 m M TrisHCl, pH 7.6, temperature 65 °C. Aliquots were withdrawn at the indicated times and frozen in EPR tubes. The EPR signal intensities of the different species were calculated by simulating the different species, reproduction of the compound spectrum and double integration of each individual component.

2.3.7.4 Effect of heterodisulfide (CH_3-S-CoM, HDS) on the active form of MCR (MCR_{red1a}):

The above data can be interpreted as the HDS inactivating MCR. To test this, the direct effect of HDS on MCR_{red1} was determined by incubating MCR_{red1} with increasing amounts of HDS and the effect over time was followed using EPR spectroscopy. **Figure 2.14** shows the changes that were detected in intensity of the MCR_{red1} EPR signal when the enzyme was incubated with different concentration of HDS for 5 min (**Fig. 2.14A**), 10 min (**Fig. 2.14B**) and 15 min **(Fig. 2.14C).** Comparison of the different figures shows that in the absence of HDS (control), MCR stayed mainly as MCR_{red1} but the intensity decreased from 86% to 63% after 15 min. In the presence of HDS, however, the red1 form disappeared much faster and the decrease was larger at higher HDS concentrations. Similarly the formation of MCR_{ox1} was only observed when HDS was present and a higher intensity was reached with higher HDS concentrations (58% with 20 mM HDS). Over time, however, the MCRox1 signal fluctuated and showed the highest intensity after 5 min but then the intensity decreased again upon longer incubation. After 15 min most of the enzyme was converted into one or more silent forms.

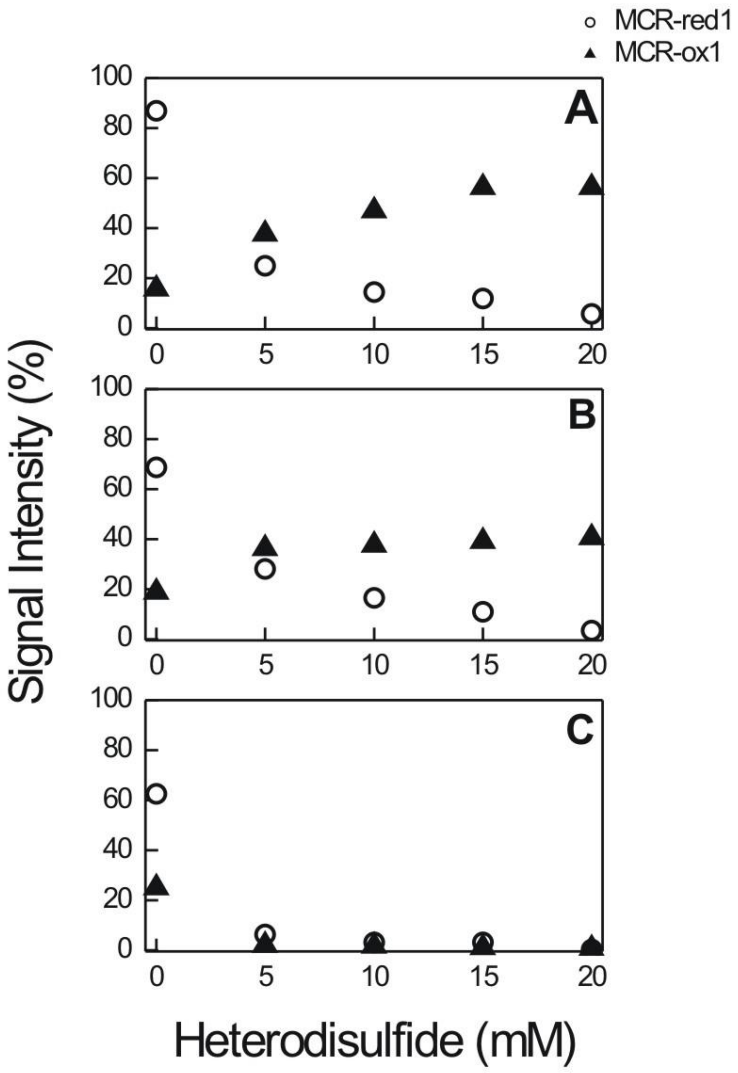

Figure 2.14: Changes in EPR signal intensities detected in MCR after incubation at 60 °C with 0, 5.0, 10.0, 15.0, and 20.0 mM of HDS for 5 min (Panel A), 10 min (panel B) and 15 min (panel C). The MCR concentration was 100 μM. Aliquots were withdrawn under exclusion of oxygen and frozen in EPR tubes. The EPR signal intensities of the different species were calculated by reproduction of the compound spectrum by simulating the different species and double integration of each individual component.

The effect of HDS on the MCR_{red1} (Ni-I) form was also analyzed by absorption spectroscopy at different time intervals (**Fig. 2.15**) at room temperature. The MCRred1 form converted into MCRox1 and MCRsilent.

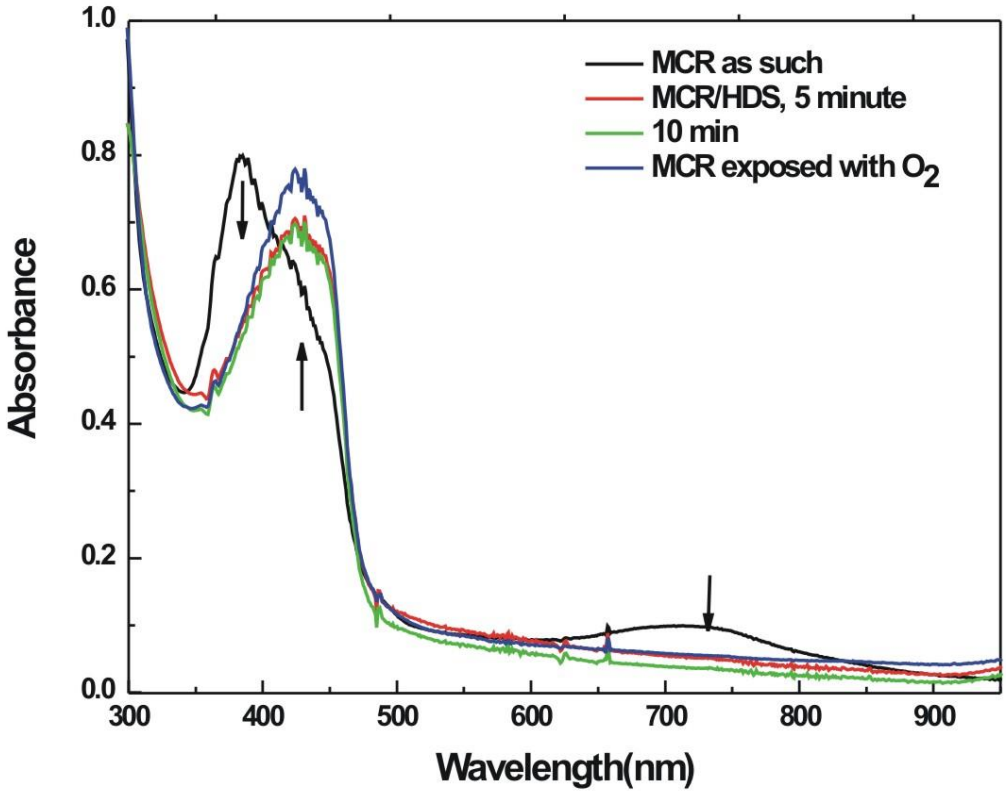

Figure 2.15: Uv-Vis spectra of MCR after incubation of the enzyme in the Red1 form with Heterodisulfide (HDS). 30 µM of MCR was incubated with 5 mM of HDS at room temperature at different time intervals (5 min and 10 min). MCR was also exposed to O_2 for comparison. Arrow indicates the disappearance of absorption maxima of red1 form at 386 nm and 720 nm in the presence of HDS and appearance of silent form of MCR at 420 nm.

2.3.7.5 Freeze-Quenching experiment of MCRred1a with heterodisulfide (CH_3-S-CoM, HDS):

In the presence of HDS, it appears that the MCR_{red1} form is first converted in to the MCR_{ox1} form and subsequently to a silent form. To characterize how fast HDS reacts with MCR, a freeze-quench study was performed. The second reason to do this experiment was to check if there are any thiyl based radical species that are formed transiently during the reaction of HDS. A radical species might be detectable if MCR_{red1}-Ni(I) is directly converted into MCR_{silent}-Ni(II). With a special setup the enzyme solution is rapidly mixed with a solution containing the HDS. With the freeze-quench (FQ) set up, reactions were quenched at time intervals between 5 ms and 500 ms. Each sample was further analyzed with EPR spectroscopy (**Fig. 2.16**). Most of Ni(I)-form converted to Ni(II)- silent form without generating any new signal or significant amounts of free radicals.

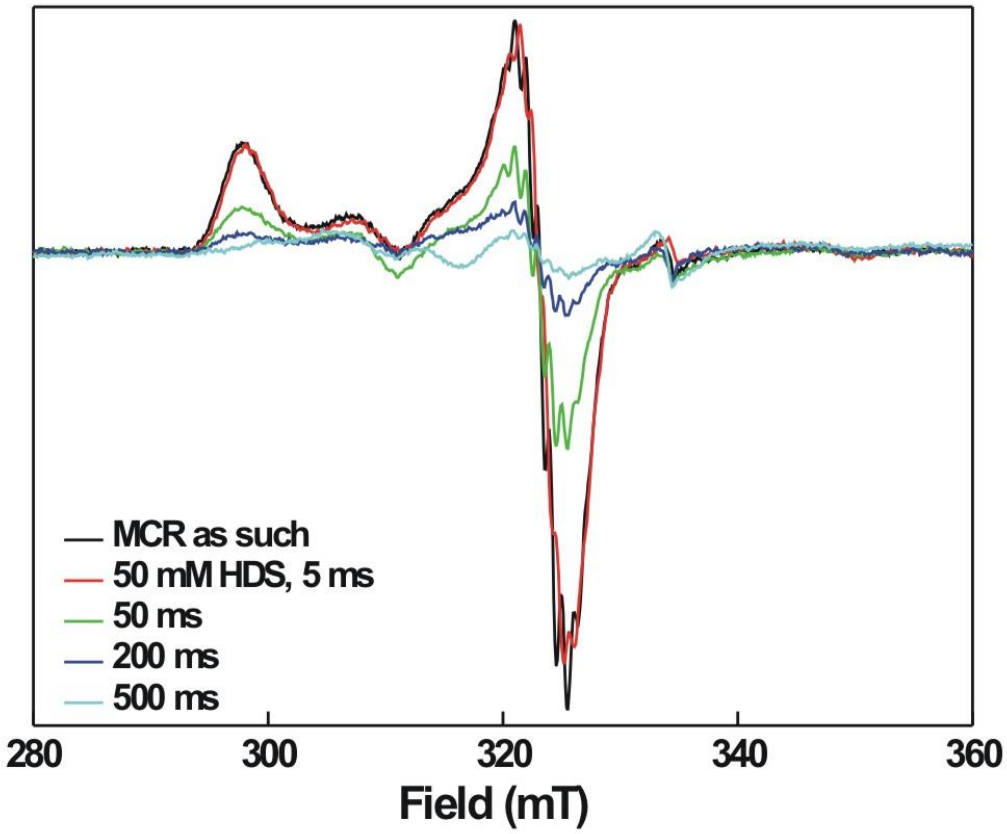

Figure 2.16: Freeze quenching experiment. 100 uM of MCR concentration was incubated with 10 mM of HDS. Aliquots were prepared under exclusion of oxygen at 5 ms, 50ms, 200 ms and 500 ms.

2.3.8 Activation of the MCR_{ox1} and MCR_{silent} forms in the presence of dithiothreitol and activating components A2 and A3a:

Both components A2 and A3a were purified to be able to investigate the mechanism of activation of MCR. For the activation assay dithiothreitol (E_m = -320 mV) was used instead of Ti(III) citrate (E_m = -500 mV). Since most of our enzyme preparations contained varying amount of MCR_{ox1} it was important to show that the observed MCR_{red1} formation was not due to the direct conversion of MCR_{ox1} into MCR_{red1} by Ti(III) citrate. Therefore, the assay contained dithiothreitol, and purified MCR, component A2, MgATP, and CH_3-S-CoM. With this assay the different column fractions were tested for the presence of the A3a component. The purification procedure started with a size-exclusion Sephacryl-300 column purification step, followed by a hydrophobic interaction Phenyl-Sepharose column step, an anion exchange Mono Q column step, and a size-exclusion Superdex 200 column step. The A3a protein comes down as a single isolated peak from the Superdex column.

2.3.8.1. Activation of the MCR_{ox1}:

Fig. 2.17 shows the activation achieved with this A3a preparation. Figure 2.15 shows how an enzyme preparation containing a mixture of 5% red1, 70% ox1 (and the rest MCR_{silent}) is converted into a sample containing 100% MCR_{red1}. This means that both ox1 and silent forms were fully converted into the red1 form.

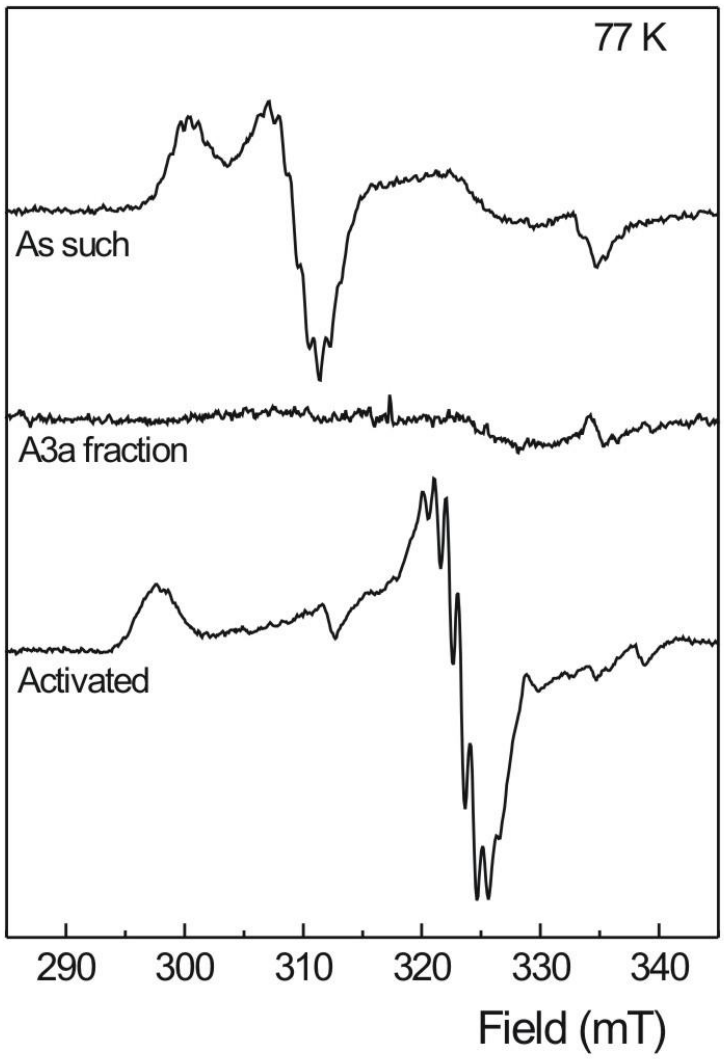

Figure 2.17: Activation of purified methyl-coenzyme M reductase (MCR) in the MCR_{ox1} form (Panel A). 100 μM MCR was incubated for 15 min at 60 °C in the presence of 20 μM component A2, 5.2 mg/ml component A3a, 10 mM MgATP, 5 mM dithiothreitol, and 10 mM methyl-coenzyme M. The 'A3a' spectra are from the A3a fraction (diluted to 5.2 mg/ml). EPR conditions: Microwave power to the cavity, 2 mW.

2.3.8.2 Activation of the MCR_{silent} forms:

Fig. 2.18, shows how a sample that contains only trace amounts of MCR_{ox1} (5.9%) is converted into a sample containing 69% MCRred1. No activation was observed in the absence of A2 or A3a protein. These data show that both the MCR_{ox1}-Ni(III) and the MCR_{silent}-Ni(II) forms can be converted into the MCR_{red1}-Ni(I) form by the same activating system. The amount of activation is also unprecedented with close to 63% activation for the silent-to-red1 conversion.

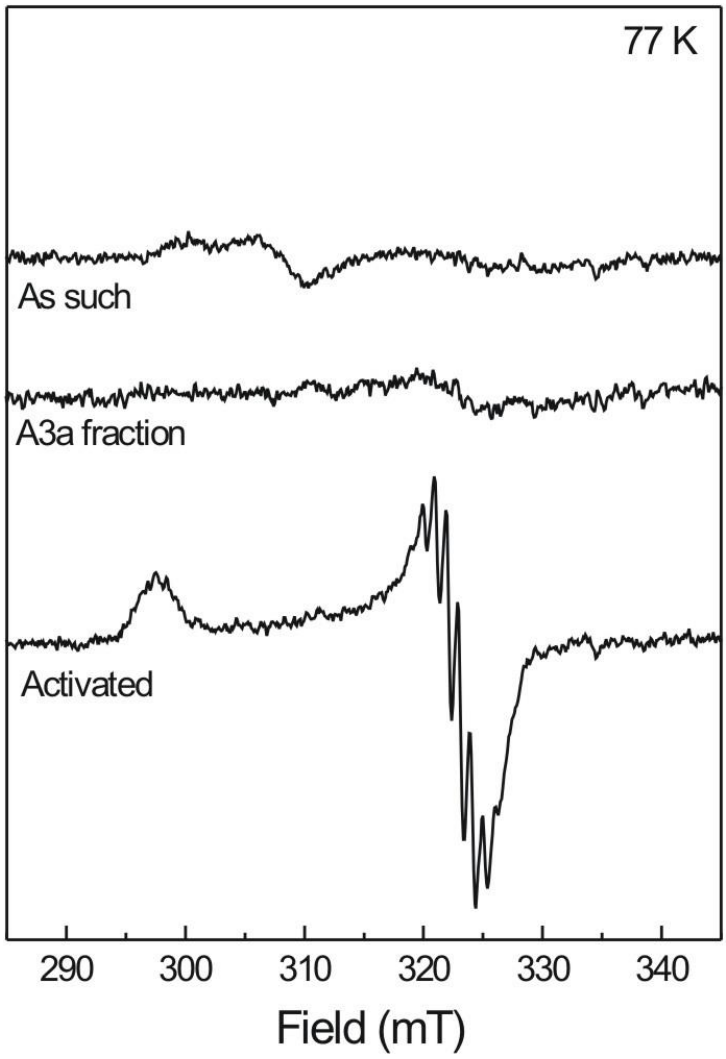

Figure 2.18: Activation of purified methyl-coenzyme M reductase (MCR) in the MCR_{silent} form. 100 μM MCR was incubated for 15 min at 60 °C in the presence of 20 μM component A2, 5.2 mg/ml component A3a, 10 mM MgATP, 5 mM dithiothreitol, and 10 mM methyl-coenzyme M. The 'A3a' spectra are from the A3a fraction (diluted to 5.2 mg/ml).

2.3.8.3 Effect of HDS on activation and activity of MCR:

The direct effect of HS-CoB and HDS were measured on activation. Activation assays were set up for 60 min and samples were withdrawn at 15 min and 60 min for EPR and activity measurements (Tables 1 and 2). In spite of the presence of all the necessary components required for activation, there was no observable formation of the active MCR_{red1} form in the presence of either HDS or both HDS and HS-CoB at 15 or 60 min. On the other hand 100% of the red1 form was formed after 15 min under the normal assay conditions and decreased to 56.9 % at 60 min. This decrease is probably due to heat instability of the enzyme. In the presence of HS-CoB (causing turn-over due to the presence of CH_3-S-CoM and therefore the formation of HDS), the signal intensity reached was only 83.6 % at 15 min and 0 % at 60 min. The activity of the activated enzyme was determined. We find only 51 µmol min^{-1} mg^{-1} (Table 2) which is less than the expected value of 100 µmol min^{-1} mg^{-1} (62). Assuming that there is only one red1 form it is not clear why this is a lower value.

Table 2.1: Effect of coenzyme B (CoB) and heterodisulfide (HDS) on the activation of MCR as detected by the different paramagnetic MCR forms in EPR spectroscopy.

Conditions	**MCR Spin concentration (%)**		
	t= 0 min	**t = 15 min**	**t = 60 min**
A: Activating components[a]	48.6% (10% red1,38.6% ox1)	100% red1	56.9% red1
B: As A with 1 mM CoB	48.6% (10% red1,38.6% ox1)	83.6% red1	0
C: As A with 1 mM HDS	48.6% (10% red1,38.6% ox1)	0	0
D: As A with 1 mM CoB and 1 mM HDS	48.6% (10% red1,38.6% ox1)	0	0

a) see Experimental Methods. Amount of MCR was 100 μM in all samples.

Table 2.2: Effect of coenzyme B (CoB) and heterodisulfide (HDS) on the activation of MCR as detected by the production of methane.

Comments	**MCRred1 signal intensity relative to enzyme concentration (%)**	**Specific activity (μmol min^{-1} mg^{-1})**
A: As such	10	3.1
B: Activating components[a]	100	51
C: B with 1 mM CoB	83.6	35
D: B with 1 mM HDS	0	0
E: B with 1 mM CoB and 1 mM HDS	0	0

a) see Experimental Methods. Amount of MCR was 100 μM in all samples.

2.3.9 Characterization of the A3a protein:

2.3.9.1 Absorption spectroscopy:

The purified A3a protein was brown in color and the electronic absorption spectrum revealed a broad absorbance maximum at 420 nm. After reduction with dithionite the absorption at 420 nm decreased, a property characteristic for proteins containing Fe-S clusters (**Fig. 2.19**).

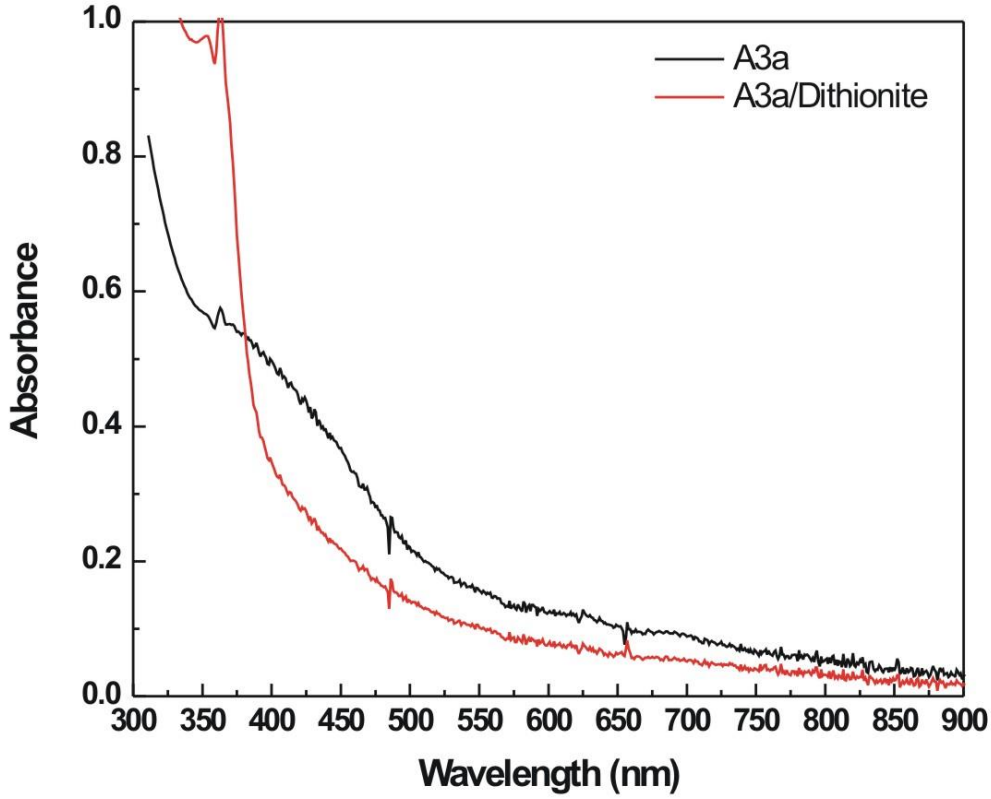

Fig: 2.19: **UV-VIS absorption Spectra of A3a Protein.** Purified A3a protein was incubated with 50 µM, 100 µM and 150 µM of Dithionite and analyzed by UV-VIS spectroscopy.

2.3.9.2 EPR spectroscopy:

Similarly, the reduced enzyme shows a broad signal in EPR spectroscopy that can be assigned to the presence of reduced [4Fe-4S] clusters (see below). The protein, however, is a multi-enzyme complex and several of the component enzymes contain iron-sulfur clusters (**Fig. 2.20**).

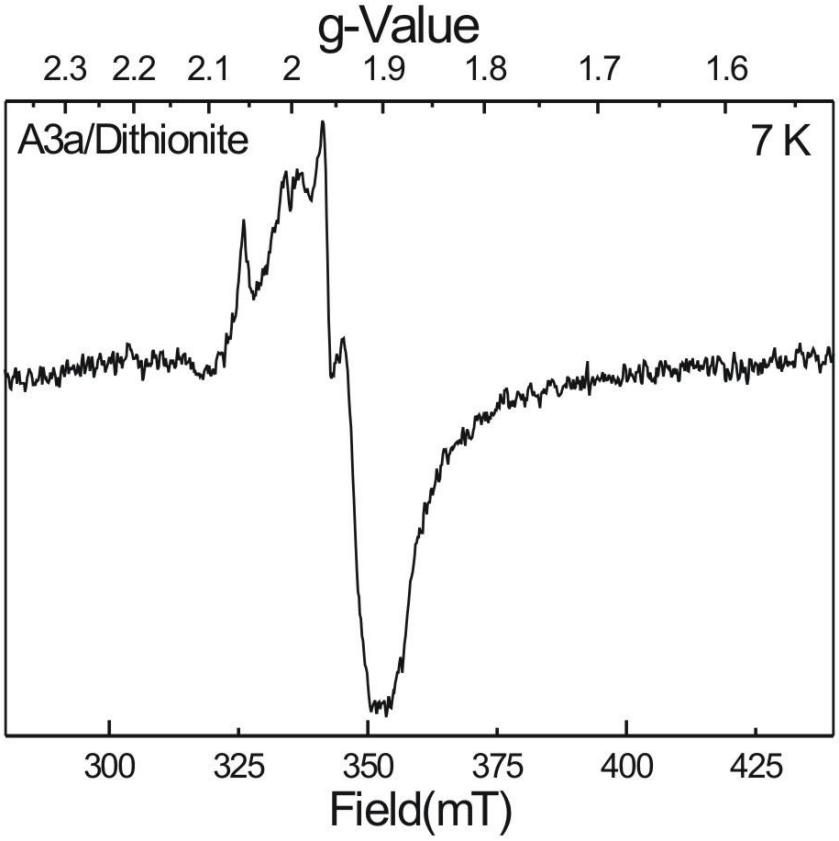

Figure. 2.20: EPR spectrum of the A3a fraction in the presence of 10 mM dithionite. EPR conditions: Microwave power to the cavity, 0.2 mW; temperature, 7 K.

2.3.9.3. Gel Electrophoresis and De-Novo sequencing:

Further characterization of A3a on a SDS-PAGE (**Fig. 2.19**) followed by de-novo sequencing showed the presence of both F_{420}-reducing hydrogenase (Frh) and F_{420}-non-reducing hydrogenase (Mvh), polyferredoxin, heterodisulfide reductase (Hdr), tungsten containing (Fwd) and molybdenum containing (Fmd) formylmethanofuran dehydrogenase, methyl coenzyme M reductase operon protein C I (McrC or McrE) and II (MtrC), acetyl-CoA decarbonylase/synthase (Cdh), 5,10-methylenetetrahydro-methanopterin reductase (Mer), Fe-protein homolog/iron sulfur cluster carrier protein (Iscc), Predicted iron sulfur flavoprotein (Pisf), and UPF0145 protein MTBMA (**Fig. 2.21 and Table 3**).

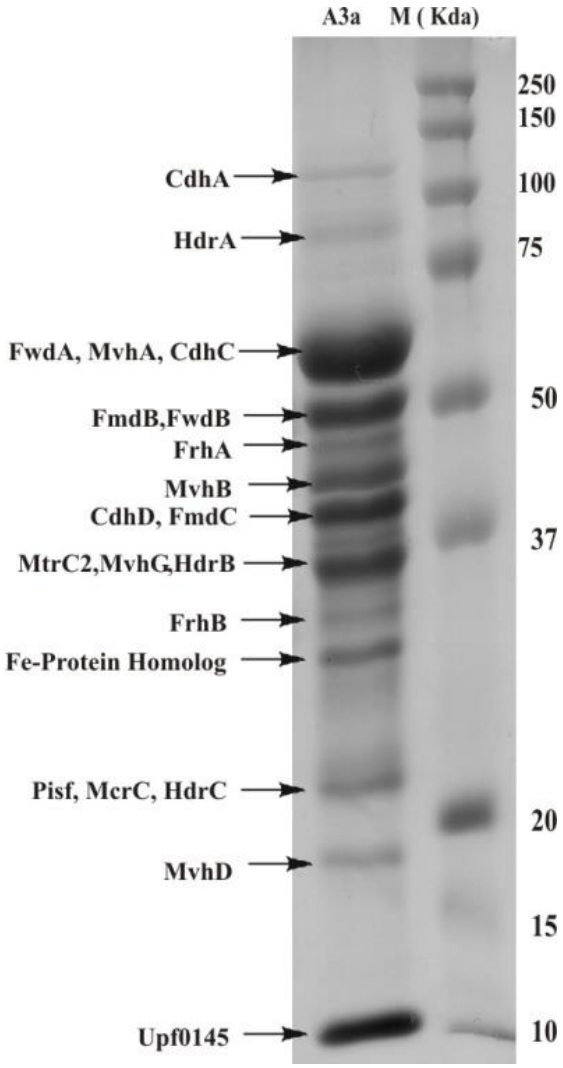

Figure 2.21: SDS-PAGE analysis of the A3a purification. The acronyms and full names can be found in Table 3. The final activator fraction after four purification steps was denatured in SDS reducing sample buffer at 95°C for 5 min and loaded onto a 12 % polyacrylamide gel. The gel was stained using Coomassie brilliant Blue R-250 I (Bio-Rad).

Table 3.3: Tabulation of the protein components present in the A3a complex with their predicted mass and accession number

Accession	Description	Predicted M.W (KDa)
D9PUJ7_METTM	acetyl-CoA decarbonylase/synthase, subunit α (CdhA)	85.8
HDRA_METTM	heterodisulfide reductase, subunit A (HdrA)	72.1
D9PU54_METTM	tungsten formylmethanofuran dehydrogenase, subunit A (FwdA)	62.8
MVHA_METTM	F_{420}-non-reducing hydrogenase, subunit A (MvhA)	52.8
D9PUJ9_METTM	acetyl-CoA decarbonylase/synthase, subunit β (CdhC)	51.5
D9PU56_METTM	tungsten formylmethanofuran dehydrogenase, subunit B (FwdB)	48.4
D9PXE7_METTM	molybdenum containing formylmethanofuran dehydrogenase, subunit B (FmdB)	48.0
D9PYF9_METTM	F_{420}-reducing hydrogenase, subunit α (FrhA)	44.7
FMDC_METTM	molybdenum containing formylmethanofuran dehydrogenase 1, subunit C (FmdC)	43.3
MVHB_METTM	F_{420}-non-reducing hydrogenase, subunit B (MvhB)	44.0
D9PUK1_METTM	Acetyl-CoA decarbonylase/synthase complex, subunit δ (CdhD)	43.2
D9PY38_METTM	Methyl coenzyme M reductase II, operon protein C (MtrC)	34.1
MER_METTM	5,10-methylenetetrahydromethanopterin reductase (Mer)	33.4
MVHG_METTM	F_{420}-non-reducing hydrogenase, subunit G (MvhG)	33.7
D9PYF6_METTM	F_{420}-reducing hydrogenase, subunit β (FrhB)	30.7
HDRB_METTM	heterodisulfide reductase, subunit B (HdrB)	33.4
D9PW01_METTM	Polyferredoxin	27.5
D9PUW4_METTM	Fe-protein homolog/iron sulfur cluster carrier protein (Iscc)	27.1
D9PU92_METTM	Predicted iron sulfur flavoprotein (Pisf)	20.6
MCRC_METTM	Methyl coenzyme M reductase I, operon protein C (McrC or McrE)	21.2
HDRC_METTM	heterodisulfide reductase, subunit C (HrdC)	20.5
MVHD_METTM	F_{420}-non-reducing hydrogenase, subunit D (MvhD)	15.9
D9PWC8_METTM	UPF0145 protein MTBMA c09310	12.4
D9PWT1_METTM	Flavoprotein	22.5
D9PW02_METTM	CBS-domain-containing protein	31.6

When the A3a fraction was applied to a native-gel 3 protein bands were observed at around 700 kDa, 160 kDa, and 40 kDa (**Fig 2.22**). It is not clear how these make up the whole protein complex. Most likely the smaller bands are breakdown products of the 700 kDa complex since these bands are not observed with size-exclusion chromatography. This would also be in line with the previous work that indicated a mass of 500 kDa for the complex purified from *Methanobacterium thermoautotrophicum* (*Methanothermobacter thermoautotrophicus*, str. ΔH) (116). Although this result would indicate further fractionation could be possible, attempts to purify a smaller complex still capable of activating MCR were not successful. Different procedures, including incubations with 50 mM CHAPS or 0.2 M urea, would provide different fractions but the SDS-PAGE would show very little variation in the complex composition. In addition the activation activity was lost and it was not possible to recombine fractions to restore this activity. The co-elution of the complex proteins after four purification steps suggests that the observed complex exists *in vivo*.

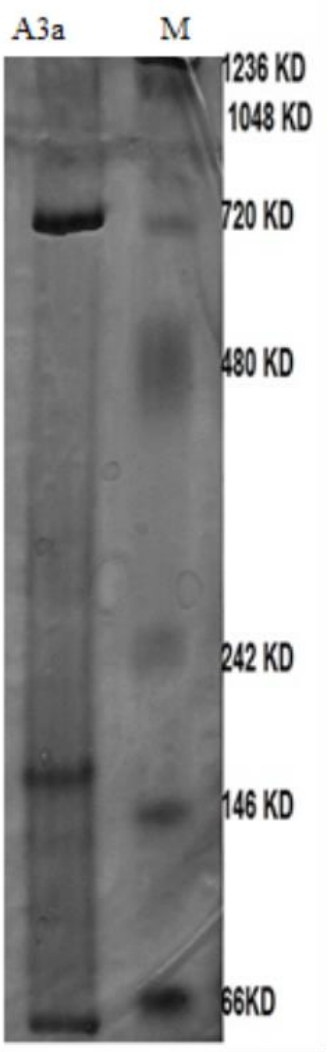

Figure 2.22: Native-PAGE analysis of the A3a purification. The final activator fraction after four purification steps was dissolved in sample buffer containing glycerol and methylene blue and loaded onto a 5 % polyacrylamide gel. The gel was stained using Coomassie brilliant Blue R-250 I (Bio-Rad).

2.4. Discussion:

2.4.1 Effect of Heterodilsulfide (HDS):

A possible explanation for the conversion into MCR_{ox1} would be that HDS binds in the active site and is reduced by the Ni(I), forming the MCRox1-Ni(III) form and HS-CoM and HS-CoB. The fact that not all of the red1 state was converted into the ox1 state could indicate that alternative reactions were taking place or could indicate an inherent instability at 60°C of both the ox1 and red1 forms. From these experiments, it can be concluded that the activation process is inhibited by HDS. In the experiments performed by the Wolfe group, the activation of MCR was measured by detecting methane formation in the head space of a closed off bottle containing a solution with Ti(III) citrate, component A2, MCR, the column fraction containing A3a, ATP, CH_3-S-CoM, and HS-CoB (101-103). Under these conditions it can be expected that HDS is formed during turn-over by the activated enzyme. Due to the direct inactivation of MCR by HDS it may be possible that the activated enzyme is quickly inactivated and less CH_4 is produced than theoretically possible**.** Therefore, to be able to detect the full activation of MCR, it is important to separate the activation step from the monitoring assay to make sure that HDS formation does not interfere with the activation itself.

The formation of HDS is an important step for archaea that have a membrane-bound heterodisulfide reductase (HDR) complex. The breakdown of HDS into coenzyme M and coenzyme B using H_2 as an electron source is used to generate a proton gradient that is used for ATP synthesis. In *M. marburgensis*, however, the HDR complex is not membrane bound but performs an electron bifurcation step to produce essential low-potential electrons (117). In both cases, one could expect HDS levels to be high to be able to perform these essential processes. Here

we show, however, that when levels are too high MCR will be inactivated. The hydrogenase:heterodisulfide reductase complex has an apparent K_m < 0.1 mM for CoM-S-S-CoB under bifurcating reaction conditions (117). This means that the HDS levels can be easily maintained below levels that inactivate MCR without compromising the function of HDR.

2.4.2 Activation complex:

Although the A3a fraction contained a diverse set of proteins, it is possible to deduce a potential model by which they facilitate the activation of MCR (**Fig. 2.23**). Activation comprises the reduction of the Ni center of cofactor F_{430} to the Ni(I) state. Activation of MCR in whole cells is possible by either by H_2 or CO (60,97). Electrons from the 2 H^+/H_2 couple represent an E_m of -414 mv under growth conditions (117). The electrons, however, can be used to reduce polyferredoxin (E_m = -500 mV) through the process of electron bifurcation. Electron bifurcation is performed by a complex containing Hdr/Mvh in *M. marburgensis* and Hdr/Mvh/Fwd and other components in *Methanococcus maripaludis* (117,118). The reductive power of these electrons, however, would not be enough to reduce the Ni in MCR. The next step is to take electrons from ferredoxin and through coupling with ATP hydrolysis bring the potential down to the level of the Ni(I)/Ni(II) couple (estimated to be -650 mV).

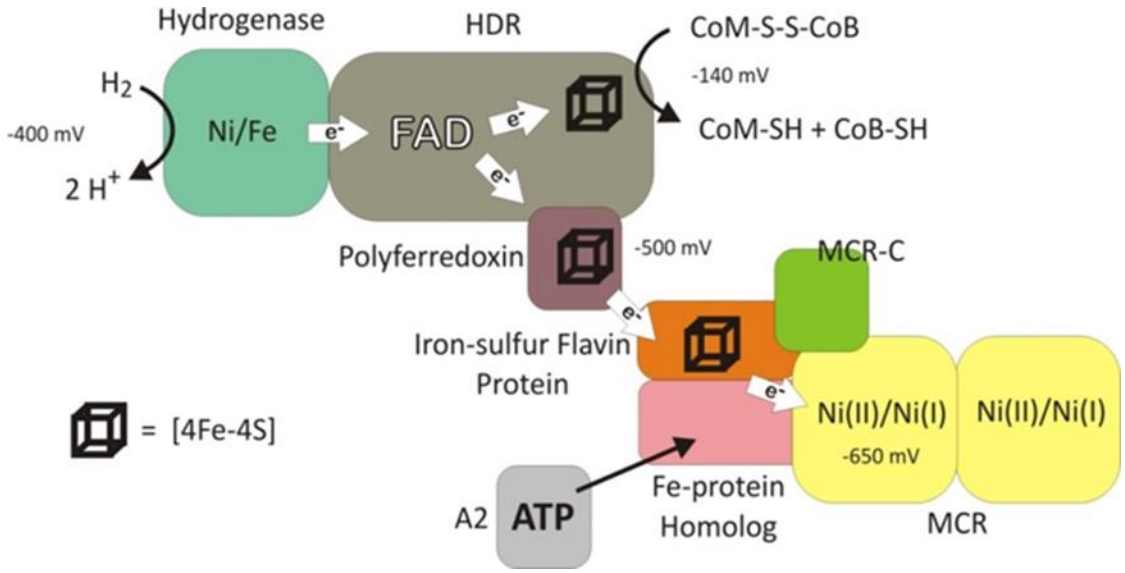

Figure 2.23: Schematic presentation of the steps leading up to the creation of low-potential electrons for the reduction of the nickel-containing cofactor F_{430} and the activation of MCR *in vivo* (47). For clarity, different components are drawn separately. The purified activation complex, however, contains all the components shown with exception of the A2 protein and MCR itself. It was not possibly to obtain through additional purification steps a smaller set of components that would still activate MCR.

This can be proposed based on the presence of the Fe-protein homolog/iron sulfur cluster carrier protein that performs such a function in the nitrogenase system. The predicted sequence of the Fe protein homolog shows the presence of an ATP-binding site (**Fig. 2.24**). The activation assay, however, does not work when ATP is present but component A2 is left out. This would indicate that A2 is responsible for delivering ATP to the Fe protein homolog and might assist in the hydrolysis. Component A2 possesses two ATP-binding domains and has sequence similarities to the ATP-binding cassette family of transport systems (119). The Fe-protein homolog/iron sulfur cluster carrier protein is not well named since its predicted sequence shows that the [4Fe-4S]-binding site is absent (**Fig. 2.24**).

Fe-protein homolog/iron-sulfur cluster carrier protein (ISCC)

MTRVITVASGKGGVGKTTITANLGVALSTYGERVVVLDADIAMANLELILGMEGKSVTLHDVLAGNASIE
DAVYEGPNGVRVVPAGISLEGLRNVKLDRLEDALAYLIEDTDILLIDAPAGLEKDAVAALAAADELLLVT
TPEVPSISDALKTKIVASKLGINIIGVVINREQYDKTFLSVEEVETILEVPVIAVIPDDPEVSRAAAFGE
PIVIKNPKSPASNSLMKLAADLIGEDYQPIEPDKQGVIAKLISGLMGRR

Predicted iron-sulfur flavoprotein (PISF)

MISASPRKESNTMMVLEHCRDAVESRGVECEIVSLRGMNIESCRACLSCAKKHRCKIDDGLNGIIERIRD
AEGLIVATPVYFGTARGDLMSALQRIGMVSRVSDGFLSWKVGGPIAVARRGGHTATIQELLMFYFINDMI
VPGSTYWNMVFGWAPGEVEDDDEGMETIRRFGENVAELIKRIQSGE

UPF0145 protein MTBMA c09310

MVEEHGDIVYVTSNYVPGHRAVETLGFVYGLTVRSRGLGGQIGAGLRSIVGGEIKEYVTMMEHSRQEALE
RMLDHARELGANAVISVRFDSDSISDIMQEILAYGTAVIVEPEE

Figure 2.24: Predicted amino acid sequences for the Fe-protein homolog/iron-sulfur cluster carrier protein (ISCC), the predicted iron-sulfur flavoprotein (PISF), and the UPF0145. The nucleotide binding site for ISCC is indicated in gray. ISCC belongs to the Fer4-NifH superfamily which share a common ATP-binding domain. Functionally, proteins in this superfamily use the energy from hydrolysis of NTP to transfer electrons or ions. The cluster binding site for PISF, recognizable by the 4 Cys residues, is marked in gray. PISF belongs to NADPH-dependent FMN reductase superfamily. UPF0145 belongs to the YbjQ-1 putative heavy-metal-binding superfamily. On the basis of comparative structural analysis, this family is likely to contain a heavy-metal binding domain. No Cys residues are present that would indicate the presence of an iron-sulfur cluster.

It is the combination of ATP hydrolysis and electron transfer from the nitrogenase Fe-protein's 4Fe cluster that provides the low-potential electrons for the nitrogenase reaction. Assuming that a similar process is needed for the activation of MCR, the presence of a 4Fe cluster might be essential. The cluster of the iron-sulfur flavoproteins could possibly have that function. It has been shown that the iron sulfur flavoprotein can accept electrons from polyferredoxin (120). The MCR operon contains five genes. The *mcrA*, *mcrB*, and *mcrG* genes form the three subunits of MCR while the *mcrC* and *mcrD* genes have an unknown function. It appears that the *mcrC* gene product might play a role in the activation of MCR. Recently it was shown that CO can also activate MCR in whole cells. The CO_2/CO couple has an E_m of -520 mv and electrons from CO dehydrogenase complex (Cdh) are unlikely to activate MCR directly. Cdh, however has been shown to be able to reduce the polyferredoxin (121,122).

Electrons for the activation of MCR can come from different known cellular processes but are most likely directly donated by polyferredoxin. Although the model predicts that MCR can be activated using H_2 as an electron source we were not able to prove this. After the multiple purification steps the hydrogenases in the A3a complex turned into the resting Ni-B/Ni-unready state (123), as detected by EPR spectroscopy. The standard method to reactivate the hydrogenases (incubation under H_2 at 65°C for longer time periods, 1-2 hrs) (123) resulted in precipitation of the A3a complex preventing testing of our model. Therefore future research will focus on the components that are unique for the activation of MCR, which are probably the McrC proteins, the Fe-protein homolog and the predicted iron sulfur flavoprotein. The next step will be to prove that MCR can indeed be activated by these three components using either polyferredoxin or an artificial electron donor.

CHAPTER THREE: Cloning, expression, and characterization of individual components of the activating complex

3.1 Introduction:

The objective of this chapter is to examine the proposed model for the activation in described in Chapter 2. First, however, we will focus on the parts that take electrons from ferredoxin and shuttle those to the Ni centers on MCR. This is because not all methanogens have the cytosolic hydrogenase:heterodisulfide reductase complex but all have ferredoxin or polyferredoxin. The A3a protein components that are unique for the activation of MCR and come after the ferredoxin in the electron path are the predicted iron sulfur flavoprotein, the McrC proteins and the Fe-protein homolog. Their role in the activation process can be demonstrated by co-expressing the selected A3a protein components in an archaeal host together with the MCR genes to reconstitute active enzyme complex. These experiments are underway and we recently expressed recombinant MCR with low activity. The coexpression of the selected genes proposed to be important for activation will be the next step. We were not able, however, to overexpress the *M. marburgensis* genes in *M. maripaludis* but only the MCR genes from *Methanococcus okinawensis*. Optimization of codon might be needed because of optimum growth temperature of M. *marburgensis* and *M. maripaludis* is different. *M. marburgensis* grow at 65°C while M. *maripaludis* grow at room temperature. It will be investigated if the *M. marburgensis* genes can be expressed by optimizing the codons or alternatively the *M. okinawensis* activating components can be coexpressed. In the meantime these protein components were separately overexpressed in an *E. coli* host and that work will be described here.

Predicted iron-sulfur flavoprotein:

There are three different uncharacterized iron-sulfur flavoprotein present in the *M. marburgensis* genome: MTBMA_c00180 Iron-Sulfur flavoprotein (**D9PU92**), MTBMA_c00560 Iron-Sulfur flavoprotein (**D9PYX1**) and MTBMA_c00580 Iron-Sulfur flavoprotein (**D9PVD2**). These proteins belong to the FMN_red superfamily characterized by an NADPH-dependent FMN reductase like domain. De-novo sequencing of the A3a complex subunits, revealed the presence of only MTBMA_c00180 iron-sulfur flavoprotein (D9PU92) as a part of the complex. Proteins in this domain contain a flavodoxin-like fold, which is characterized by an open twisted/alpha beta structure consisting of five parallel beta-sheets connected by alpha-helices which surround the sheet. Flavodoxins are electron-transfer proteins that function in various electron transport systems. They bind one FMN molecule, which serves as a redox-active prosthetic group and are functionally interchangeable with ferredoxins. This domain can be found in flavodoxins, FMN-dependent NADH-azo compound oxidoreductases, ribonucleotide reductase stimulatory proteins, glutathione-regulated potassium-efflux system ancillary protein KefG, N-terminal of the sulfite reductase [NADPH] flavoprotein alpha-component and the C-terminal of the anaerobic nitric oxide reductase flavorubredoxin. Other proteins with this domain include iron-sulfur flavoproteins and chromate reductase.

Based on the overall sequence identity and presence of a compact cysteine motif, the ISF (*i*ron-*s*ulfur *f*lavoprotein) family is distinct from other flavin mononucleotide (FMN)-containing flavoproteins (124). The first prototype of Iron sulfur protein was identified and characterized from *Methanosarcina thermophila* (125). Ever since then, homologs of ISF have been identified in the genomes of many anaerobic prokaryotes belonging to the domains Bacteria and Archaea (124).

Interestingly, many species contain multiple ISF homologs. The *Methanosarcina acetivorans* genome is annotated with 19 Iron Sulfur Protein homologs (126). The *M. marburgensis* genome is also annotated with three Iron Sulfur Flavoprotein homologs and multiple sequence alignment of all these ISF with iron-sulfur protein [*Methanosarcina acetivorans*] and iron-sulfur flavoprotein [*Methanosarcina mazei*] showed the presence of a compact cysteine motif ($CX_2CX_2CX_5C$) and two conserved Arg and Leu amino acids residue that may be involved in Flavin binding as shown in **Fig. 3.1.** The Role of these proteins in *M. marburgensis* is not known. However, an Iron-Sulfur Protein from *Methanosarcina mazei* functions as an archaeal dihydromethanopterin reductase (DmrX) (127). In *M. marburgensis* genome the genes that code for **D9PYX1** and **D9PVD2** are on the same operon. Most likely, one of the gene products function as a Dihydromethanopterin reductase (DmrX) in *M. marburgensis*.

As mentioned in Chapter 2 and described below, the Fe protein homolog does not contain an iron-sulfur cluster. The MTBMA_c00180 Iron-sulfur flavoprotein would therefore be the only A3a component that could possibly bind an iron-sulfur cluster. If the activation of MCR has similarities to that of the Nitrogenase system one of the components needs to bind a cluster that can accept electrons from ferredoxin that can be used to reduce the Ni center in MCR in combination with ATP hydrolysis.

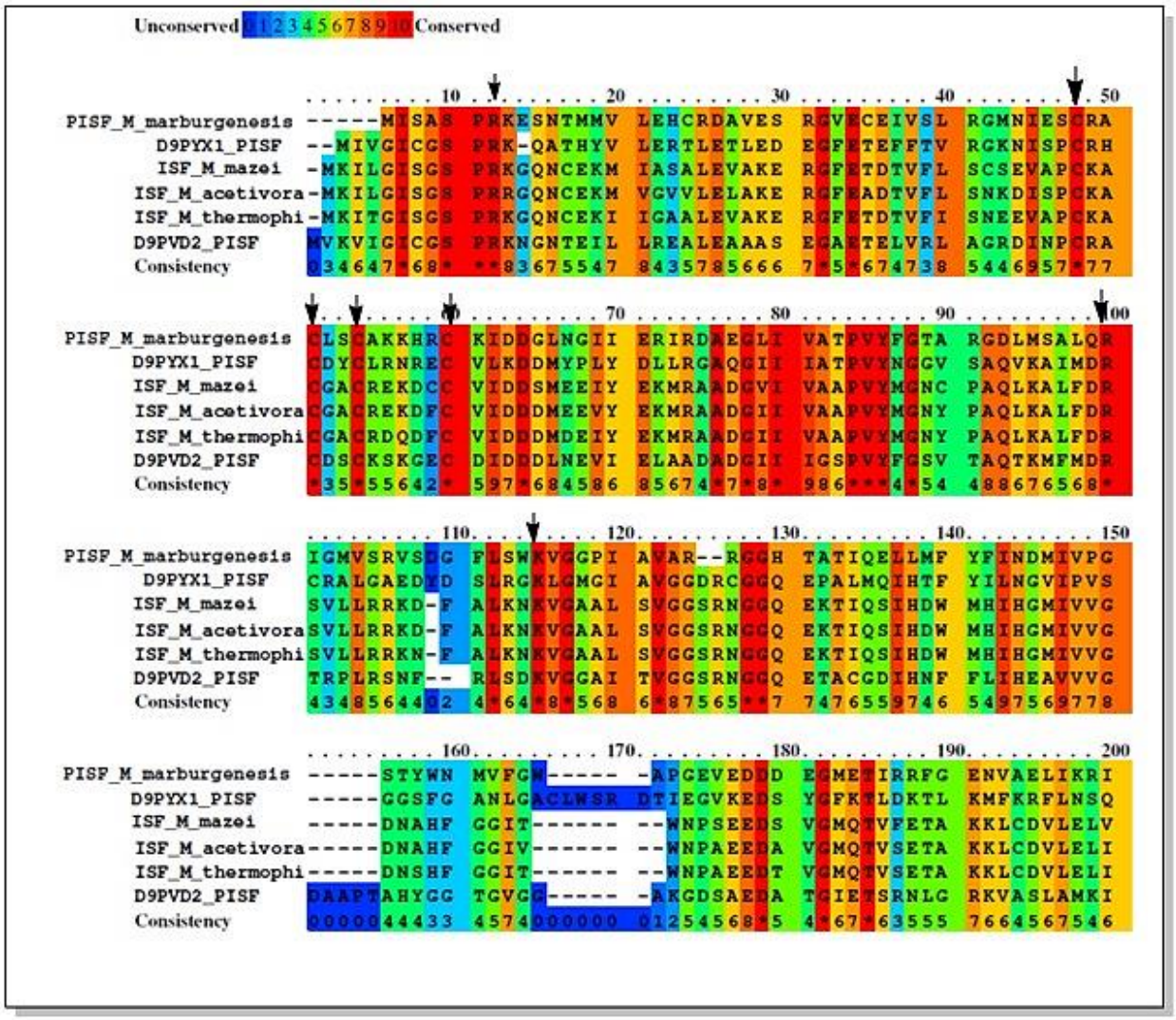

Figure 3.1: Partial amino acids sequence alignment Iron Sulfur Flavoproteins.

D9PU92_METTM Predicted iron-sulfur flavoprotein (PISF_*M.marburgensis*), D9PYX1_METTM Predicted iron-sulfur flavoprotein, D9PVD2_METTM Predicted iron-sulfur flavoprotein, iron-sulfur flavoprotein [Methanococcus maripaludis], iron-sulfur flavoprotein [*M. thermophila*], iron-sulfur flavoprotein [*M. mazei*] and iron-sulfur protein [*Methanosarcina acetivorans*].

Fe-protein homolog/iron-sulfur cluster carrier protein (ISCC)*:*

This protein belongs to the Fer4-NifH superfamily. The Fer4_NifH superfamily contains a variety of proteins which share a common ATP-binding domain. Functionally, proteins in this superfamily use the energy from hydrolysis of NTP to transfer electrons or ions. ISCC is related to the nitrogenase Fe protein. The predicted sequence of the Fe protein homolog shows the presence of a nucleotide-binding site (**Figs. 2.24 and 3.2**), switch I/II and P-loop. However, the [4Fe-4S]-binding site is absent unlike in the Fe-protein. Members of this family are often found in archaeal genomes but the function is unknown.

In our model we predict that the ATP hydrolysis takes place on ISCC and that a concurrent conformational change causes a change in the midpoint potential of the cluster of the iron-sulfur protein that is interacting with the ISCC subunit. The ATP hydrolysis, however, does not happen in the absence of A2. Apparently A2 is responsible for both delivering the ATP to the Fe protein homolog and assisting in the hydrolysis.

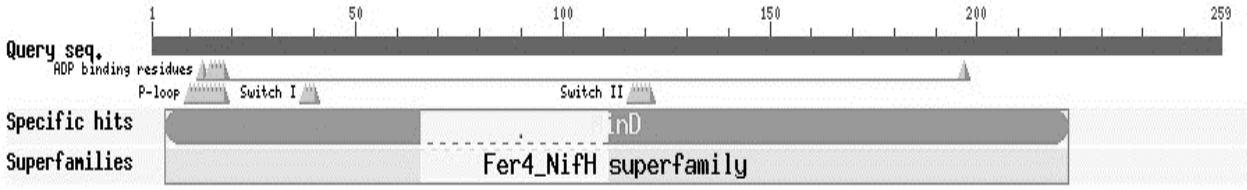

Figure 3.2: Sequence analysis of ISCC/ Fe-protein homolog

Methyl-coenzyme M reductase I operon protein C (McrC) and Methyl coenzyme M reductase II operon protein C (MrtC):

As depicted in **Fig. 3.3**, the genes encoding the three subunits of the isoenzyme I (MCR) form a transcription unit (*mcrBDCGA*). In addition to the 3 genes that code for the 3 subunits of the enzyme, two open reading frames are present that encode for two polypeptides, McrC and McrD. The molecular masses of the gene products are estimated to be around 20 kDa (45-47). Both gene products, McrC and McrD can be detected in cell extracts (47,48) but they are not part of the active form of the enzyme (49-52).

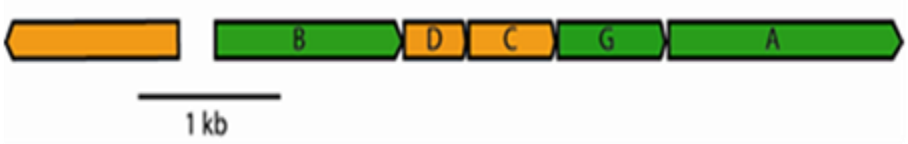

Figure 3.3: Methyl Coenzyme M Reductase Operon

The genes encoding the three subunits of the isoenzyme II (MRT) also form a transcription unit *(mrtBDGA)* which contains only one additional open reading frame encoding a protein with sequence similarity to McrD (41). However, a gene with a sequence similar to *McrC*, the *mrtC* gene, is coded elsewhere in the genome. The function of the *mcrC*, *mcrD*, *mrtC* and *mrtD* gene products is not known (43). Recently, however, we found that the *mcrC* and *mrtC* gene products are part of the A3a activating complex and involved in the activation of MCR (47). Sequence analysis of McrC revealed the absence of both a typical Fe-S cluster and a nucleotide binding consensus sequence (**Fig. 3.4**). Therefore, it doesn't seem to be involved in either ATP hydrolysis or electron transfer. As it is a part of the A3a complex, it is possible that it assists in assembling

the activating complex. The presence of MtrC in the A3a protein complex suggest that A3a can activate both MCR isoenzyme I and isoenzyme II (MRT).

Methyl-coenzyme M reductase I operon protein C (McrC)

MIGKCTHVVDCRETMGMGEGGGIAQRGTFAQCGSEVLAVAMSPGRRHITKPVCEITFALREANIMTSTLV

LNAGAGVPQDAPSAGAGSLFGLTPAEVEQMKRHRLLVVHLGGVKNHITYKARLILRNVDRPCIVICEYPV

DFEDFAKIGVKTRVVMPDEPKTKGTIVDIVSGVIRGETCPQEKLDEIIRKVKLALGGA

Methyl coenzyme M reductase II, operon protein C (MtrC)

MYETLTYQGGVHRHEEMKELIEDLGGFVLQENMLQMDLILTLAVPIEDVDKVREKARELLGKVKVAPMAG

TEIAIVSPTLARHHLPHSACDISEYLRRYGAKDNMIGLARGAGKGISRISEDEKRLIEEHDLAVFALGSF

EQCIKDKAHLFSDINIPVVVTGSPEKIDLSELPGADAYVGGLGRIPRRLKRGEDIRALRKLVEVVEDILD

RRRREMAADPPLVPSILVKTEIENQVPAVKEVYSPTPVTSQLDGVRVKLNYDRYHDEIADVRVSDYRLGD

ISEIRKSMMYDYILVKLLPESSIL

Figure 3.4: McrC and MtrC sequence analysis

In addition to the predicted iron sulfur flavoprotein, the McrC proteins, and the Fe-protein homolog proteins, two other uncharacterized proteins, a CBS-domain-containing protein and a Flavoprotein, with unknown function were detected in the A3a complex.

The CBS domain, named after human CBS, is a small domain originally identified in cystathionine beta-synthase and is found in a wide range of different proteins. It usually occurs in tandem repeats. Crystallographic study of bacterial CBS domain containing proteins revealed that they associate to form a so-called Bateman domain or a CBS pair. These domains have been shown to bind ligands with an adenosyl group such as AMP, ATP and S-AdoMet.

The Flavoprotein found in the A3a protein complex is similar to AfpA (Archaeoflavoprotein) from *Archaeoglobus fulgidus*. AfpA forms a homodimer with two non-covalently bound FMN cofactors can receive electrons from ferredoxin, but not from a number of other electron donors such as NADH or rubredoxin. It can then donate electrons to various acceptors like Ferricyanide, 2,6-dichlorophenolindophenol, several quinones, ferric citrate, bovine cytochrome c, and O_2 (128). Since cytochrome c and quinones electron carriers are not present in *M. thermoautotrophicus*, the physiological significance of these electron acceptors for AfpA is questionable. The role of the Flavoprotein is yet to be determined in *M. thermoautotrophicus* and the closely related *M. marburgensis*. Flavoprotein and Cbs-domain-containing protein were also overexpressed in the *E. coli* host to study their possible roles in the A3a complex and the activation of MCR.

The model for the activation of MCR described in Chapter 2 and in our recent report (47) postulates that reduced polyferredoxin is the direct source of electrons for reduction of the iron-sulfur cluster of the predicted iron sulfur flavoprotein (PISF). Depending on the growth conditions, reduction of polyferredoxin is possible either by electron bifurcation or the CODH/ACS complex.

However, under *in vitro* conditions, reduction of the iron-sulfur cluster of PISF is possible by artificial electron donors like sodium dithionite or Ti(III) citrate. Hence, to confirm the postulated model of activation of MCR, either of these can be used in an assay that contains the other recombinant activating components. **Fig. 3.5** depicts the *in vitro* model of activation of MCR, where dithionite or Ti(III) citrate donates electrons to the Fe-S cluster of PISF and hydrolysis of ATP by A2 and the Fe-protein homolog decrease the potential of electron further to enable reduction of the Ni center in MCR. McrC possibly assists in assembling the activating complex.

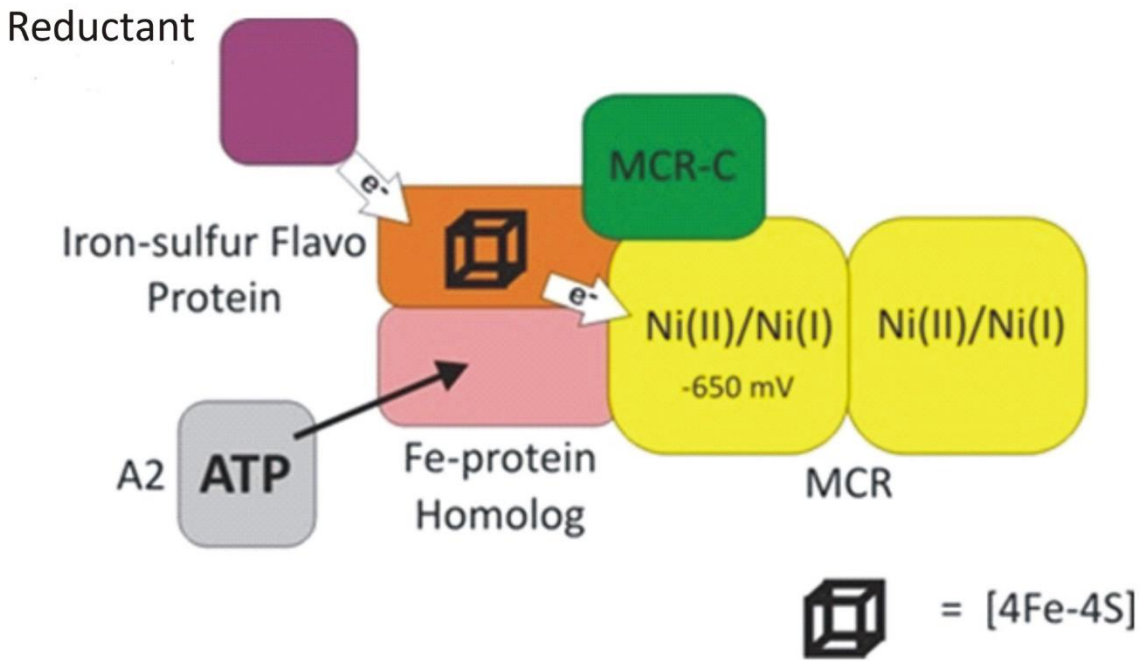

Figure 3.5: Schematic presentation of the steps leading up to the creation of low-potential electrons for the reduction of the nickel-containing cofactor F_{430} and the activation of MCR ***In Vito.*** For clarity different components are drawn separately. The purified activation complex, however, contains all the components shown with exception of the A2 protein and MCR itself.

3.2 Materials and Methods:

3.2.1 Reagents:

In-Fusion cloning kit was purchased from Takara Clontech (Mountain View, CA). pET-32 EK/LIC kit , Enterokinase capture kit and different competent cells were purchased from Novagen, USA. Thermostable DNA polymerase *Pfu* was purchased from Agilent Technologies (Clara, CA). pQE-80L vector, universal T5-promoter primer, plasmid isolation kit and gel extraction kit were purchased from Qiagen (Valencia, CA). The primers were purchased from Integrated DNA Technologies (San Jose, CA) and the restriction enzymes were purchased from New England Biolabs (Ipswich, MA). ATP Affinity Kit was purchased from Jena Bioscience (Jena, Germany). Phosphate detection kit, Biomol Green Kit was purchased from Enzo.

3.2.2 Cloning of Iron Sulfur Cluster Carrier, Fe-Protein homolog Protein, Methyl coenzyme M reductase I, operon protein C (McrC), Methyl coenzyme M reductase II, operon protein C (MtrC2), Flavoprotein, Cbs-domain-containing protein by In-Fusion cloning:

The *iscc*, *cbs-domain-containing*, *flavoprotein*, *McrC*, *polyferredoxin* and *mtrc2* genes specific primers with 15 bp extensions homologous to pQE-80Lvector at *Bam*H1 and *Hin*dIII ends were designed as shown in **table 3.1.** The desired inserts were amplified directly from *M. marburgensis* genomic DNA using appropriately designed PCR primers (**table 3.1.**) with the high fidelity thermostable DNA polymerase Phusion. To enhance the cloning efficiency the resulting PCR products were incubated with cloning enhancer for 15 min at 37°C followed by 15 min at 80°C. In-Fusion cloning reactions were set up for ligation of inserts with vector as per instruction. Cloning enhancer treated genes were incubated with In-Fusion Enzyme premix and linearized pQE-80L vector at *Bam*H1 and *Hin*dIII restriction sites. The recombinant plasmids pQE80-L-

McrC, pQE80-L-*MtrC2*, pQE80-L-*ISCC*, pQE80-L-*CBS-domain* and pQE80-L-*flavoprotein* were transferred into Stellar competent cells by heat shock treatment at 42°C. The integrity of the recovered plasmids was confirmed by restriction endonuclease digestion and sequencing of the *McrC, mtrC2, flavoprotein, ISCC, CBS-domain* containing inserts using a universal T5-promoter primer. For overexpression, recombinant plasmids were transformed into *E. coli Rosetta-gami* competent cells containing pRARE plasmid by heat shock treatment. Expression of these genes produce proteins that are tagged at the N-terminus with six histidine residues.

TABLE 3.1: Tabulation of forward and reverse primers with overhang sequence homologs to vector (underlined containing *Bam*H1 (GGATCC, bold) and *Hind*III (AAGCTT, bold)).

Description	Forward Primer	Reverse Primer
Fe-protein homolog / iron sulfur cluster carrier protein (Iscc)	5'- TCA CCA TCA C**GG ATC** **C**AT GAC AAG AGT GAT TAC AGT CGC A -3'	5'- TCA GCT AAT T**AA GCT** **T**TC ACC TTC GCC CCA TCA A -3'
Cbs-domain-containing protein	5'- TCA CCA TCA C**GG ATC** **C**AT GAA AGT TAA GGA GAT AAT GGA TAA GG -3'	5'- TCA GCT AAT T**AA GCT** **T**TT ACT TCC TTG CCC TCG C -3'
Methyl coenzyme M reductase I, operon protein C (McrC or McrE)	5'- TCA CCA TCA C**GG ATC** **C**AT GTA CGA AAC TTT AAC CTA TCA GGG -3'	5'- TCA GCT AAT T**AA GCT** **T**TC ACA GTA TGG AGC TTT CAG GTA G -3
Methyl coenzyme M reductase II, operon protein C (MtrC2)	5'- TCA CCA TCA C**GG ATC** **C**AT GAT CGG AAA GTG CAC TCA C -3'	5'- TCA GCT AAT TAA GCT TTC ATG CAC CTC CTA AAG CTA ACT -3'
Flavoprotein	5'- TCA CCA TCA C**GG ATC** **C**AT GAC TGA AAA ACT GAC TGT TGC -3'	5'- TCA GCT AAT TAA GCT TTC ATT GAT CCT TGG GGT AGG -3'
Polyferrodoxin	5'- TCA CCA TCA C**GG ATC** **C**AT GAT AGT TGT CAA CAA AGA GGA CTG -3'	5'- TCA GCT AAT T**AA GCT** **T**TT ATT TCA GTG ACA GTG CAC CC -3'

3.2.3 Cloning of Predicted Iron-Sulfur Falvoprotein (PISF):

The gene coding for Predicted Iron-Sulfur Flavoprotein was cloned into four different expression vectors: pQE-80L, pET28b, GEV-2 and pET-32 EK/LIC.

3.2.3.1 Cloning of *pisf* into pQE-80L and pET-28b vector:

The *pisf* gene was cloned into pQE-80L and pET28b as method described in method 3.2.1 by using primers listed in Table 3.2.

3.2.3.2 Cloning of *pisf* into GEV-2 vector:

The GEV2 vector contains a linker (LVPRGS) with a thrombin cleavage site between the GB1 domain and the N-terminus of the protein of interest (129) (**Fig. 3.6)**. Genes can be inserted between a *Bam*HI site at the 5' end and several possible restriction sites at the 3' end (129). Cloning into the *Xho*I site allows incorporation of a poly His-tag. The gene coding for PISF was generated by amplifying the *pisf* gene directly from *M. marburgensis* genomic DNA by PCR using the forward and the reverse primers containing *Bam*H1 and *Xho*I restriction sites (indicated in table 3.2.) with the high fidelity thermostable DNA polymerase Phusion.The resulting PCR product was digested with *Bam*HI and *XhoI* and ligated into a *Bam*HI-*XhoI*I-digested GEV-2 vector. The recombinant plasmids pQE80-L-*pisf* was transferred into Stellar competent cells by heat shock treatment at 42°C. The integrity of the recovered plasmid was confirmed by restriction endonuclease digestion and sequencing of the *pisf* inserts using a universal T5-promoter primer. For overexpression, The recombinant plasmid GEV-2-*pisf* was transferred into *Rosetta-gami 2(DE3)pLysS* competent cells by heat shock method. Expression generates a recombinant protein

that is tagged at the N-terminus with the GB1 domain of protein G linked via a linear peptide with a Thrombin cleavage site (LVPRGS), and six histidine residues on C-terminus.

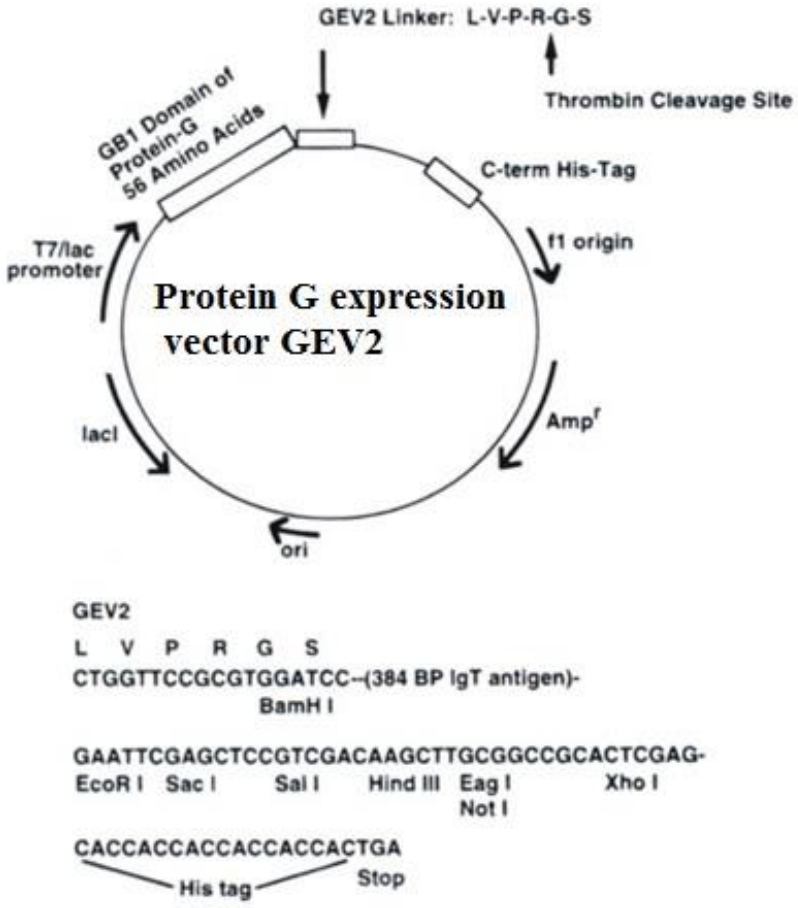

Figure 3.6: Map of the GEV-2 vector.

3.2.3.3 Cloning of *pisf* into pET-32 EK/LIC vector:

The pET-32 Ek/LIC vector is an Ek/LIC version of pET-32b (+) (130). The pET-32 Ek/LIC designed for cloning and high-level expression of target proteins fused with the 109aa Trx•Tag™ thioredoxin protein, His•Tag, and S.Tag coding sequences that are cleavable with enterokinase (Ek) protease (**Fig. 3.7A and B**). The plasmid contains a strong T7*lac* promoter, an optimized RBS, the coding sequence for the Ek protease cleavage site (AspAspAspAspLys↓), and a multiple cloning site to facilitate insert transfer. An optional C-terminal His•Tag coding sequence is compatible with purification, detection, and quantification. LIC is a cloning method that makes use of annealing of single-stranded complementary overhangs on the target vector and a PCR-generated insert of at least 12 bases. Single-stranded overhangs can be generated by using T4 DNA polymerase and only one dNTP in the reaction mix, leading to an equilibrium of 3'->5'-exonuclease and 5'->3'-polymerase activity at the site of the first occurrence of this nucleotide (**Fig. 3.8**). The *pisf* gene specific primers with 12 bp extensions homologous to pET-32 Ek/LIC linear vector at single strands ends were designed as shown in **Table 3.2** and **Figure 3.7**. The desired insert sequence was amplified directly from *M. marburgensis* genomic DNA using appropriately designed PCR primers (**Table 3.1**) and cleaned by QIAquick PCR purification kit (Qiagen). The compatible overhang on the amplified *pisf* was generated with T4 DNA Polymerase in the presence of dATP and DTT. The sample was incubated for 22°C for 30 min to generate the *pisf* overhang. To generate a pET32EK/LIC-*pisf* recombinant plasmid, the *pisf* overhang was simply incubated with linear pETEK/LIC vector at 22°C for 5 min. The recombinant plasmids pET32EK/LIC-*pisf* was transferred into NovaBlue GigaSingles™ competent cells by heat shock treatment at 42°C. The integrity of the recovered plasmid was confirmed by restriction endonuclease digestion and sequencing of the *pisf* insert using a universal T7-promoter primer. For overexpression,

recombinant plasmids were transformed into *Rosetta-gami 2(DE3)pLysS* competent cells by the heat shock method.

A

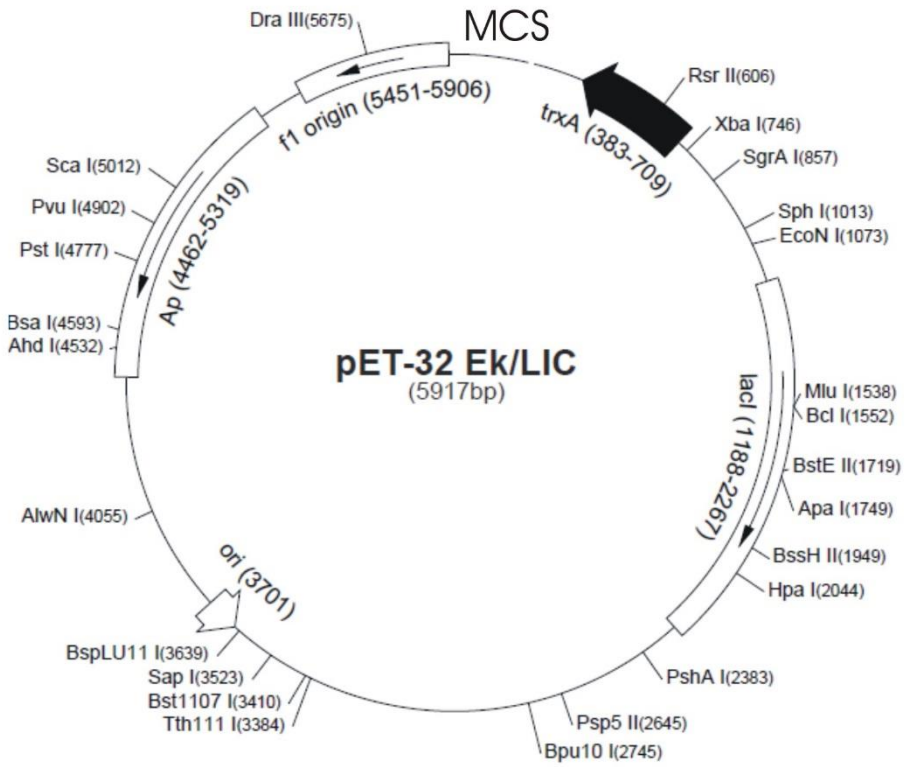

B

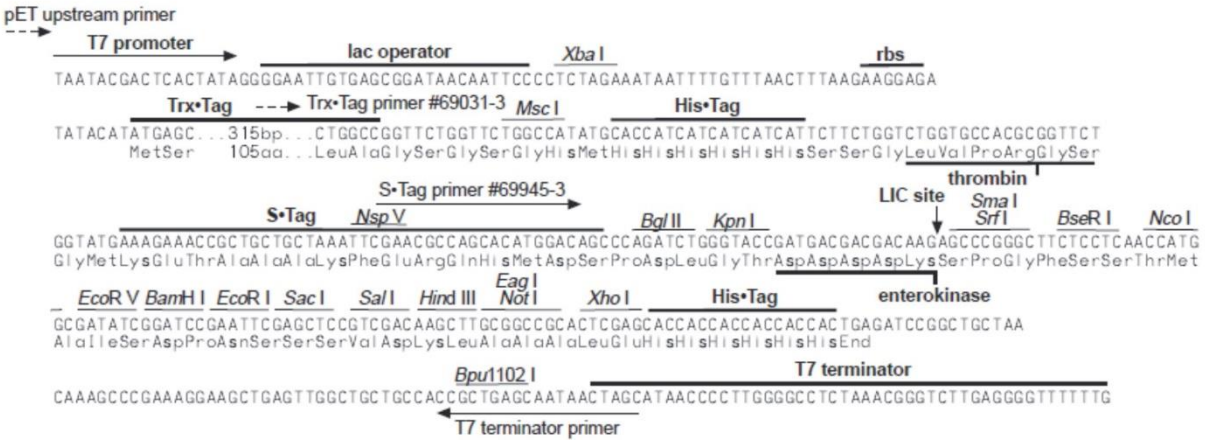

Figure 3.7: Panel A: Map of vector pET-32 Ek/LIC. Panel B: The Cloning/Expression region of pET-32 EK/LIC.

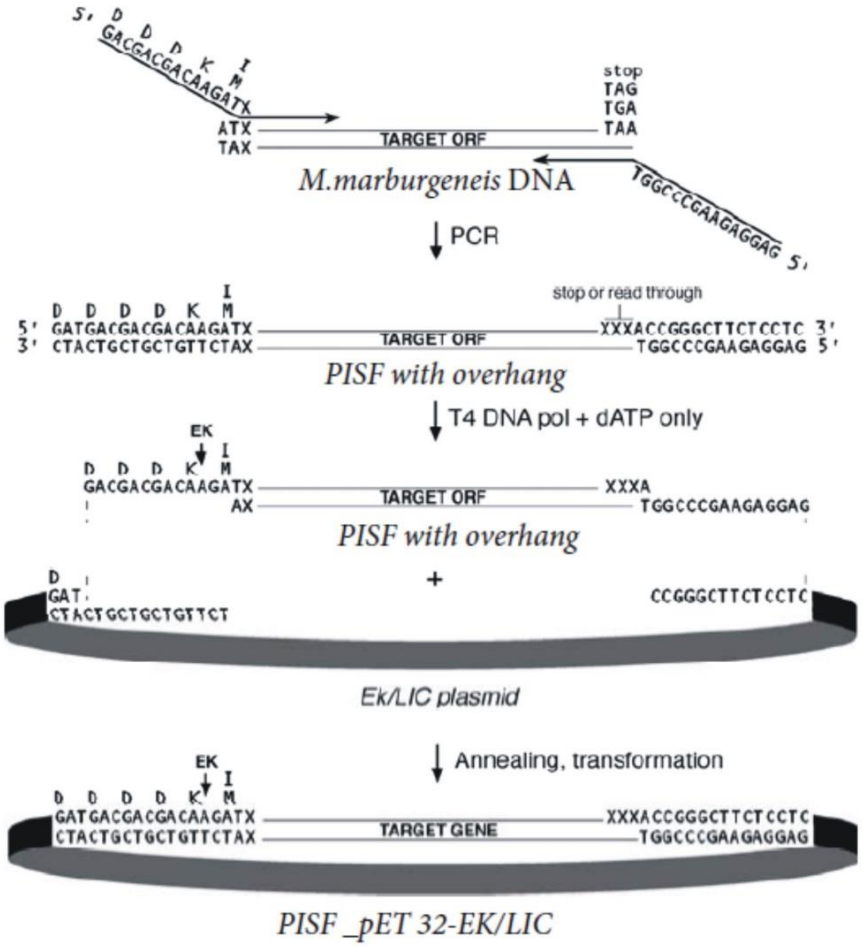

Fig 3.8: Strategy to clone the PISF gene into pET-32 EK/LIC vector.

TABLE 3.2: Tabulation of *pisf* forward and reverse primers.

Description	Forward Primer	Reverse Primer
PISF gene clone into pQE-80L vector	5'- TCA CCA TCA C**GG ATC C**AT GAT ATC TGC AAG TCC AAG GA -3'	5'- TCA GCT AAT T**AA GCT T**TT ACT CCC CGC TTT GAA TCC -3'
PISF gene clone into pET-28b(+) vector	5'- CGC GCG GCA GC**C ATA TG**A TGA TAT CTG CAA GTC CAA GGA -3'	5'- GTG CGG CCG C**AA GCT T**TT ACT CCC CGC TTT GAA TCC -3'
PISF gene clone into GEV-2 vector	CAT **GGA TCC** ATG ATA TCT GCA AGT CCA AGG AA	CAT **CTC GAG** CTC CCC GCT TTG AAT CCT
PISF gene clone into pET-32 EK/LIC vector	5'- GAC GAC GAC AAG ATC ATG ATA TCT GCA AGT CCA AGG AA -3'	5'- GAG GAG AAG CCC GGT TAC TCC CCG CTT TGA ATC C -3'

3.2.4 Expression and purification of Iron Sulfur Cluster Carrier/ Fe-Protein homolog Protein, Methyl coenzyme M reductase I, operon protein C (McrC), Methyl coenzyme M reductase II, operon protein C (MtrC2), Flavoprotein and Cbs-domain-containing protein :

Overexpression and purification of ISCC, Flavoprotein, McrC, MtrC2 and Cbs-domain-containing protein were performed similar to the previously described for the AtwA protein (47). *E. coli Rosetta-gami* cells harboring selective different plasmids were grown in the LB medium supplemented with Ampicillin (100 µg/ml) at 37°C with shaking (at 250 rpm) to an A_{600} of 0.5-0.6; then isopropyl-β-D-thiogalactopyranoside (IPTG) was added to a final concentration of 1 mM. The cells were incubated for a further 5 hours before being lysed to purify recombinant protein. The protein was purified by immobilized metal affinity chromatography using a 5 ml Ni-Sepharose column (GE Healthcare) connected to an Äkta fast protein liquid chromatography (FPLC) system. The cell pellet from a 1 L of *E. coli* DH10B culture harboring the recombinant plasmid was resuspended in 80 ml 50 mM Tris-HCl buffer, pH 8, with 100 mM NaCl (buffer A). Cells were lysed by sonication followed by centrifugation at 20,000 *g* x 30 min at 4°C to collect cell free extract (CFE). The supernatant containing the protein was filtered using a 0.22 µm filter unit and loaded on the Ni-Sepharose column. The protein was then eluted using a linear imidazole gradient from 0% to 100% buffer B containing 50 mM TrisHCl, pH 8, 100 mM NaCl, and 500 mM imidazole. The fractions containing the pure protein were pooled. Imidazole was removed by repeated concentration and dilution steps with buffer A (3x) using a centricon centrifugal filter unit (Millipore) with a cutoff of 10 kDa. The protein concentration was determined by the Bradford assay and the purity was determined by SDS-PAGE and amino acids sequencing.

3.2.5 Expression of Predicted Iron-Sulfur Falvoprotein (PISF) cloned into pQE-80L, pET28b and GEV-2 vector:

Because of insolubility of the PISF protein *E.Coli Rosetta-gami* cells harboring recombinant plasmids (pET32EK-LIC_*Pisf*) were grow at both 37°C and 18°C. It was observed that amount of soluble protein enhance at 18C as compared to 37C. *E. coli Rosetta-gami* cells harboring pET32-EK/LIC-*pisf* plasmid were grown in the LB medium supplemented with Ampicillin (100 µg/ml) at both 37°C or 18°C with shaking (at 200 rpm) to an A_{600} ~ 0.5 at 37°C or ~0.1 at 18°C then isopropyl-β-D-thiogalactopyranoside (IPTG) was added to a final concentration of 1 mM. After 12 hrs cells were harvested at 1000 rpm for 25 min and stored at -80°C.

3.2.6 Purification of Predicted Iron-Sulfur Falvoprotein (PISF) cloned into pQE-80L from inclusion body:

The Pellet from 1 L PISF cells was resuspended in 50 ml of 200 mM NaCl and 50 mM PO_4 buffer (Buffer A). 100 µl of 50 mM of PMSF was added to the cell suspension which was homogenized with a bead beater homogenizer followed by sonication for 3.5 min (42 sec on and off) on ice. 20 µl of benzonae nuclease was added to the sonicated suspension and stirred at RT for 2 h and centrifuged at 10,000 rpm for 15 min. After centrifugation, supernatant was discarded and the pellet was re-suspended in 25 ml of buffer A containing 4 M urea (Buffer B) followed by centrifugation at 10000 RPM for 15 min. Supernatant was loaded Ni-NTA column pre-equilibrated with with Buffer B. Further, the column was washed with 20 mM Imidazole in Buffer B and eluted with 400 mM Imidazole in Buffer A. Eluted fractions were analyzed by 12 % SDS-PAGE.

3.2.7 Expression and purification of Predicted Iron-Sulfur Flavoprotein (PISF) cloned into pET32-EK/LIC vector:

E. coli Rosetta-gami cells harboring pET32-EK/LIC-*pisf* plasmid were grown in the LB medium supplemented with Ampicillin (100 µg/ml) at 18°C with shaking (at 200 rpm). When an O.D of 0.1 (A_{600}) was reached, isopropyl-β-D-thiogalactopyranoside (IPTG) was added to a final concentration of 1 mM. The cells were incubated for a further 12 hours at 18°C before being lysed to purify the recombinant protein. The protein was purified by immobilized metal affinity chromatography using a 5 ml Ni-Sepharose column (GE Healthcare) connected to an Äkta fast protein liquid chromatography (FPLC) system. The cell pellet from a 1 L *E. coli* DH10B culture harboring the pET-32 EK/LIC-*pisf* plasmid was resuspended in 80 ml 50 mM Tris-HCl buffer, pH 8, with 100 mM NaCl (buffer A). Cells were lysed by sonication followed by centrifugation at 20,000 g x 30 min at 4°C to collect cell free extract (CFE). The supernatant containing the protein was filtered using a 0.22 µm filter unit and loaded on the Ni-Sepharose column. The protein was then eluted using a linear imidazole gradient from 0% to 100% buffer B containing 50 mM TrisHCl, P^H8, 100 mM NaCl, and 500 mM imidazole. The purity was determined by SDS-PAGE and amino acid sequencing.

3.2.8 Cleavage and removal of the Thioredoxin (Trx) tag from the fusion Trx-PISF protein:

Similar to native Enterokinase, Recombinant Enterokinase (rEK) recognizes the AspAspAspAspLys↓, cleavage site. The Enterokinase Cleavage Capture Kit is designed for highly specific cleavage of fusion proteins followed by the rapid affinity-based capture and removal of rEK. Following cleavage of the target protein, rEK is removed from the reaction with > 99% efficiency by affinity capture on EKapture™ Agarose. The EKapture Agarose is then removed by

spin-filtration. Optimization of rEK against PISF was performed at small scale by incubating different concentration of the PISF (10 µg, 20 µg and 30 µg) with 5 µl of 10X rEK cleavage buffer, 1 µl of diluted rEK (I unit/µl) to the final volume to 50 µl at room temperature. 10 µl of samples was removed at 16 h for SDS-PAGE analysis.

3.2.9 Fe-determination of PISF:

The iron determination was carried out with a rapid ferrozine-based colorimetric method. Protein samples used for the iron determination were run over a Chelex column (Bio-Rad) to remove adventitiously bound iron. All containers and pipette tips used for this determination were repeatedly soaked in boiling 1 M HCl and washed with ultra-pure water. The iron standards (0, 10, 20, 30, 40, 50 µM) were made by dissolving ferrous ethylenediammonium sulfate in 0.01 M HCl. Iron releasing reagent (0.5 ml–containing equal amounts of 0.6 M HCl and 0.142 M potassium permanganate) was added to both the iron standard samples and the protein samples (1 ml). The samples were incubation at 60 °C for 2 hrs. The samples were centrifuged to remove precipitated protein. The iron chelating and reducing reagent was added to the samples (0.1 mL -containing 6.5 M ferrozine, 13.1 mM neocuprine, 2 M ascorbic acid, and 5 M ammoniumacetate), which were incubated for at least another 30 minutes. The absorbance at 562 nm was recorded for creation of the standard curve and determination of the iron concentration in the protein samples.

3.2.10 ATP-affinity Column:

The ATP Affinity Test Kit contains a set of 4 typical ATP-Agarose chromatography materials and blank Agarose for negative control: Aminophenyl-ATP-Agarose, C10-spacer (*APATP-Agarose*), 8-[(6-Amino) hexyl]-amino-ATP-Agarose (*8AHATP- Agarose*), N6-(6-

Amino) hexyl-ATP-Agarose (*6AH-ATPAgarose*), 2'/3'-EDA-ATP-Agarose (*EDA-ATPAgarose*), and *Agarose* (blank) (**Fig. 3.9**). With these four materials, the ideal material for purification of a particular protein of interest can be identified in a simple screening experiment. In *6AH-ATP-Agarose* and *8AH-ATP-Agarose* the ATP is immobilized via the adenine base but varies by the actual position of the linker (C6 and C8, respectively). *AP-ATP-Agarose* and *EDA-ATPAgarose* are phosphate and sugar modified derivate, respectively.

The binding affinity of A2 protein with different types of ATP-Agarose column were tested. 50 µl of ATP-agarose beads were transferred to 1.5 ml centrifuge tube and equilibrated three times with 500 µl of 1x wash buffer (Hepes, NaCl, $MgCl_2$, and 0.25% NP-40, 200 mM Sodium Orthovanadate, 100 mM DTT and 100x Protease Inhibitor Mix) by centrifuging the tube at 1000 g for 1 min and 0.5 ml of A2 protein was mixed with equilibrated ATP-agarose and incubated at 4°C for 2-3 hours by slight agitation for binding. After, 3 hours of incubation, the resin was washed three times with 500 µl of 1 X wash buffer to remove non-specifically bound protein to the resin. After washing, A2 protein were eluted two times with 150 µl 1X elution buffer (Hepes, ATP, and 0.25% NP-40, 200 mM Sodium Orthovanadate, 100 mM DTT and 100x Protease Inhibitor Mix) by spinning the column at 1000g for 1 min.

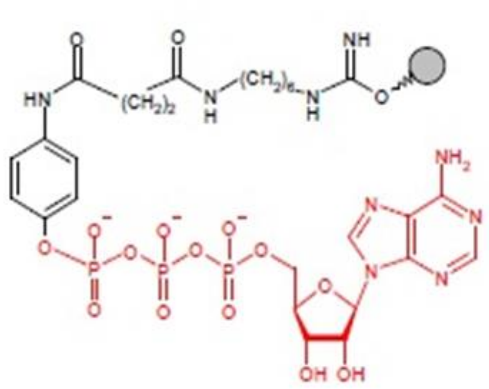

AP-ATP-Agarose

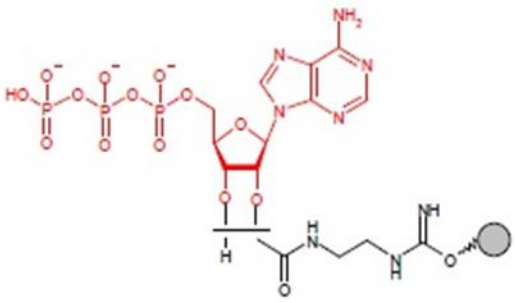

EDA-ATP-Agarose

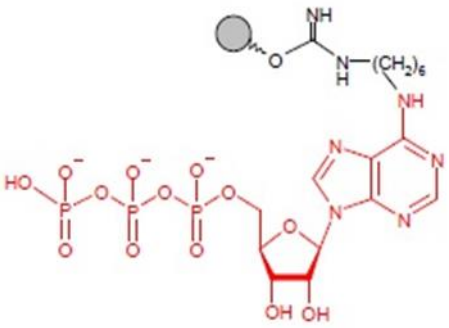

6AH-ATP-Agarose

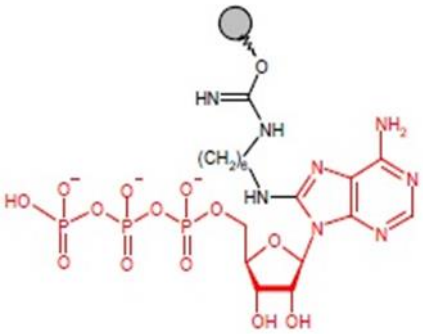

8AH-ATP-Agarose

Fig: 3.9: Structure of the different ATP-Agarose materials.

3.2.11 A2 Pull down assay:

Pull-down assays probe potential interactions between proteins of interest (e.g., bait) and the potential interacting partners (prey).

A2 pull down assay with *M. marburgensis* cell extract:

6xHis-A2 (bait protein) was purified as mentioned in **section 2.2.6**. Imidazole was removed by repeated (2X) concentration and dilution steps with 30 mM Tris-HCl, 100 mM NaCl and 10mM ATP (buffer A) using a Centricon centrifugal filter unit (Millipore) with a cutoff of 10 kDa. 6xHis-A2 protein was then immobilized to the Ni-NTA column. This forms a complex, a ″secondary affinity support″, which is then incubated with *M. marburgensis* cell lysate (source of Prey protein) dissolved in Buffer A containing 10 mM ATP, 400 mM $MgCl_2$ for 12 hours. The protein was then eluted using a linear imidazole gradient from 0% to 100% buffer B containing 50 mM TrisHCl, pH 8, 100 mM NaCl, 10 mM ATP, 400 mM $MgCl_2$ and 500 mM imidazole. The fractions containing the pure A2 protein were pooled and analyzed by SDS-PAGE and de-nova sequencing for the possible prey protein.

A2 pull down assay with Predicted Iron-sulfur flavoprotein, Iron Sulfur Cluster Carrier/ Fe-Protein homolog Protein, Methyl coenzyme M reductase I, operon protein C (McrC) , Methyl coenzyme M reductase II, operon protein C (MtrC2), Flavoprotein and Cbs-domain-containing protein:

Bait protein (6xHis-A2) and potential prey proteins (Predicted Iron-sulfur flavoprotein or Iron Sulfur Cluster Carrier/ Fe-Protein homolog Protein or Methyl coenzyme M reductase I or operon protein C (McrC) or Methyl coenzyme M reductase II or operon protein C (MtrC2) or Flavoprotein or Cbs-domain-containing protein) were purified as mentioned in section 2.2.6.

Imidazole was removed by repeated (3x) concentration and dilution steps with 30 mM Tris-Hcl, 100 mM Nacl and 10mM ATP (buffer A) using a Centricon centrifugal filter unit (Millipore) with a cutoff of 10 kDa. Then the 6xHis-A2 protein was immobilized to an ATP-agarose column. This forms a complex, a ″secondary affinity support″, which is then incubated with source of Prey protein for 12 hours. After, 12 hours of incubation, the proteins of interest were washed three times with 500 ul of 1 X wash buffer to remove non-specifically bound protein to the resin. After washing the proteins of interest were eluted with 150 ul 1X elution buffer (HEPES, ATP, and 0.25% NP-40, 200 mM Sodium Orthovanadate, 100 mM DTT and 100x Protease Inhibitor Mix) by spinning the column at 1000g for 1 min. The eluted fraction was analyzed by SDS-PAGE to observe the possible prey protein binding to the A2 (bait) protein.

3.2.12 ATP hydrolysis assay:

The BIOMOL® GREEN Reagent was used for measuring free-phosphate released during enzymatic phosphatase assays (at A_{620} nm). It is a modification of the classic Malachite green reagent. The phosphate standards (0, 10, 20, 30, 40, 50 nmol) were prepared by serial dilution of a stock phosphate standard (BML-KI102) in 50 mM tris-HCl buffer. Protein samples used for ATPase activity was incubated with 10 mM ATP, 400 mM $MgCl_2$ for 20 min at RT. Further, 1 ml of BIOMOL® Green reagent was added to 100 µl of standards and protein samples. Addition of BIOMOL® Green stopped the reaction and begins color development, which was read 20-30 min. later. The absorbance at 620 nm was recorded for creation of the standard curve and determination of the phosphate concentration in the protein samples.

3.2.13 Activation of different forms of MCR:

100 µM MCR was incubated for 15 min at 60°C in the presence of 100 µM component A2, 20 µM PISF, 20 µM Fe-Protein homolog, 20 µM Flavoprotein, 20 µM McrC, 20 µM MtrC2, 20

μM Cbs-domain-containing protein, 10 mM MgATP, 5 mM dithiothreitol and 10 mM methyl-coenzyme.

3.3 Results:

3.3.1 Cloning of the iron-sulfur-cluster carrier/Fe-protein homolog protein, methyl-coenzyme M reductase I operon protein C (McrC), methyl-coenzyme M reductase II operon protein C (MtrC), flavoprotein, CBS-domain-containing protein:

Specific primers for the *iscc*, *cbs-domain-containing protein*, *flavoprotein*, *mcrC*, *polyferredoxin* and *mtrC* genes with 15 bp extensions homologous to the pQE-80Lvector at *Bam*H1 and *Hind*III ends were designed as shown in **Table 3.1.** The desired insert sequences were amplified directly from *M. marburgensis* genomic DNA using appropriately designed PCR primers (**Table 3.1.**) with the high fidelity thermostable DNA polymerase Phusion. Amplified *iscc*, *cbs-domain-containing protein*, *flavoprotein*, *mcrC* and *mtrC* were analyzed by 1.5% agarose gel electrophoresis (**Fig. 3.10, panel A**) and *polyferredoxin* was analyzed by 0.8 % agarose gel electrophoresis (**Fig. 3.10, panel B**). Agarose gel analysis showed a single band for all amplified products except *cbs-domain-containing.* Therefore, the band corresponding to the *cbs-domain-containing* gene was cut out and purified using a DNA Agarose gel Extraction kit. The amplified gene products was treated with cloning enhancer and ligated in the presence of In-Fusion enzyme to generate a protein that is tagged at the N-terminus with six histidine residues. The integrity of the recovered plasmid was confirmed by restriction endonuclease digestion and sequencing of the gene containing insert pQE-80L plasmids using the T5- promoter primer.

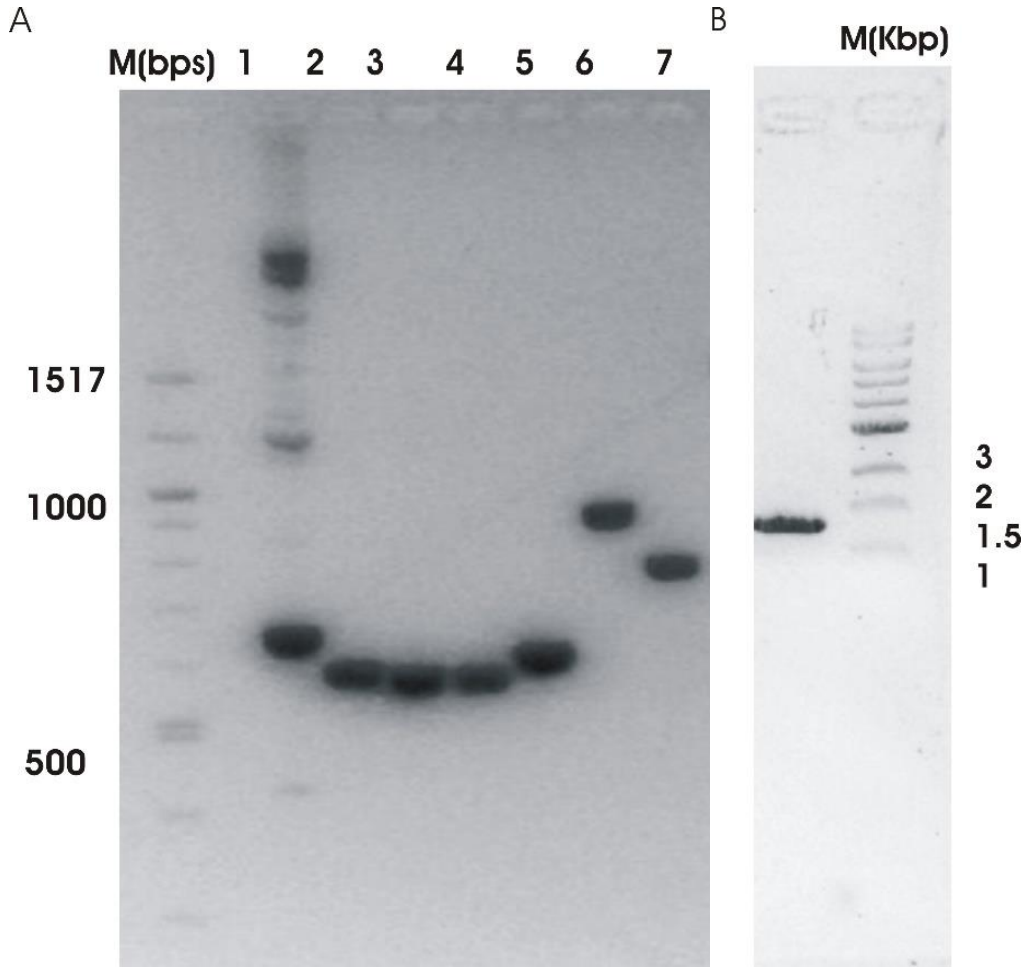

Fig: 3.10: Agarose gel DNA electrophoresis profile of PCR amplified fragments *iscc, cbs-domain-containing, flavoprotein, McrC, polyferredoxin* and *mtrc2.* Panel A, 1.5 % agarose gel profile Numbers in figure indicate: 1. *cbs-domain-containing (716 bps)*, 2. *Flavoprotein (648 bps)*, 3. *Pisf (635 bps), 4. Pisf (635 bps), 5. mtrc (673 bps) and 6. McrC(997 bps*). **Panel B.** 0.8 % agarose gel profile: *F_{420}-non reducing hydrogenase, polyferredoxin* (1.3 Kbps).

3.3.2 Cloning of *pisf* into pET-32 EK/LIC vector:

The *pisf* gene specific primers with 12 bp extensions homologous to the pET-32 Ek/LIC linear vector at single strands ends were designed as shown in **Table 3.2** and **Fig. 3.7**. The desired insert sequences were amplified directly from *M. marburgensis* genomic DNA using appropriately designed PCR primers (**Table 3.2**) with the high fidelity thermostable DNA polymerase Phusion. The amplified gene was analyzed by 1 % agarose gel electrophoresis (**Fig. 3.11**). The amplified gene products was inserted into a pET-32EK/LIC vector using an EK/LIC ligating mixture. The integrity of recovered recombinant pET-32 EK/LIC_*pisf* plasmid was confirmed by restriction endonuclease digestion of recombinant pET-32 EK/LIC_*pisf* plasmid at XbaI and BamH1 restriction sites. Including the attached thioredoxin, the size of the insert is 936 bps (635 bps pisf + 301 bps Trx), however, restriction digested fragment showed a larger size above 1 kbp, because the XbaI restriction site is far from the N-terminal region of Thioredoxin (**Fig. 3.6 B).** The integrity of the clone was also confirmed by sequencing of the pET-32EK/LIC_*Pisf* plasmids using a T7-promoter primer.

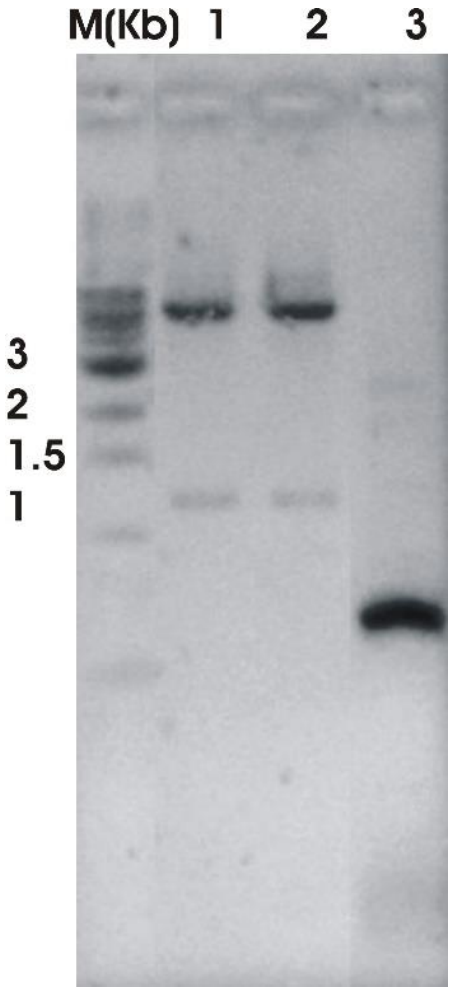

Fig.3.11: Cloning of Predicted Iron Sulfur Flavoprotein (pisf) gene. 1% agarose gel profile of restriction digestion of the *pisf* clone at the XbaI and BamHI sites (number 1 and 2) and amplified *pisf* gene (number3).

3.3 Purification of iron-sulfur-cluster carrier/Fe-protein homolog protein, methyl-coenzyme M reductase II operon protein C (MtrC) and CBS-domain-containing protein:

The proteins were individually overexpressed in *E. coli* and purified from the cell extract using a Ni-Sepharose column. The purity of the proteins was determined by SDS-PAGE (**Fig. 3.12**). The purity level of the purified proteins was estimated to be 85% or higher based on the band patterns on the gel. The protein concentration of each sample was determined using the Bradford assay. As indicated in panel A, MtrC showed a prominent band at 34Kda and CBS domain containing protein showed a prominent band at 23 kDa. Fe-Protein homolog or Cluster carrier showed the prominent band at 27 kDa (panel B).

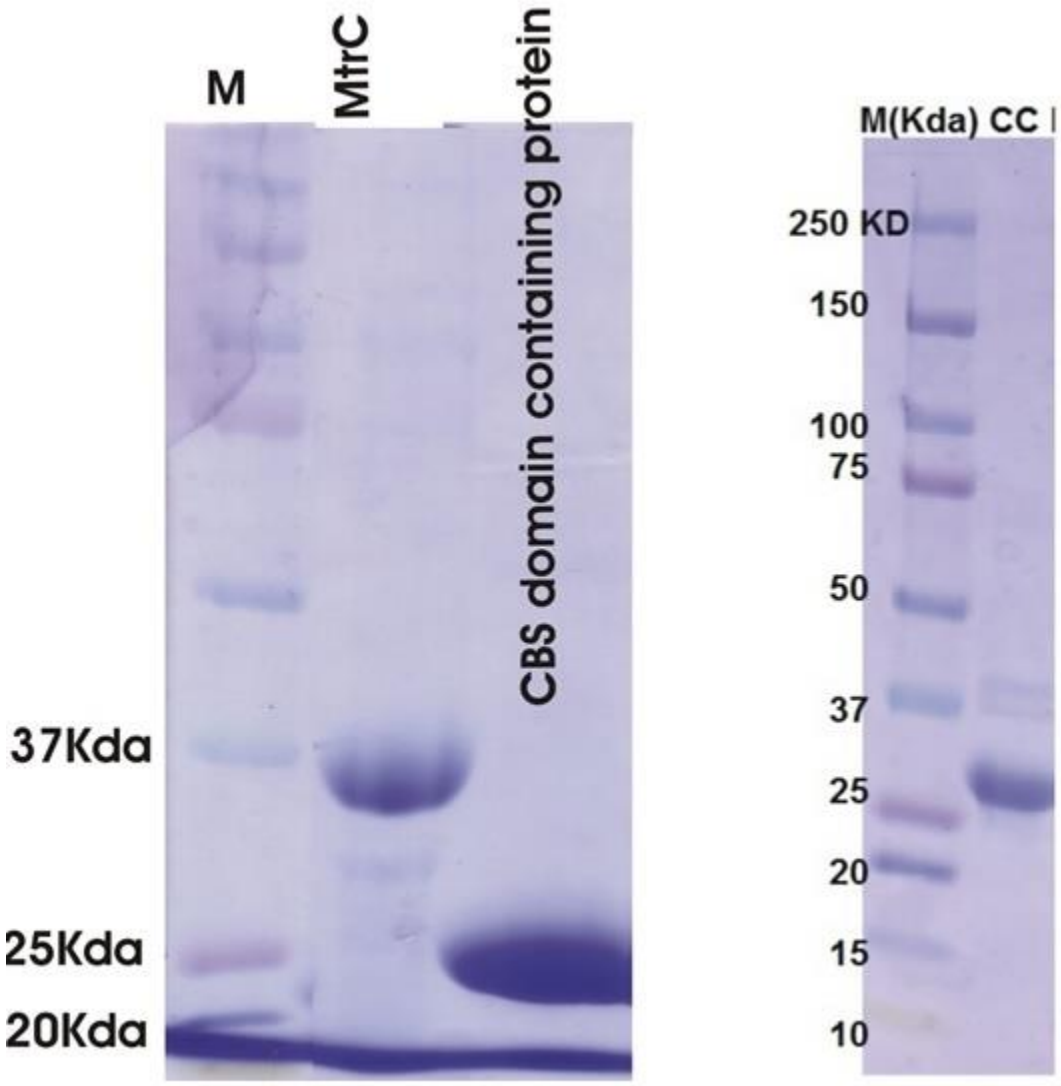

Fig.3.12: SDS-PAGE analysis of the Methyl coenzyme M reductase II, operon protein C (MtrC) and the CBS-domain-containing protein (Panel A) and Iron Sulfur Cluster Carrier/ Fe-Protein homolog (panel B). Proteins after the Ni-NTA column steps were denatured in sample buffer at 95°C for 5 min and loaded onto a 12 % polyacrylamide gel. The gel was stained using coomassie brilliant Blue R-250 I (Bio-Rad).

3.3.4 Purification and characterization of Methyl-coenzyme M reductase I operon protein C (McrC):

The McrC was overexpressed in *E. coli* and purified from the cell extract using a Ni-sepharose column. The purity of the protein was determined by SDS-PAGE. A prominent band is detected at the expected molecular weight of 21 kDa (**Fig. 3.13**). The purity of the protein was estimated to be 90%. The protein concentration was determined by the Bradford assay**.**

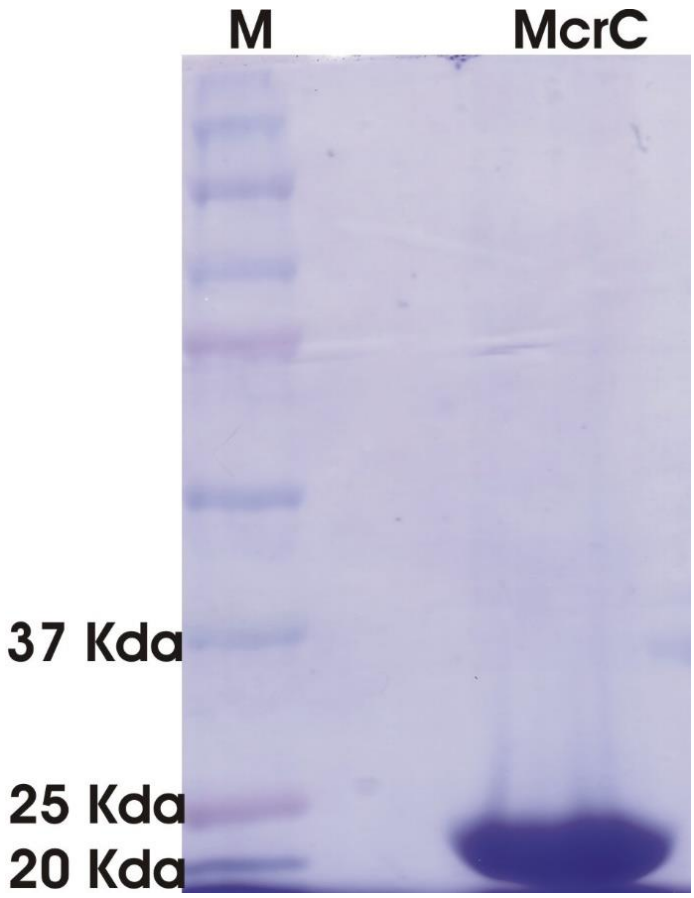

Fig.3.13: SDS-PAGE analysis of, the Methyl coenzyme M reductase I, operon protein C (McrC). Protein fractions after the Ni-sepharose column step was denatured in sample buffer at 95°C for 5 min and loaded onto a 12 % polyacrylamide gel. The gel was stained using coomassie brilliant Blue R-250 I (Bio-Rad).

Although the sequence analysis of McrC does not indicate the consensus sequence for an Fe-S cluster, purified McrC protein was brown in color. Therefore, it was further characterize by electronic absorption spectroscopy to explore the possibility of the presence of an Fe-S cluster. As indicated in **Fig. 3.14**, overexpressed purified McrC has a sharp absorption band around 320 nm and a small band at 420 nm. This type of spectra was observed by Dr. Weiya Xu for the iron-sulfur-cluster containing LytB protein. The unstable [4Fe-4S] cluster fell apart in the presence of oxygen resulting in the appearance of an absorption band at 320 that was assigned to single Fe-ion still bound in the original cluster sites. These Fe-ions could be easily removed by passage of the protein samples through a Chelex column. It is possible that McrC contains a cluster which is not stable and easily damaged due to the presence of oxygen. Although the purification of the protein was done in the Coy anaerobic chamber no particular methods were applied to remove any residual oxygen in the cells/cell pellets before cell disruption.

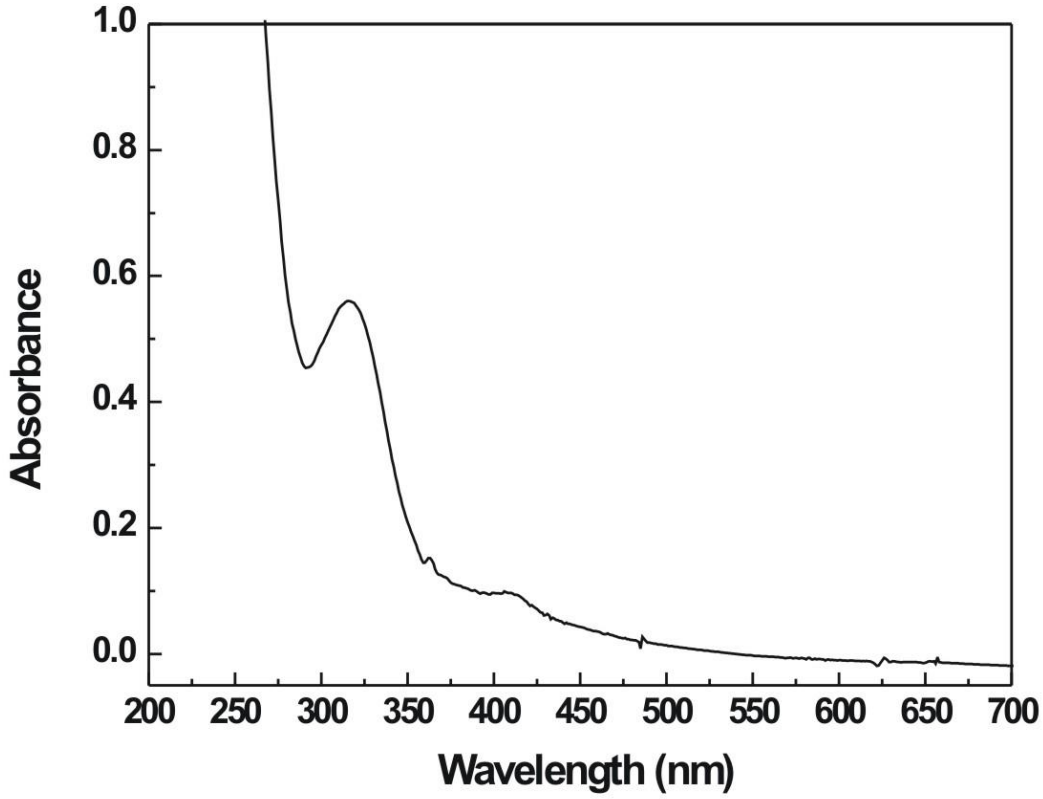

Figure 3.14: UV-VIS absorption spectra of the McrC.

3.3.5 Purification and characterization of Flavoprotein:

The flavoprotein was overexpressed in *E. coli* and purified from the cell extract using a Ni-sepharose column. The purity of the protein was determined by SDS-PAGE. A prominent band is detected at the expected molecular weight of 22 kDa (**Fig. 3.15**). The purity of the protein was around 95%. The protein concentration was determined by the Bradford assay.

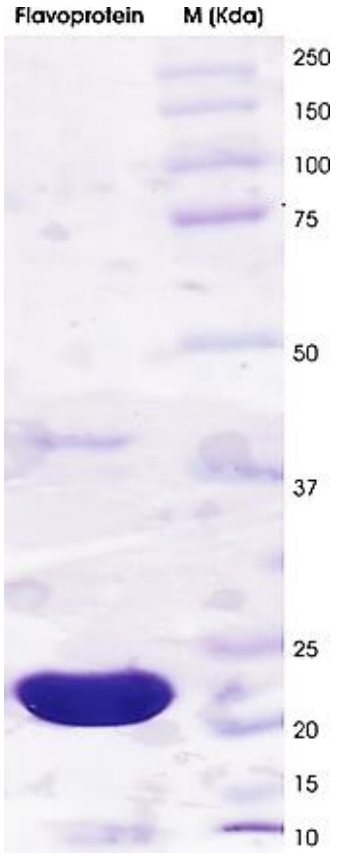

Fig.3.15: SDS-PAGE analysis of the flavoprotein. Protein fractions after the Ni-NTA column steps were denatured in sample buffer at 95°C for 5 min and loaded onto a 12 % polyacrylamide gel. The gel was stained using coomassie brilliant Blue R-250 I (Bio-Rad).

The flavoprotein protein displayed a yellow color and the electronic absorption spectrum revealed an absorbance maxima at 380 and 460 nm corresponding to an anionic flavin semiquinone radical and oxidized flavin respectively.The Absorption maximum at 360 nm indicate that anaerobically purified flavoprotein exhibits stoichiometric amounts of free radical. After reduction with dithionite the absorption peaks at 380 and 460 nm disappeared, a property characteristic for proteins containing flavins (**Fig. 3.16**).

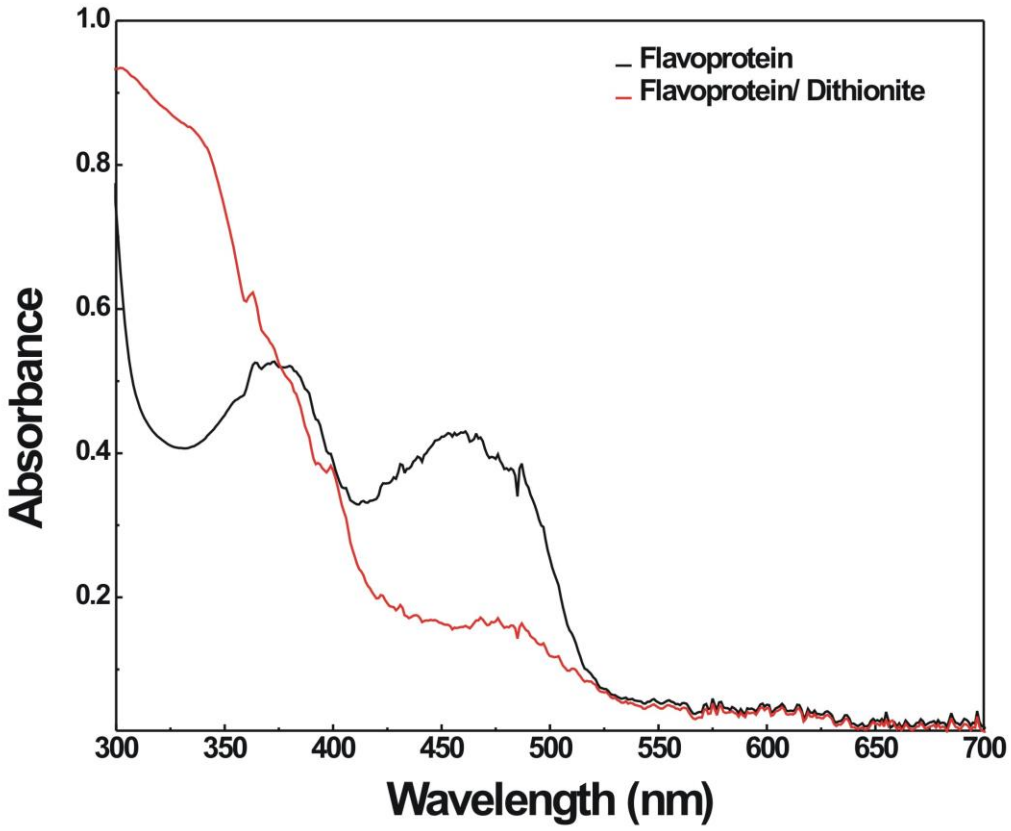

Figure 3.16: **UV-VIS absorption Spectra of the Flavoprotein.** 40 µM Purified Flavoprotein was incubated with 30 mM of Dithionite.

3.3.6 Purification of the predicted iron-sulfur flavoprotein (PISF) cloned into pQE-80L and GEV-2:

Overexpressed PISF protein cloned into the pQE-80L, pET28b (+) or GEV-2 vectors formed inclusion bodies. The PISF protein was purified from the inclusion bodies in the presence of 4 M urea. As shown in **Fig. 3.17**, the PISF protein eluted as a single band at around 20 kDa on SDS-PAGE after purification on a Ni-NTA column. SDS-PAGE profile indicates that the purified PISF protein was 90% pure. The expression level of PISF was very high (**as indicated in Fig. 3.17**) even though it was expressed from a T5 promoter. Attempts were made to refold the purified protein by dialysis against the following types of buffers: a) 50 mM Tris-HCl pH 8.0, 0.1 M NaCl, 500mM Imidazole and 5 mM DTT, b) 50 mM Tris-HCl pH 8.0, 1 M NaCl and 5 mM DTT, c) 50 mM Tris-HCl pH8.0, 1 M NaCl, 5 mM DTT and 10 % Glycerol at 4°C and in anaerobic condition. PISF was not stable under these conditions. Generally PISF started to precipitate within 60 min. An additional attempt to refold the denatured protein was by using refolding buffer containing 50 mM Tris-HCl, pH 8.0, 5 mM reduced gluthione, 0.5 mM glutathione disulfide, 5 mM DTT and 10 % Glycerol.

In a final attempt it was decided to use a fusion protein to improve the solubility of PISF. Two fusion protein containing vectors were used to improve solubility. GEV-2 (GB1 domain of protein G (5 kDa)) and pET-32EK/LIC (Thioredoxin (12 kDa)). No improvement in solubility of PISF was observed by cloning using the GEV-2 vector. The PISF-Thioredoxin fusion protein turned out to be expressed as a cytosolic enzyme and could easily be purified using a Ni-NTA column.

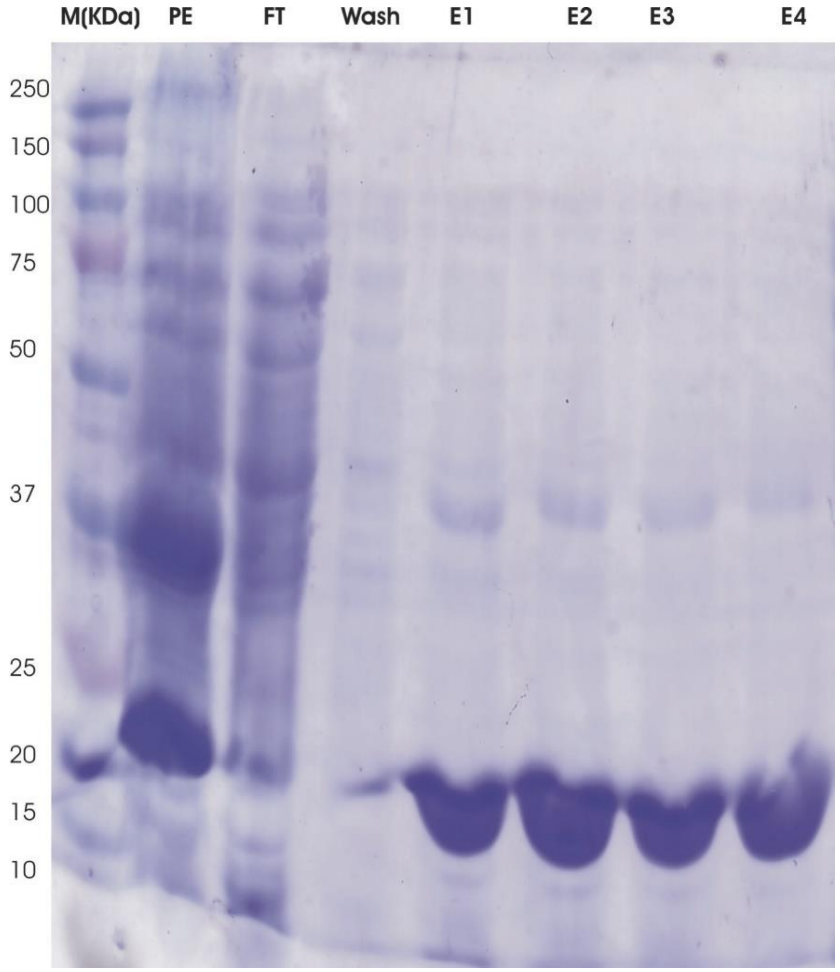

Figure 3.17: SDS-PAGE analysis of the purified PISF protein from inclusion bodies. Protein fractions after the Ni-NTA column steps were denatured in sample buffer at 95°C for 5 min and loaded onto a 12 % polyacrylamide gel. The gel was stained using coomassie brilliant Blue R-250 I (Bio-Rad). PE: pellet, FT: Flow through, Wash, E1-E4: different elution fractions.

3.3.7 Purification of the predicted iron-sulfur flavoprotein cloned into pET-32EK/LIC:

Addition of Thiredoxin fusion partner via enterokinase cleavage site containing peptide (AspAspAspAspLys↓) to PISF protein helped to improve the solubility of PISF protein. Further, quantity and purity of soluble protein enhanced by growing the cells at 18°C as compared to normal growth temperature (37°C). **Fig. 3.18** show the SDS-PAGE purification profile of (TRX-PISF) protein overexpress at 18°C.

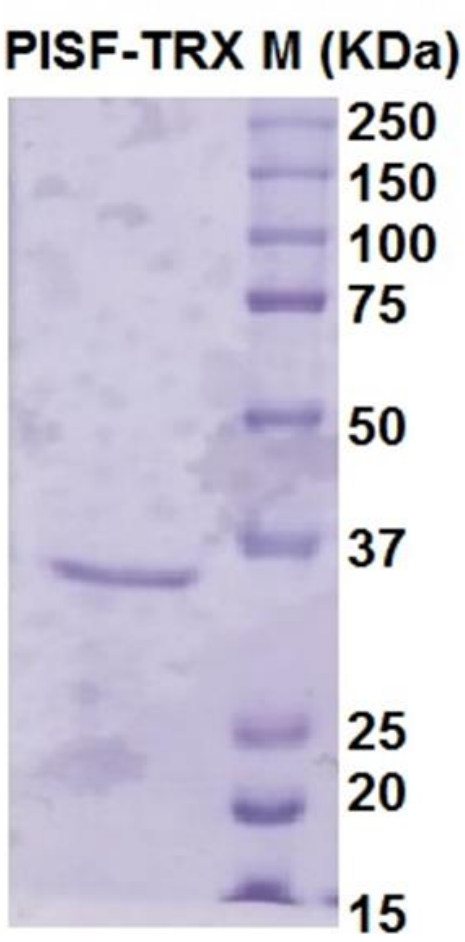

Fig. 3.18: SDS-PAGE analysis of the PISF protein cloned into pET-32EK/LIC. Protein fractions after the Ni-NTA column steps were denatured in sample buffer at 95°C for 5 min and loaded onto a 12 % polyacrylamide gel.

3.3.8 Cleavage of Thioredoxin (Trx) tag from fusion Trx-PISF protein:

The thioredoxin tag from the fusion protein Trx-PISF was removed by incubating the protein for 16 h with recombinant enterokinase (rEK). As shown in **Fig. 3.19**, the fusion protein Trx-PISF shows a prominent band at 36 kDa and after incubation with rEK, there are two bands detectable with less intensity. The bands at around 20 kDa and 16 kDa correspond to respectively PISF and Trx. Most of the thioredoxin tag attached PISF protein precipitated during the incubation with enterokinase cleavage reaction, hence activation of MCR was tested without removing the thioredoxin tag from purified TRX-PISF protein.

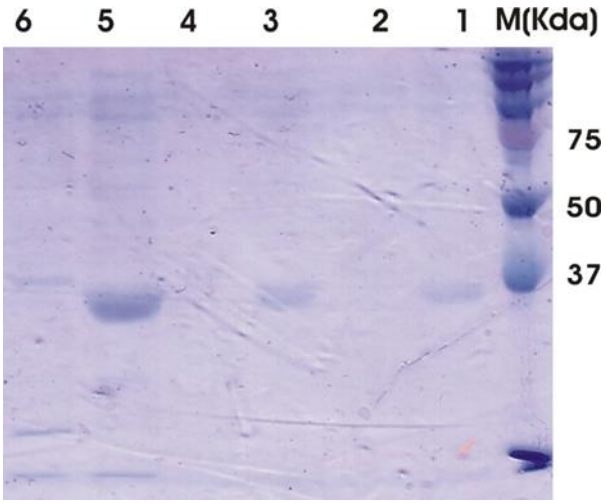

Fig. 3.19: SDS-PAGE analysis of the fusion Trx-PISF protein after incubating with eEK for 16 hrs. Protein after the Ni-NTA column step was incubated with rEK for 16h and further denatured in sample buffer at 95°C for 5 min and loaded onto a 12 % polyacrylamide gel. The number in the gel indicate the following **1**:10 µg, **3**: 20 µg, **5** : 30 µg of untreated TRX-PISF while **2**, **4** and **6** indicate the same amounts of TRX-PISF treated with rEK.

3.3.9 Characterization of the PISF-Trx fusion protein:

The absorption spectra of the purified PISF-Trx fusion protein showed a broad absorption maxima at 420 nm unlike typical iron-sulfur flavoprotein (ISF) that usually exhibit absorption maximum at 410 or 420 nm (corresponding to Fe-S center) and 360, 480 nm (corresponding to the Flavin center). The absorption maximum at 420 nm decreased in the presence of dithionite (**Fig. 3.20**). This is typical for the presence of either a [3Fe-4S] or [4Fe-4S] cluster. The percentage iron content of protein was 51.39±12.83. Cluster content in case of [4Fe-4S] cluster is 12.84±3.20.

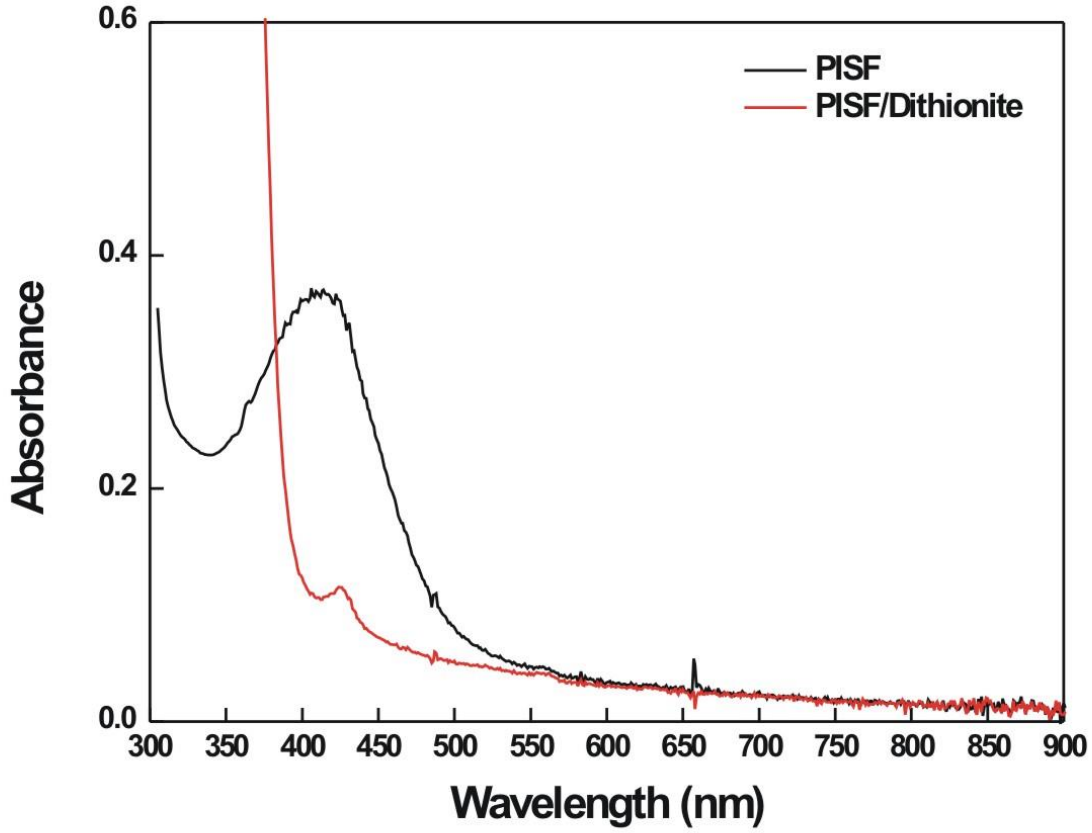

Fig: 3.20: **UV-VIS absorption Spectra of the predicted iron-sulfur flavoprotein.** 40 µM Purified PISF protein was incubated with 30 mM of Dithionite for Uv-Vis analysis.

The EPR spectrum of the PISF-Trx fusion protein in the presence of dithionite does not display any peaks that can be assigned to a 4Fe cluster. It is possible that the reduced form of the cluster is unstable in the absence of other activating components (**Fig.3.21**).

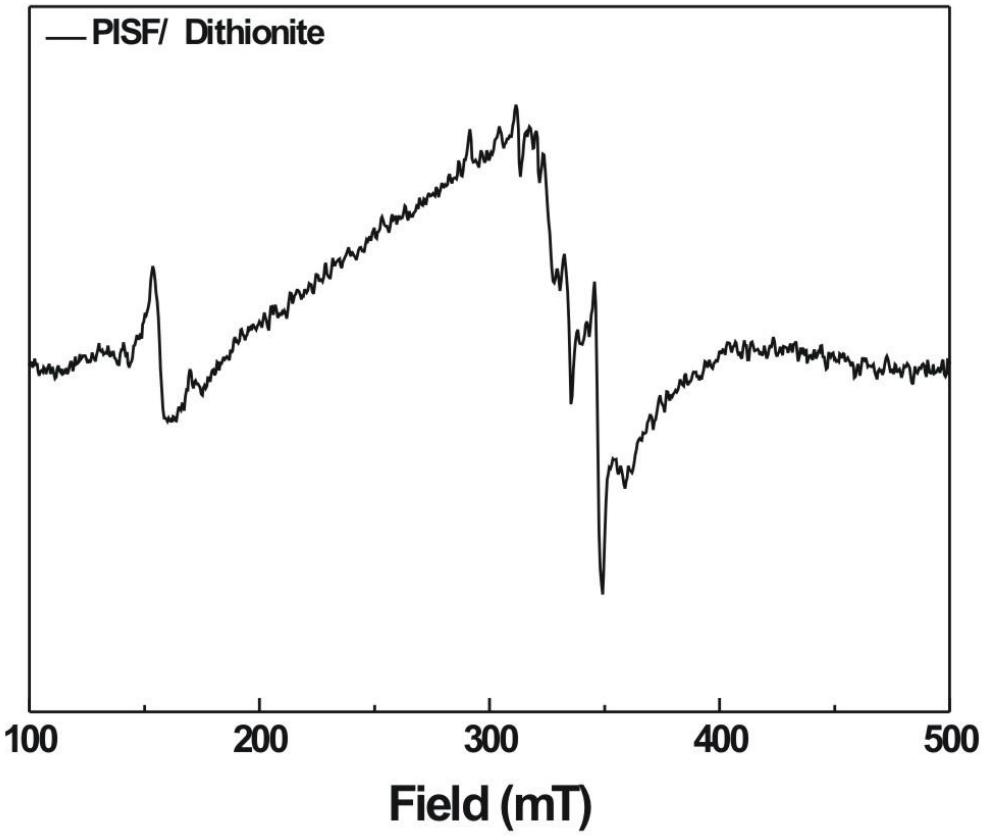

Fig. 3.21: EPR spectroscopy of the purified reduced PISF. 100 µM of PISF was incubated with 30 mM of Dithionite to reduce the Fe-S center for the EPR analysis.

3.3.10 Activation of MCR in the presence of overexpressed A2a and A3a protein:

As indicated in **Fig. 3.22** and **Table 3.3** , no increase in activity was observed when the as-such form of MCR that contains mostly the silent form was incubated with all the activating A3a components in the presence of dithionite as an electron source. Activation of MCR was observed only when Ti(III) citrate was used as an electron source for the activation (Samples C and D). Methane formation increased almost two fold as compared to control when Ti(III) citrate was used as an electron source with the different A3a protein components. There was no significant increase in activity of activated MCR when also Flavoprotein and the CBS-domain-containing protein were added in addition to PISF, McrC and the Fe protein homolog. It indicates that both the Flavoprotein and the CBS domain containing proteins are probably not involved in the activation of MCR.

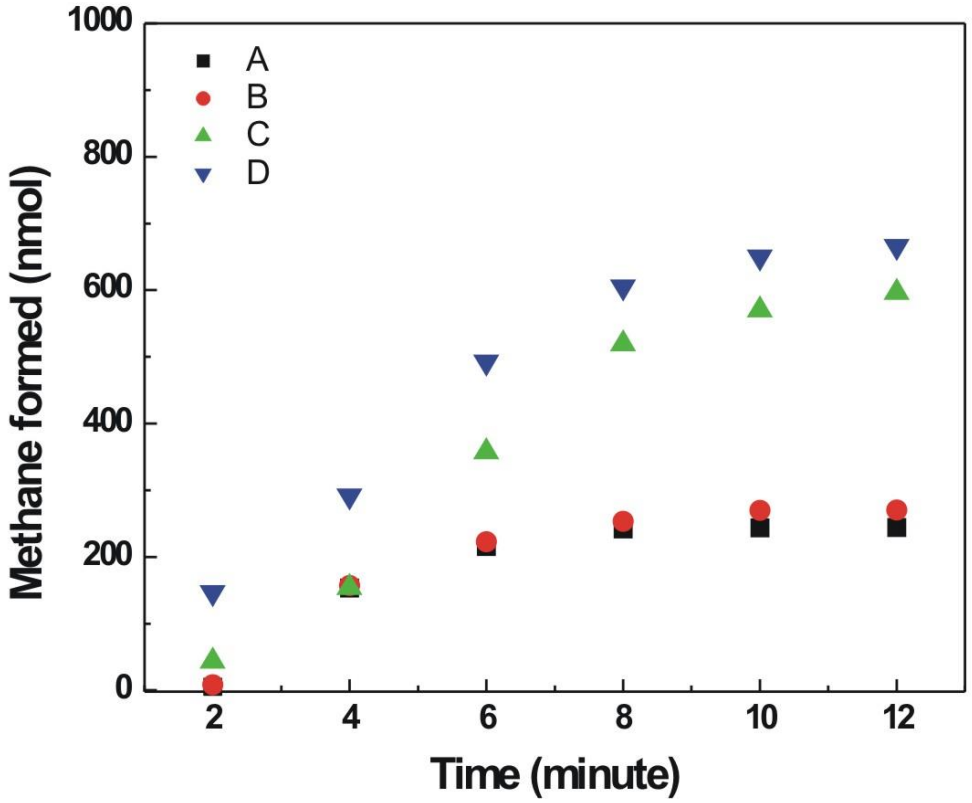

Fig.3.22: Methane formation from 400 µl of assay solution containing 10 mM MCoM, 1mM CoB, 25 mM Ti (III)Citrate, 0.3 mM Hydroxycobalamine and containing 1.1 mg of MCR **A)**.treated with 6 mM Ti(III) Citrate, **B)**.treated with 6 mM Dithionite with 100 µM component A2, 20 µM PISF, 20 µM Fe-Protein homolog, 20 µM Flavoprotein, 20 µM McrC, 20 µM MtrC2, 20 µM Cbs-domain-containing protein, 10 mM MgATP, and 10 mM methyl-coenzyme at 60°C for 15 min . **C).** treated with 6 mM Ti(III) Citrate with 100 µM component A2, 20 µM PISF, 20 µM Fe-Protein homolog, , 20 µM McrC, 10 mM MgATP, and 10 mM methyl-coenzyme at 60°C for 15 min. **D).** treated with 6 mM Ti(III) Citrate with 100 µM component A2, 20 µM PISF, 20 µM Fe-Protein homolog, 20 µM Flavoprotein, 20 µM McrC, 20 µM MtrC2, 20 µM Cbs-domain-containing protein, 10 mM MgATP, and 10 mM MCoM at 60°C for 15 min.

Table 3.3: Activity displayed as nmol/min/mg for the different samples.

Comments	Activity (nmol/min)
Sample A	38.75
Sample B	40.06
Sample C	81.54
Sample D	78.81

Description of samples A,B, C and D are in Fig. 3.22.

3.3.11 ATP hydrolysis assay:

According to our postulated model of activation, the A2 protein donates ATP to the Fe-protein homolog and hydrolysis of ATP occurs by the Fe-protein homolog to generate a low potential electron to reduce the Ni center in MCR. To study this effect in more detail it is important to find out what combination of proteins is needed to stimulate the ATP hydrolysis. As shown in **Fig. 3.23**, there was no phosphate released when the Fe-Protein homolog was incubated with ATP, however, there was ATP hydrolysis when ATP was incubated in the presence of the A2 protein.

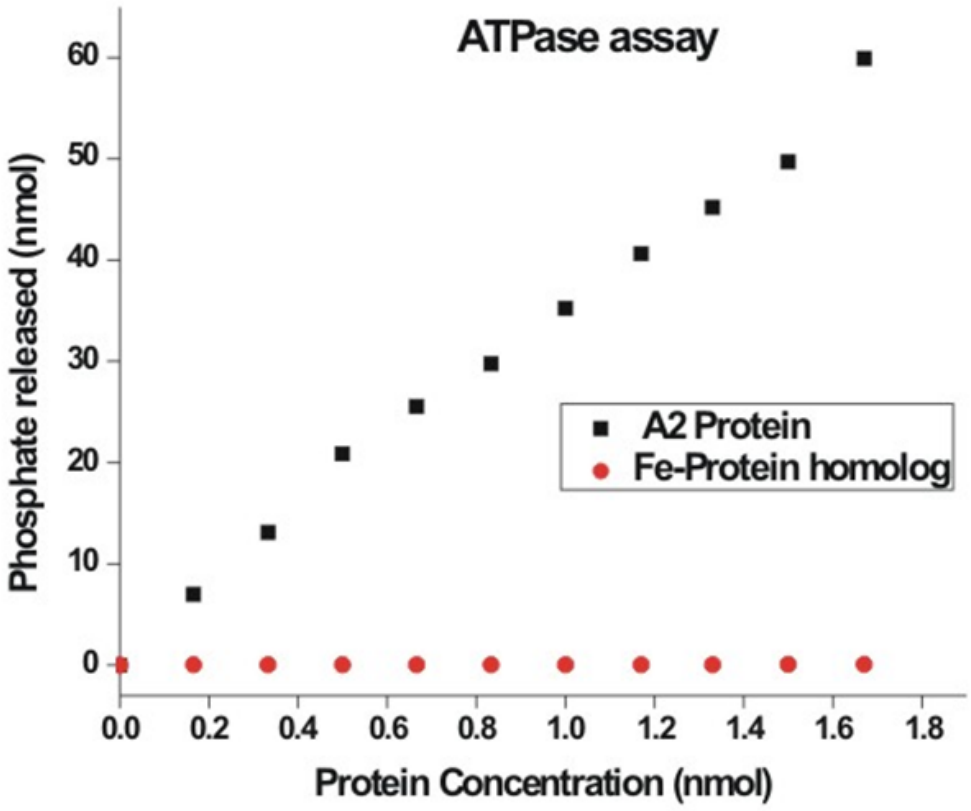

Fig 3.23: ATP hydrolysis assay of the A2 and the Fe-protein homolog.

It could be possible that the Fe-Protein Homolog assists the A2 protein in the hydrolysis of ATP, hence the phosphate released was measured in the presence of both the A2 and the Fe-protein homolog. In the presence of the Fe protein homolog, there was an increase in ATP hydrolysis (**Table.3.4)**

Table.3.4: ATP hydrolysis assay in the presence of A2 and Fe-Protein homolog.

Comments	Phosphate released (nmol)
A2	32.15
A2 and Fe-Protein homolog	49.93

30 nmol of A2 protein and with Fe-protein homolog was used for the assay.

3.3.12 Protein-protein interaction studies:

Two soluble protein components are required for the activation of MCR; A2, with an ATP binding site and A3a, an Fe-S cluster containing protein complex. According to our hypothetical model (47), the A2 protein donates ATP to the Fe-Protein homolog present in the complex and subsequent hydrolysis of ATP decrease the midpoint potential of the Fe-S center on PISF. In the course of these processes there is a high possibility that the A2 protein would interacts or even binds to subunits of the A3a protein complex. Pull-down experiments were performed to study the possible interaction between the different protein components.

A2 pull-down assay with *M. marburgensis* cell extract:

Purified A2 protein was loaded onto a Ni-sepharose column. Subsequently *M. marburgensis* extract was loaded and the column was washed with buffer. The A2 protein and interacting proteins were eluted from the column using buffer containing 500 mM Imidazole. As a control cell extract was loaded directly on the Ni-NTA column in the absence of A2. No proteins binds under these conditions. In the presence of A2 several other proteins are present in the eluate. These where all separated on SDS-PAGE and the individuals bands were sequenced using mass spectrometry. The relevant enzymes that were detected were: methyl-coenzyme M reductase II operon protein C and the CBS-domain-containing protein (**Table 3.5**).

Table 3.5: Tabulation of protein components interact with A2 protein from cell extracts:

Accession	**Description**	**Mass (Kda)**
D9PUZ4_METTM	Predicted activator of 2 hydroxyglutaryl CoA dehydratase	44.02
D9PXZ6_METTM	Methyl-coenzyme M reductase II	47.14
D9PY38_METTM	Methyl-coenzyme M reductase II operon protein C (MtrC)	34.17
D9PV71_METTM	30S ribosomal protein S4P	19.75
D9PU72_METTM	CBS-domain-containing protein	14.68
D9PX22_METTM	Hydrogenase maturation factor HypB	23.89
D9PYW7_METTM	Imidazoleglycerol phosphate dehydratase	20.77
D9PXN7_METTM	Methyl-coenzyme M reductase component A2	59.4

A2 pull-down assay with Predicted Iron-sulfur flavoprotein, Iron Sulfur Cluster Carrier/ Fe-Protein homolog Protein and Methyl coenzyme M reductase I, operon protein C (McrC) and M Methyl coenzyme M reductase II, operon protein C (MtrC):

It is possible that the binding affinity of the A2 protein for the Fe-protein homolog might be altered in the presence of the N-terminal 6-His tag on the A2 protein. Therefore it was important to study the interaction of these proteins individually.

Except for Predicted Iron-sulfur flavoprotein cleavage of the His-tag was not possible from either bait protein (A2) or from any prey protein source (Iron Sulfur Cluster Carrier/ Fe-Protein homolog Protein, McrC and MtrC) because these proteins were cloned into pQE-80L vector and this vector does not have any linker between 6-his tag and multiple cloning site. Hence, pull-down study by using a Ni-NTA column were not possible. To circumvent this problem, an ATP affinity column was used. Since, the A2 protein has an ATP binding site there was the possibility that the A2 protein could bind non-covalently with high affinity to the column containing ATP. There is, however, a fundamental problem with using ATP in affinity chromatography, for attachment to a matrix ATP needs to be chemically modified with a linker (**Fig. 3.7**). This linker may interfere with the protein-ATP interaction and thereby reduce the binding. This problem can be overcome by attaching ATP at a different positions at the adenine base (6-AH-ATP-Agarose and 8-AH-ATP-Agarose), the sugar (EDA-ATP-Agarose) or the phosphate moiety (AP-ATP-Agarose). These four different types of ATP-Agarose column and a control column (agarose without ATP) were tested for the binding of the A2 protein.

Purified A2 protein after the Ni-NTA was loaded to these different types of columns and eluted in the presence of ATP. Interestingly, SDS-PAGE analysis of the eluted fractions indicate that the A2 protein interacts with all four types of column (**Fig. 3.23**) except the control (column without

ATP). The intensity of the bands on the gel indicate that the A2 protein bind most effectively to the 6-AH-ATP-Agarose column.

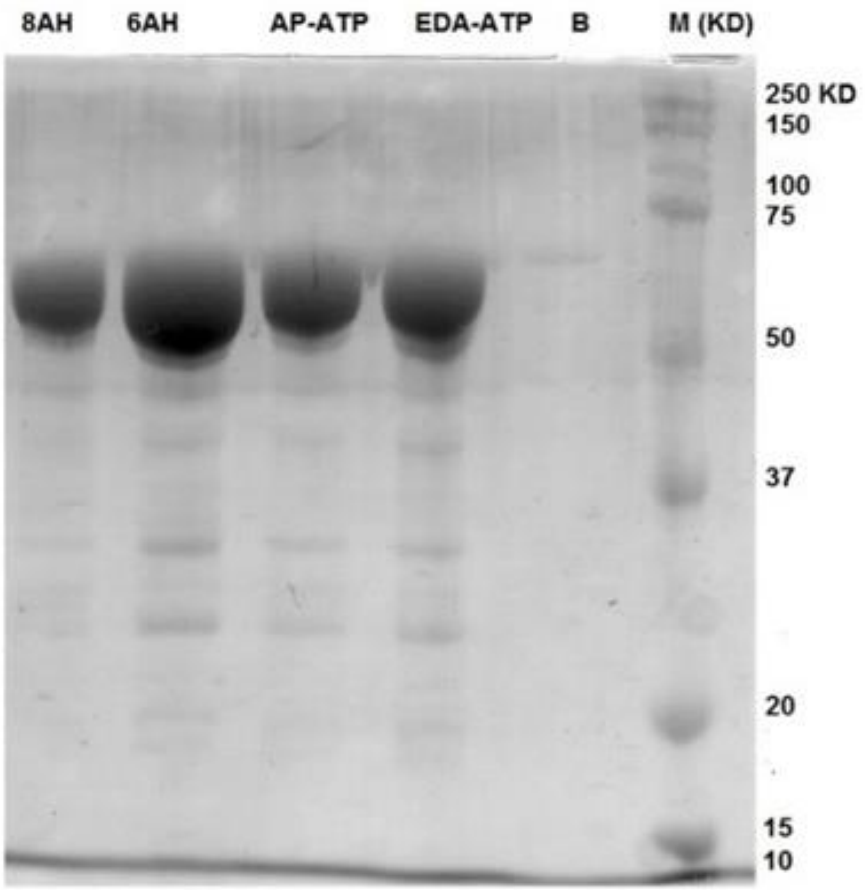

Figure 3.24: ATP affinity test of the A2 Protein. Eluted A2 Protein after eltion from different columns were denatured in sample buffer at 95°C for 5 min and loaded onto a 12 % polyacrylamide gel. The gel was stained using coomassie brilliant Blue R-250 I (Bio-Rad). **B:** Blank (Agarose), **EDA-ATP:** 2'/3'-EDA-ATP-Agarose (***EDA-ATPAgarose***), **AP-ATP:** Aminophenyl-ATP-Agarose, C10-spacer (***APATP-Agarose***), **6 AH:** N6-(6-Amino) hexyl-ATP-Agarose **(*6AH-ATPAgarose*), 8 AH:** 8-[(6-Amino)hexyl]-amino-ATP-Agarose (***8AHATP-Agarose***).

Since A2 binds to the ATP-Agarose columns, pull down experiments of A2 with either Predicted Iron-sulfur flavoprotein, Iron Sulfur Cluster Carrier/Fe-Protein homolog Protein, Methyl coenzyme M reductase I, operon protein C (McrC), Methyl coenzyme M reductase II, operon protein C (MtrC2) or Flavoprotein were performed. Since the binding of A2 was maximal with the 6-AH-ATP-Agarose column this column was used for the pull down experiments. The eluted pull down fractions were analyzed by SDS-PAGE to observe the possible prey protein binding to the A2 protein (**Fig. 3.24**). In this case no other protein besides the A2 protein was observed.

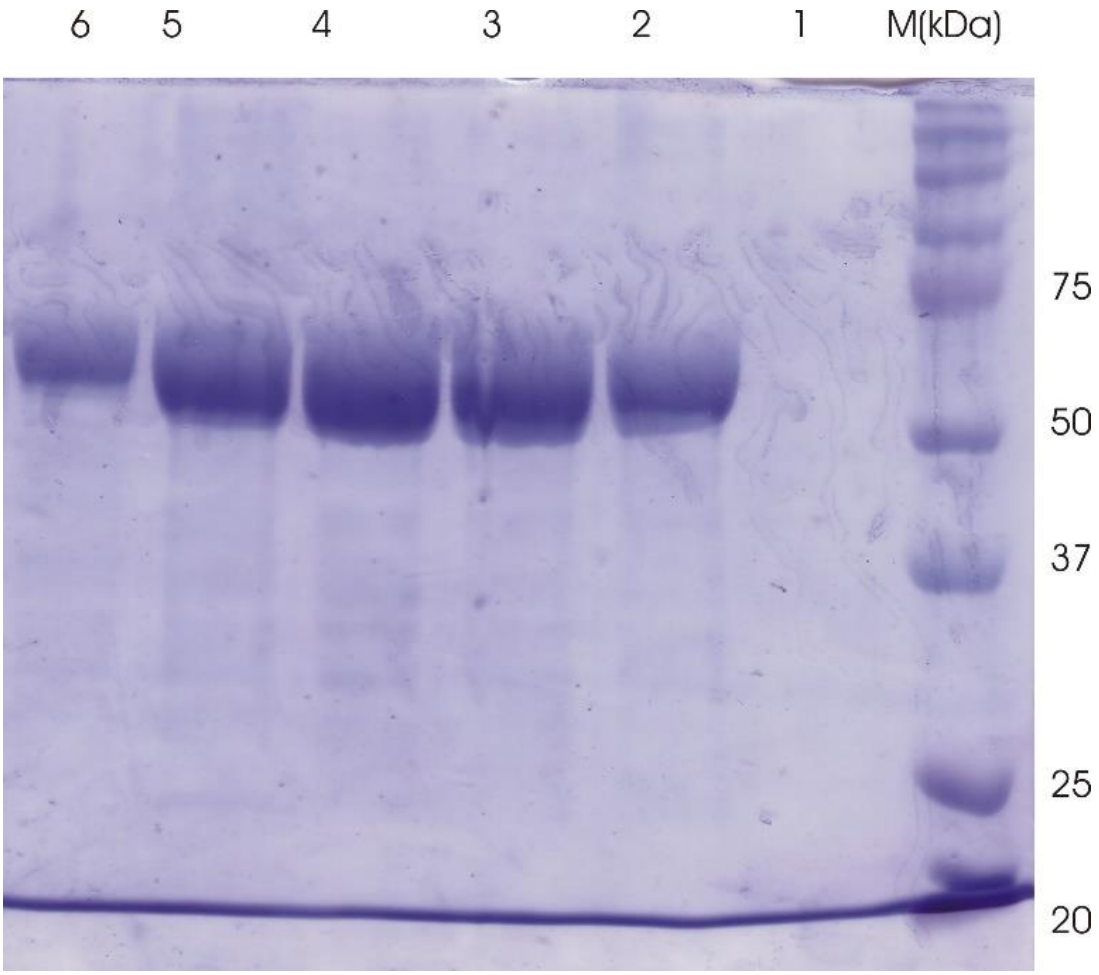

Figure 3.25: SDS-PAGE analysis of pull-down experiment of A2 with A3a protein components. The Numbers in the figure indicates samples: **1**. Control (Agarose column with A2 protein), **2**. 6- A2 with Predicted Iron-sulfur flavoprotein **3**. A2 with Iron Sulfur Cluster Carrier/ Fe-Protein homolog Protein and **4**. A2 with Methyl coenzyme M reductase I, operon protein C (McrC), **5**. A2 with, Methyl coenzyme M reductase II, operon protein C (MtrC), **6**. Pull down of A2 with Flavoprotein.

3.4. Discussion:

According to our postulated model of activation, electrons from polyferredoxin or an artificial electron source with a potential close to that of polyferredoxin ($E^{o'}$ ~ -500 mV at pH 7 vs. SHE) can reduce the Fe-S cluster in PISF and concomitant hydrolysis of ATP by the A2 protein/Fe protein homolog will lower the potential of this cluster allowing reduction of the Ni centers on MCR. Attempts to overexpress the polyferredoxin in an *E. coli* host were not successful, probably because of the 12 Fe-S cluster requirement. *E. coli* cells containing the pQE-80L_Polyferredoxin plasmid did not grow. Hence, activation studies were performed in the presence of the artificial electron sources dithionite ($E^{o'}$ ~ -420 mV at pH 7 vs. SHE) or Ti (III) citrate ($E^{o'}$ ~ -500 mV at pH 7 vs. SHE). The rate of methane formation increased almost two fold in the presence of McrC, PISF, the Fe-protein homolog, the A2 protein, and Ti(III) citrate as an artificial electron source. There was no activation observed when dithionite was used instead of Ti(III) citrate. The mid-point difference of dithionite and Ti(III) citrate is around 80 mV. The fact that activation is only observed in the presence of Ti(III)citrate which has a midpoint potential close to that of polyferredoxin ($E^{o'}$ ~ -500 mV at pH 7 vs. SHE), would be in line with our proposal that polyferredoxin is the direct electron donor. The reduction of polyferredoxin via flavin-based electron bifurcation is only possible in the presence of heterodisulfide (HDS). The activation assay described in chapter 2, used overexpressed A2, the purified A3a protein complex, and dithiothreitol (DTT, $E^{o'}$ ~ -500 mV at pH 7 vs. SHE) as the electron source. Since there is no heterodisulfide present in the assay it is not clear how the low-potential electrons are generated, unless, this is done by one of the other components in the A3a complex.

Sequence analysis of the then uncharacterized proteins present in the purified A3a complex revealed that only PISF contains a consensus sequence for binding of a 4Fe-4S cluster. Therefore,

we postulated that the reduction of the Ni center in MCR by polyferredoxin or an artificial electron source is possible via the cluster present in PISF. McrC does not have consensus sequence for Fe-S clusters, however, overexpressed purified McrC protein was brown in color and it has a sharp absorption maxima around 320 nm and a small bump at 420 nm. This could be the result of breakdown of an unstable 4Fe cluster. Purification of McrC under strictly anaerobic condition or reconstitution of the cluster will be needed to prove this. Addition of a cluster containing McrC to the activation assay would indicate of both Fe-S protein containing protein McrC and PISF might needed for the activation.

Both the A2 protein and the Fe-Protein Homolog contain nucleotide binding sites. We postulated that the A2 protein donates the ATP to the Fe-Protein Homolog and hydrolysis of ATP would occur by the Fe-Protein Homolog to generate a low potential electron. However, the ATP hydrolysis assay revealed that hydrolysis of ATP occurs by the A2 protein alone. No ATP hydrolysis was observed in the presence of the Fe-Protein homolog. There was an additional small increase in ATP hydrolysis in the presence of both A2 and Fe-protein homolog. This would indicate that both proteins have to interact for the hydrolysis to happen. This observation is somewhat strange since one would expect that ATP hydrolysis will only happen when the whole activation complex has been formed. It is possible, however, that ATP hydrolysis might not be coupled directly to electron transfer as shown in a recent paper on this process in nitrogenases where it was shown that the electron transfer from the Fe protein to the MoFe protein happens before the ATP hydrolysis on the Fe protein (100) and hydrolysis of ATP is only required to induce a conformational change to release the Fe protein from the MoFe protein. It will also be important to test how much ATP is hydrolyzed when MCR is activated to see if the detected level of hydrolysis by A2 is relevant or not. The ATP hydrolysis increased in the presence of both the A2

protein and the Fe-protein homolog which would indicate that both proteins are interacting. Pull-down experiments, however, did not show an interaction between these two proteins.

As activation of MCR was not possible in the absence of the A2 protein it is very likely that the A2 protein interacts with the A3a protein. Hence, pull down experiments were performed to study the interaction of A2 with A3a protein components in the presence of ATP. As a source of A3a, *M. marburgenesis* cell extract and purified recombinant PISF, Fe Protein homolog, MtrC, Flavoprotein and McrC were used for the interaction. The pull down experiments with A2 bound to the Ni-sepharose column with cell extract showed the binding of McrC and the CBS domain containing protein. However, there was no binding observed of A2 MtrC2 when the same experiment was performed with A2 bound to the ATP-agarose. A possible explanation would be that MtrC2 and A2 can only interact when the correct surfaces on the proteins are exposed which is the case when A2 is bound to the column via the his-tag but not when it is bound to the ATP agarose. This could indicate that MtrC2 would be interacting with the ATP molecule. In light of the possibility that MrcC could be an iron-sulfur-cluster this would indicate a more Fe-protein-like role for this protein and in turn would question the need for the Fe-protein homolog and the PISF protein in the activation process.

Another concern with the PISF protein is that is does contain an iron-sulfur cluster but not the Flavin. The crystal structure of ISF from *M. Thermophila* (ISF3-Af) indicate that it has a flavodoxin like fold and amino acids Arg11, Arg105 and Lys 94 are required for the flavin binding (131). Sequence alignments (**Fig. 3.1**) and secondary structure prediction (**Fig.3.25**) of PISF revealed the presence of three conserved flavin binding amino acids, Arg7, Arg95 and Lys 110 and a flavodoxin like fold with repeating α/β units. These features indicate our PISF could bind a flavin. Titration experiments did not indicate flavin binding.

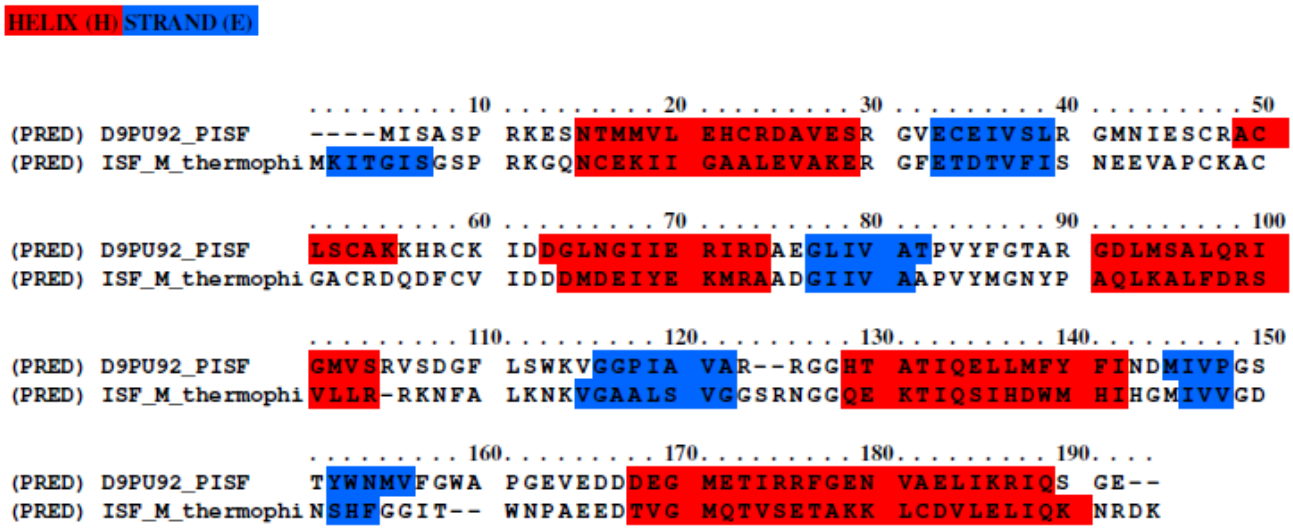

Figure 3.26: Secondary structure prediction of *M.marburgensis* PISF (D9PU92_PISF) and *M.thermophila* ISF.

In a typical iron-sulfur flavoprotein, the mid-point potential of the flavin mononucleotide (FMN) and the Fe-S cluster are reported to be -0.207 V and -0.43 V respectively (132,133). To reduce the Ni center of MCR, electrons having a potential lower than -0.650 V are required. The midpoint potential of the FMN is almost 450 mv higher than that of the cofactor F_{430} bound Ni(II)/Ni(I) couple. It can be safely assumed that if the protein is properly folded that the absence of the flavin cofactor would not be a great concern since it would not be able to participate based on the higher midpoint potential. The absence of the flavin, however, could cause the protein to be unstable. Utilization of FMN as electron source for activation is not favorable for methanogens unless it behaves like the flavin center involved in recently reported electron bifurcation process where FAD is involved in reduction of the low potential ferredoxin (28-30). However, the previously mentioned, lack of understanding of how dithiothreitol can be an electron source if there is no heterodisulfide available to steer the bifurcation process opens up the possibility that another flavin enzyme might be involved and it should be investigated if PISF could possibly have such a role.

CHAPTER FOUR: The Effect of 3-Nitrooxypropanol, a Growth Inhibitor of Rumen Methanogens, on Methyl-Coenzyme M Reductase.

4.1 Introduction:

Methane is an important greenhouse gas and it has a global warming potential 21 times more than that of carbon dioxide. Digestive processes of ruminants contribute a significant amount of methane. It has been estimated that cattle alone are responsible for emission of around 11-17% of methane globally (134). Additionally, between 2-12% of ingested gross energy of ruminants is lost due to the formation of methane (135). This loss of energy could be potentially used by the animal. Hence, controlling methane formation is important from the perspective of both environmental impact and animal productivity. Numerous efforts to control the methane emission from livestock have been tried (136-139). These include changes in the source of carbohydrate (e.g., starch or sugar vs. fiber), supplemental hydrogen acceptors (such as nitrate or sulfate), the feeding of precursors of propionate such as fumaric and malic acid or the feeding of bioactive compounds such as ionophores and natural compounds like tannins and saponins. Bioactive compounds can reduce methane emissions from ruminants through inhibition of methanogenesis or by shifting fermentation pathways to promote alternative hydrogen sinks, such as propionate production, thus reducing methane emissions (140,141). However, probably due to differences in rumen ecology and dynamics, these countermeasures are not uniformly effective in livestock. For example, supplements that are effective at reducing methane production in sheep were found to be ineffective in cattle. Therefore, research groups around the world are interested in the development of alternative countermeasures to inhibit methane formation in the form of synthetic compounds

that can act as potent inhibitors of methanogenesis without toxic or harmful effects on the rumens and the environment.

Through in-silico screening by the group of Dr. Maik Kindermann at DSM Nutritional Products, Basel, Switzerland, 3-Nitrooxypropanol (3-NOP) has been identified (142) and shown to be effective at inhibiting methane production both *in vitro* (143) and *in vivo* (144-146) with no signs of animal toxicity. Although use of 3-NOP is a promising approach to reduce enteric methane emissions from ruminants, further studies are required to understand the mode of methane inhibition. 3-NOP is speculated to inhibit the key enzyme of methanogenesis, i.e. MCR, however, no studies describing the effect of 3-NOP against MCR have been reported in the literature to date. Similar to 2-bromoethanesulfonate (BES), a potent inhibitor of methanogenesis, 3-NOP is also a structural analog of methyl-coenzyme M (**Fig. 4.1**). Hence, 3-NOP is thought to inhibit MCR similar to BES. It has been shown that 2-BES reacts with free $Ni(I)F_{430}$ to form bromide, ethene and sulfite (147):

$$2\ Ni(I)F_{430} + Br\text{-}CH_2CH_2SO_3^{1-} \longrightarrow 2\ Ni(II)F_{430} + Br^- + CH_2{=}CH_2 + SO_3^{2-}$$

Probably the following reaction sequence takes place before release of sulfite:

$$Ni(I)F_{430} + Br\text{-}CH_2CH_2SO_3^{1-} \longrightarrow Ni(II)F_{430} + Br^- + CH_2CH_2SO_3^{1-}\ (\text{radical})$$

$$CH_2CH_2SO_3^{1-}\ (\text{radical}) \longrightarrow CH_2{=}CH_2 + SO_3^{1-}\ (\text{radical})$$

$$Ni(I)F_{430} + SO_3^{1-}(\text{radical}) \longrightarrow Ni(II)F_{430} + SO_3^{2-}$$

However, not all these steps are feasible in the active site of MCR because per active site these is only one $F_{430}Ni(I)$ present, specially the last step in which the sulfite anion radical is reduced must be different. The sulfite anion radical is a strong oxidant and it was postulated that thioglyciyl or tyrosine amino acids present in active site might oxidized to a thioglycine or a tyrosyl radical (148). Within the active site there is a thioglycine and two tyrosine residues that could be

oxidized by the sulfite anion radical to a thioglycyl radical or a tyrosyl radical, respectively. The split EPR signal is most similar to that reported for the glycyl radical in proteins. More detailed studies are needed to make an assignment. The splitting in EPR signal reported to almost similar to the glycyl radical in proteins (149).

The objective of this chapter is to examining the reactivity of the Ni center in the active site of methyl-coenzyme M reductase in the presence of 3-NOP. Based upon the previously reported mechanism of inhibition of MCR by BES (27), we hypothesized that 3-NOP inhibits MCR by binding with the active form of MCR (MCRred1-Ni(I)) followed by release of Nitrite or Nitrate.

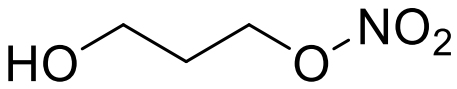

3-Nitrooxypropanol (3-NOP)

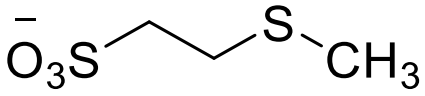

Methyl-coenzyme M

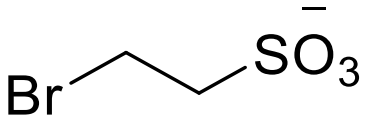

2-Bromoethanesulfonate (2-BES)

Figure 4.1: Structural formulas of 3-nitrooxypropanol, methyl-Coenzyme M and 2-bromoethanesulfonate.

4.2 Materials and Methods:

4.2.1 Reagents:

3-nitrooxypropanol (3-NOP) was provided by DSM Nutritional, Basel, Switzerland. A Griess reagent kit (G-7921) for nitrite determination was purchased from Invitrogen. Isopentane and other reagents were purchased from Sigma Aldrich.

4.2.2 Effect of 3-NOP on hydrogen induced cell extract:

M. marburgensis cells were grown at 65 °C in a 13 L glass fermenter (New Brunswick) containing 10 L of growth medium. The growth media contained medium (52,110) contained 65 mM KH_2PO_4, 50 mM NH_4Cl, 30 mM Na_2CO_3, trace elements (0.5 mM nitrilotriacetic acid, 2 mM $MgCl_2$, 50 μM $FeCl_2$, 1 μM $CoCl_2$, 1 μM Na_2MoO_4, 5 μM $NiCl_2$) and 20 μM resazurin. For growth, the cell culture has to be gassed with the 80% H_2/20% CO_2 mixture. A small amount of H_2S (~1%) is also needed. The resazurin was added to the medium to indicate when sufficient anaerobic conditions were reached. After 2 h of equilibration, the medium was inoculated with 200-300 ml of fresh cell culture. In the beginning the cells grew exponentially (doubling time about 2 h). After 15 h of inoculation, cell density reached around 6 at 578 nm. Cells were harvested after 15 h. In order to induce the red1 form, the gas was switched to pure hydrogen for 20 min before harvesting. The cell culture was cooled down over a 20 min period to 10 °C under continuous gas flow and the cells were subsequently harvested anaerobically by centrifugation using a flow-through centrifuge (Hettich, contifuge 17 RS). Approximately 60 g of wet cells were usually obtained using this procedure. All the following steps were performed in an anaerobic chamber (Coy Instruments) filled with 95% N_2/5% H_2. After the cells were collected by centrifugation, the rotor was brought in the anaerobic tent. The cell pellet was resuspended in 50

ml 10 mM Tris-HCl buffer, pH 7.6, and sonicated 3 times for 7 min each at 80% power on ice, followed by ultra-centrifugation at 350,000 x g for 20 min at 4 °C. Further, hydrogen induced cell extract was incubated with 10 mM, 3-NOP for 15 minute and analyzed with electron paramagnetic resonance at 77 K.

4.2.3 Purification of MCR_{red1} form:

The MCR red1 form was purified as described in Chapter 2.

4.2.4 Nitrite determination:

The Griess diazotization reaction was used to measure the nitrite formation (**Fig. 4.2**). In the presence of nitrite, sulfanilic acid is quantitatively converted to a diazonium salt. Further, the diazonium salt is coupled to N-(1-naphthyl) ethylenediamine to form an azo dye that can be determined in the range of 520-590 nm.

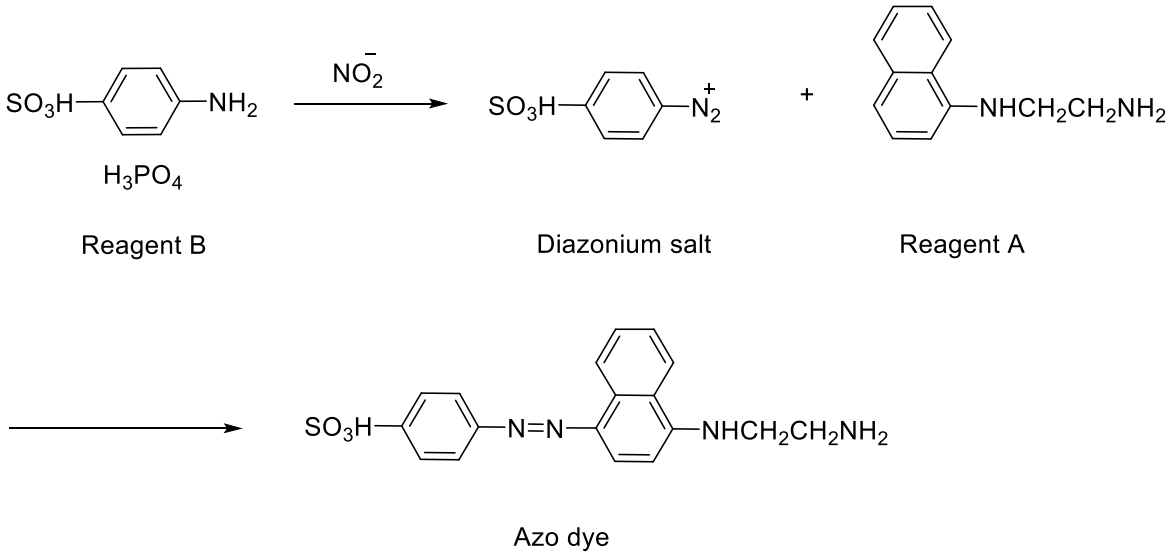

Figure 4.2: Principle of nitrite measurement using the Griess reaction. Formation of the Azo dye was detected at 548 nm.

MCR in the MCRred1 form was incubated with 3-NOP for 15 min after which the amount of formed nitrite was measured. Equal volumes of Sulfanilic acid (1 mg/ml, in 5 % phosphoric acid solution) and N-(1-naphthyl) ethylenediamine (1 mg/ml) were mixed together to form the Griess reagent. 150 µl of inhibitor treated MCRred1 sample was mixed with 20 µl of Griess reagent containing 130 µl of deionized water on a microplate. A photometric reference sample was also prepared by adding 20 µl of Griess reagent to 280 µl of deionized water. Samples were incubated for 30 min at room temperature and measured at 595 nm by an ELISA Plate reader. Nitrite standard (1.66 µM, 3.33 µM, 6.66 µM, 10 µM, 20 µM, 30 µM, 40 µM, 50 µM, 60 µM, 70 µM, 80 µM and 100 µM) was prepared by dissolving the $NaNO_2$ (1 mM) stock solution in deionized water.

4.2.5 Freeze quench experiment:

With a special setup shown schematically in **Fig. 4.3**, the enzyme solution is rapidly mixed with a solution containing the inhibitor. The mixed solution goes through an aging tube and empties out in a Dewar containing cold isopentane (~ -140°C) causing the sample to immediately freeze. The ‘snow’ is subsequently collect in an EPR tube for measurement. The reaction was quenched at different time interval (4.6 ms, 10 ms, 20ms, 40 ms, 70 ms, 100 ms, 150 ms , 500 ms, 1s, 5 s and 5 s) and the frozen samples were analyzed by EPR spectroscopy.

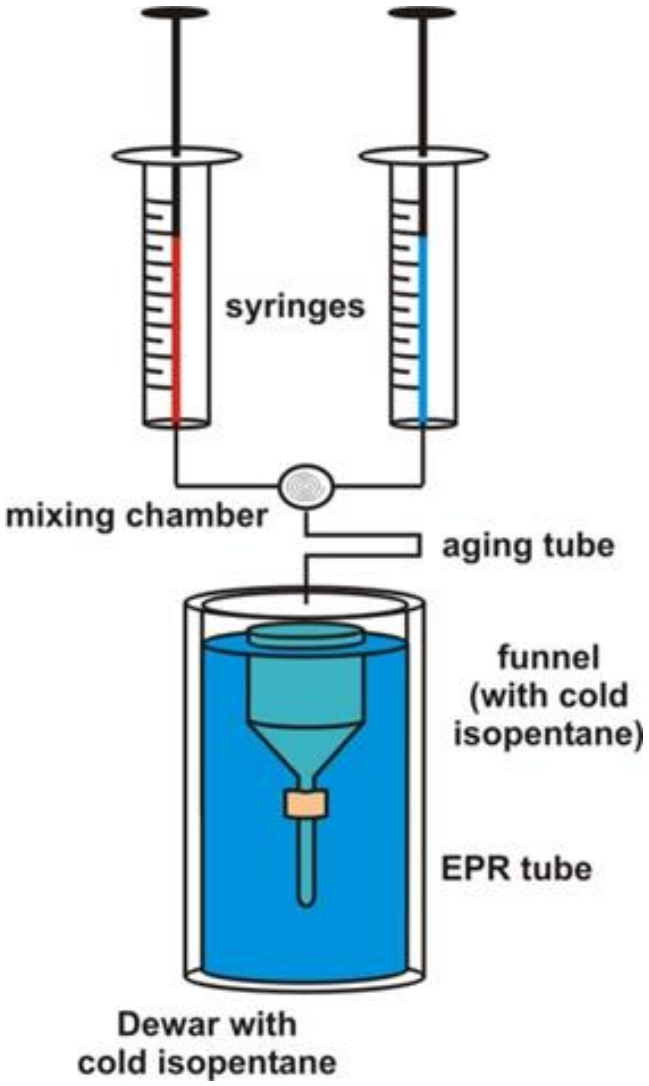

Figure 4.3: Schematic set up of freeze-quench experiment.

4.3 Results:

4.3.1 Effect of 3-nitrooxypropanol on hydrogen-incubated cell extract:

M. marburgensis utilizes CO_2 and H_2 as substrate, where reduction of carbon dioxide to methane occur via coenzyme-bound C_1-intermediates by using electrons from the oxidation of H_2. Therefore H_2 is a reductant in this pathway and gassing the cells with 100% H_2 results in the detection of the reduced forms for different enzymes in this pathway: MCR, in both the red1 and red2 forms, hydrogenase, in the Ni-C form, and formylmethanofuran dehydrogenase (**Fig. 4.4, panel A**). Gassing the cells with 80% N_2/20% CO_2 causes the oxidation of these enzymes: MCR is converted into the MCR_{ox1} forms, the hydrogenase into the Ni-A form and the formylmethanofuran dehydrogenase is not detectable anymore (**Fig. 4.4, panel B**).

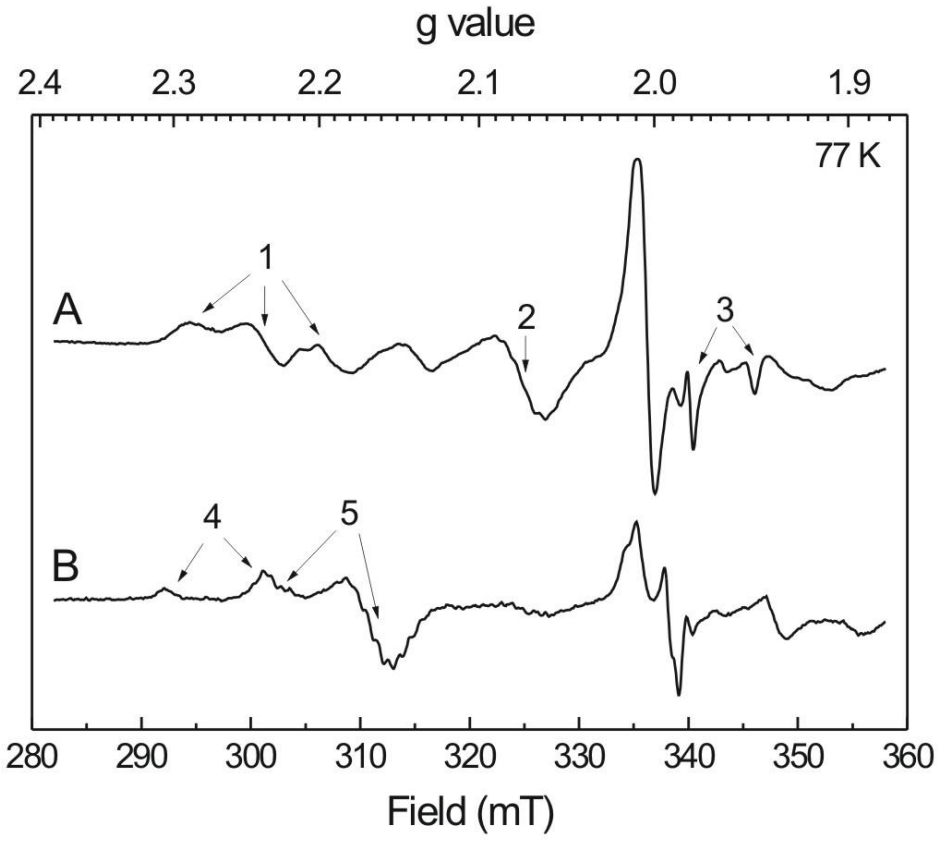

Fig. 4.4: EPR spectra of cells from *M. marburgensis*. Panel (A) Cells after 30 min gassing with 100% H_2. Panel (B) Cells after 30 min gassing with 80% N_2/20% CO_2. Numbers in Figure indicate the following enzymes: 1) Methyl-coenzyme M reductase in the MCR_{red2} form; 2) Methyl-coenzyme M reductase in the MCR_{red1} form, 3) NiFe-Hydrogenase in the Ni-C form, 4) Formylmethanofuran dehydrogenase; 5) Hydrogenase in the Ni-A form, and 6) Methyl-coenzyme M in the MCR_{ox1} form.

Since 3 important metabolic enzymes can easily be detected in whole cells it was first checked what the effect of 3-NOP is on hydrogen exposed cells. The cells where incubated with 10 mM 3-NOP for 15 min and analyzed by EPR spectroscopy at 77 K. As depicted in **Fig. 4.5.,** the effect of incubating whole cells with 3-NOP on the EPR signals is somewhat similar to the effect of removing H_2 from the gas phase. Red1 is gone but now MCR_{ox1} is detectable. None of the hydrogenase species are detected and the signal due to formylmethanofuran dehydrogenase has become less intense. Although, it is not clear from these measurements if 3-NOP has reacted with any of the other enzymes, there appears to be a clear effect on the MCRred 1 form.

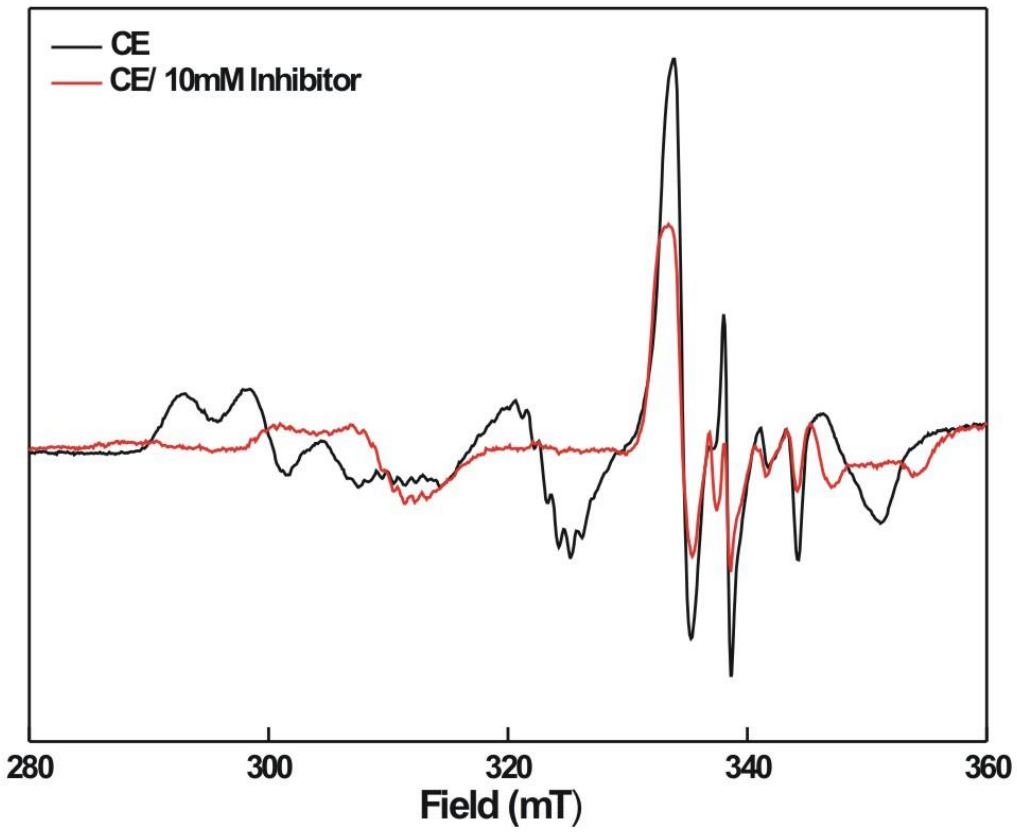

Figure 4.5: Effect of 1-Nitrooxypropanol on the EPR of whole cells of *Methanothermobacter marburgensis.*

4.3.2 Direct effect of 3-NOP on purified MCR in the MCR_{red1} form:

The MCRred1 signal was quencehed in the presence of 3-NOP in cell extract (not shown). Therefore to observe the direct effect of 3-NOP, purified MCR in the red1 form was incubated with 3-NOP for 15 min and analyzed by UV-VIS and EPR spectroscopy **(Fig. 4.6 and 4.7**).

As shown in **Fig. 4.6**, enzyme as purified, is in the red1 form characterized by the absorption maxima at 387 nm and a broad band at 720 nm. In the presence of 10 mM 3-NOP, the red1 form was converted to the silent form as observed from the shift in the absorption maxima from 387 nm to 420 nm. Most of the protein was converted within the first 5 min of incubation. The obtained absoption spectra was similar to MCR red1 exposed with oxygen and thus represents the MCRred1-silent form.

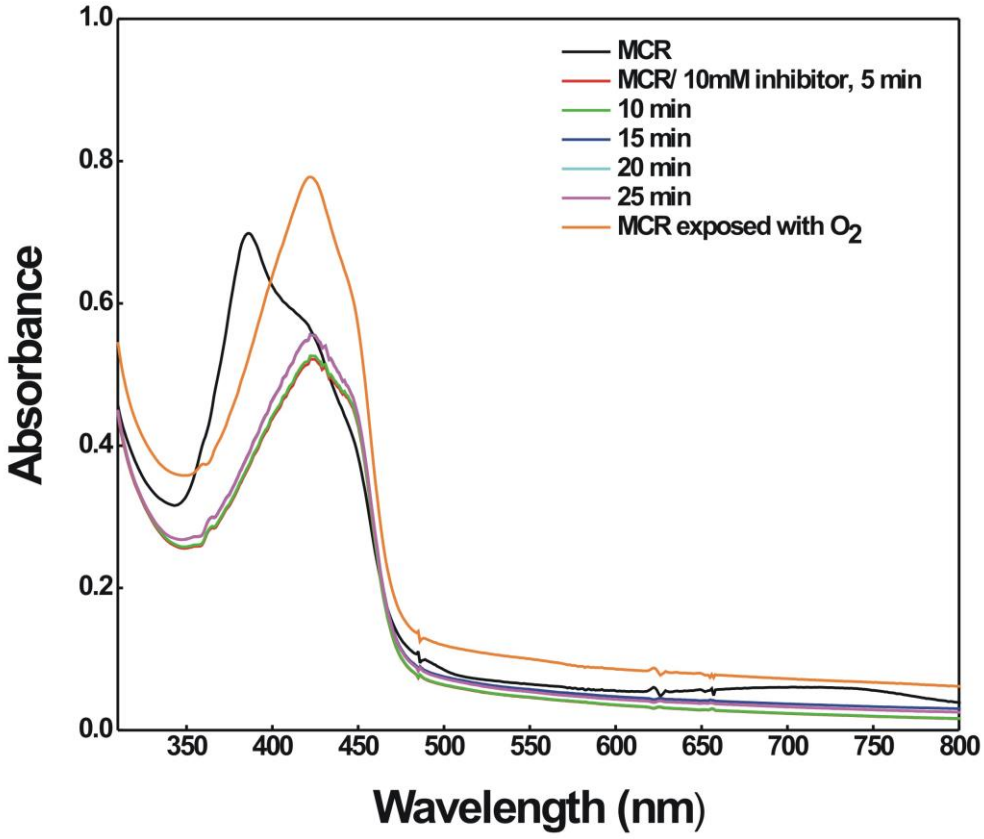

Figure 4.6: UV-VIS spectrum of MCR with inhibitor. 40 µM of MCR was incubated with 10 mM 3-NOP and analyzed at 5 min, 10min, 15 min, 20 min and 25 min.The Inhibitor treated enzyme was also compared with oxygen exposed enzyme in the red1 form.

EPR analysis of MCR in the presence of 3-NOP was in line with the absoprtion results. **Fig. 4.7, Panel A,** shows the effect of the compound on a preparation that contains mainly MCRred1 (85%) and a small amount of MCRox1 (15%). The addition of the 3-NOP resulted in the disappearance of the MCRred1 signal. There does not appear to be much of an effect on the MCRox1 form. This is confirmed by a similar experiment on a sample that contains 70% MCRox1 and 30% MCRred1 (F**ig. 4.7, Panel B**). Again the addition of the compound resulted in the disappearance of the MCRred1 signal and there is no effect on the MCRox1 form.

In panel A, a small radical species can be detected in the 'as such' sample that became less intense when the inhibitor was added. An opposite effect can be detected in panel B. Now a radical species is induced. Because of the random behavior of this, it is not clear if there is any radical chemistry involved in this process.

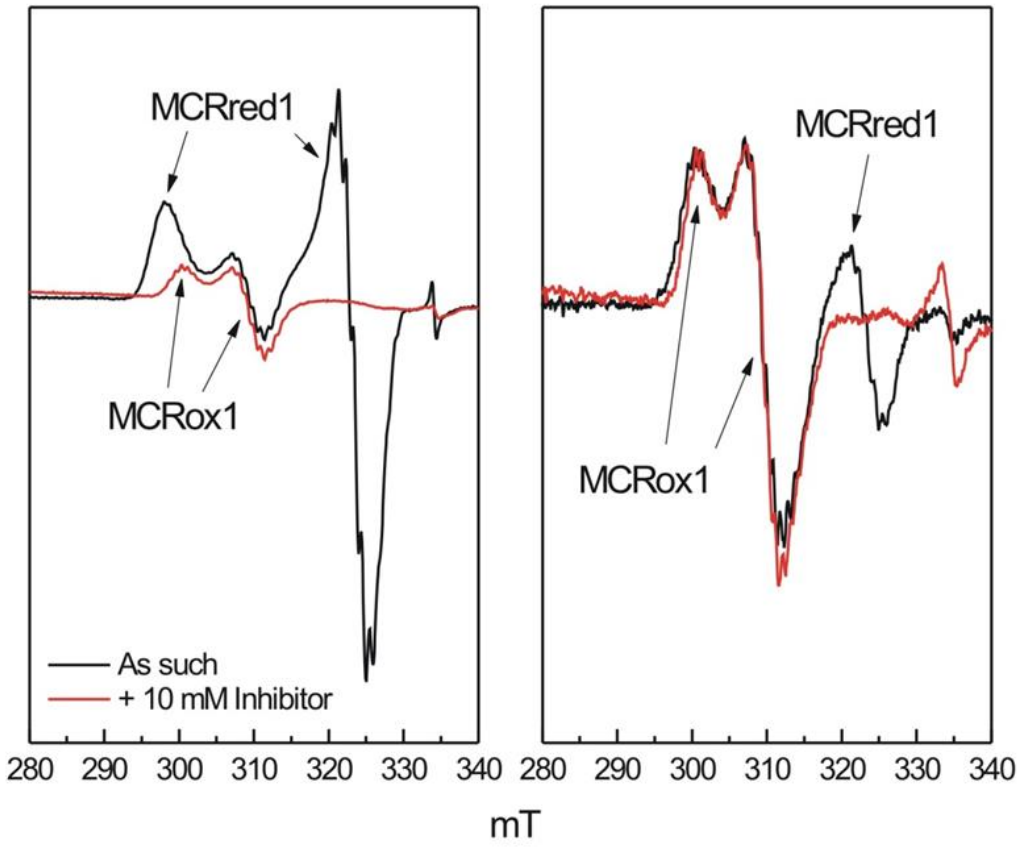

Figure 4.7: Effect of 3-Nitrooxypropanol on different forms of MCR: Panel A , effect of 10 mM 3-NOP on MCRred1: 200 µM of MCR containing mainly MCRred1 (85%) and a small amount of MCRox1 (15 %) was incubated with 10 mM 3-NOP at RT for 15 min. **Panel B, effect of the 10 mM 3-NOP on MCRox1 :** 200 µM of MCR containing approximately 70% MCRox1 and 30% MCRred1 was incubated with 10 mM 3-NOP at RT for 15 min. Samples were analyzed at 77 K and microwave power to the cavity of 2mW.

4.3.3 Direct effect of 3-NOP on MCR in the presence of substrates:

Previously, it was shown that binding of coenzyme B to the MCRred1c form resulted in the formation of the MCRred2 form while there is a small effect of binding of methyl-coenzyme M to the MCR red1c form, a more pronounced hyperfine structure. This effect is more pronounced when methyl-coenzyme M is added to the MCRred1a form. In the presence of the substrates, methyl-coenzyme M and coenzyme B enzyme can behave differently in the presence of an inhibitor. Hence the effect of 3-NOP was tested on MCRred1 in the presence of the different substrates (**Fig. 4.8**). The MCRred1 form disappeared under all conditions tested, while the ox1 form was observed to also disappear when methyl-coenzyme M is present. The MCRox1 signal is not affected when both coenzyme B and 3-NOP are present. In the presence of methyl-coenzyme M and 3-NOP there was a slight increase in the signal intensity of the free radical-type species detected at around 333 mT.

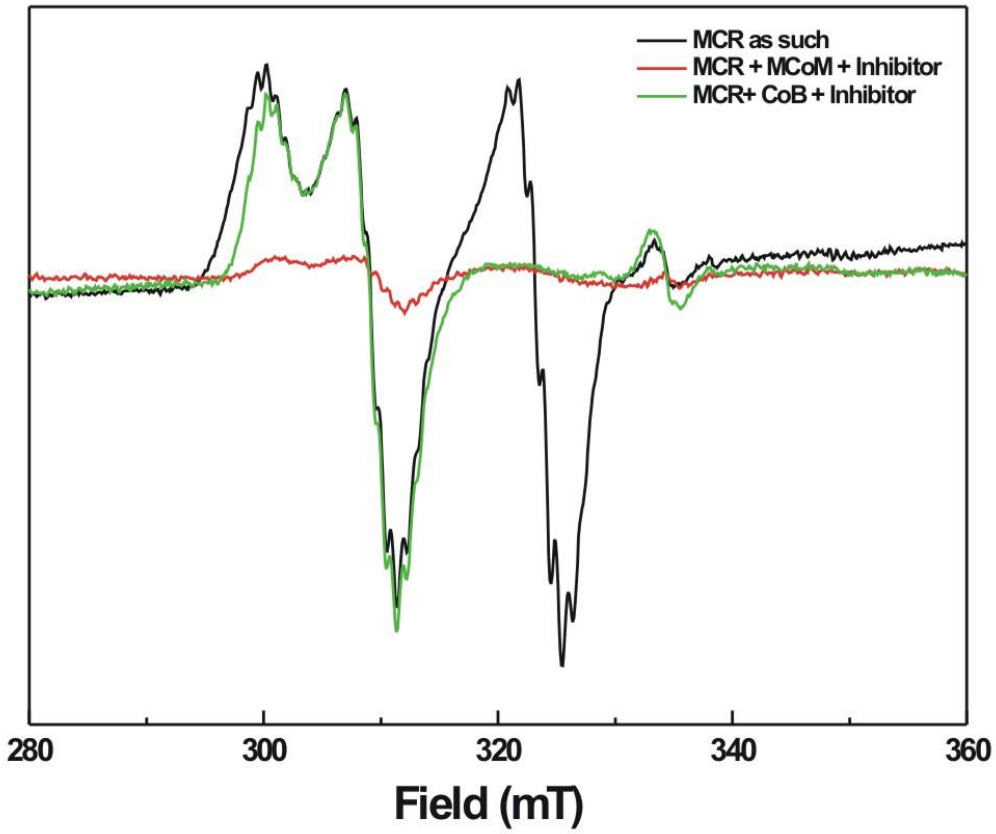

Figure 4.8: Effect of Inhibitor on MCR in the presence of coenzyme B and methyl-coenzyme M. 10 mM of 3-NOP was added to 100 µM of MCR with 10 mM methyl-coenzyme M and 100 µM of MCR with 10 mM coenzyme B for 15 min at RT and frozen in EPR tubes. Samples were analyzed at 77 K and a microwave power to the cavity of 2mW.

4.3.4 Titration of MCR with 3-NOP:

The above experiments revealed that 3-NOP only reacts with active form of MCR in the absence of any other compound and converts this to the MCRsilent form. These experiments were performed in the presence of excess of 3-NOP (10 mM). To be able to get an idea about the binding stoichiometry of the inhibitor with the active enzyme, MCR in the MCRred1 form was titrated with increasing amounts of 3-NOP. Different amounts of 3-NOP were added to a sample that contained a mixture of both the MCRred1 and MCRox1 forms (red1: 38 μM, ox1: 32 μM). The experiment was performed at room temperature. The samples were incubated for 15 min after the addition and subsequently frozen in the EPR tubes in liquid nitrogen and stored until the measurement. **Fig. 4.9, panel A** shows the effect on the whole EPR spectrum and **panel B** highlights the effect on the respective signal intensities. The MCR_{ox1} from is stable in the presence of 3-NOP. The MCR_{red1} form, however, appears to react rapidly with the inhibitor and reacts close to a 1 to 1 ratio.

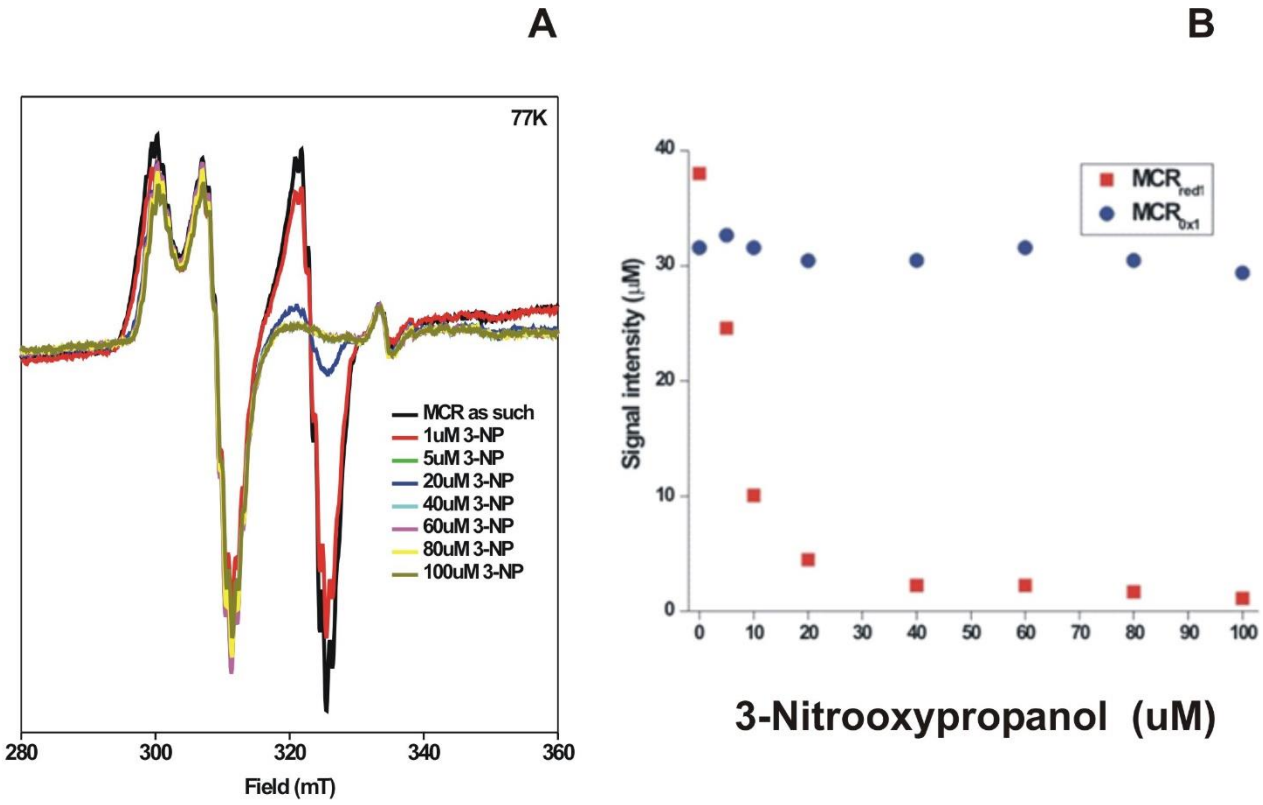

Figure 4.9: Titration of MCR with 3-Nitrooxypropanol (3-NOP). **Panel A,** MCR signal**:** 70 µM of MCR containg approximately 38 µM red1 and 32 µM ox1 was incubated with 5 µM, 20 µM, 40 µM, 60 µM, 80 µM and 100 µM of 3-NOP for 15 min at RT and analyzed by EPR**. Panel B:** MCR signal intensity with different 3-NOP concentration.

4.3.5 Time dependency of inhibition of MCRred1 form by 3-NOP:

To get an idea of how fast 3-NOP reacts with MCR a freeze-quench study was performed. The second reason to do this experiment was to check if there are any radical species that are formed transiently during the reaction. The fact that the MCRred1-Ni(I) species is converted into the MCRsilent-Ni(II) species means that only one electron is transferred between MCR and 3-NOP. Dependent on the half-life of an inhibitor-based radical species it might be detectable in a freeze-quench experiment. The overall trend indicates that the reaction is very fast: in 10 s almost all MCRred1 signal is lost (**Fig. 4.10**). At around 333 mT a radical-type signal can be detected which appears to reach its highest intensity at around 70 ms. The 3-NOP concentration was kept 50 mM to get an optimal effect since the K_i is not known.

The radical species does not show a typical hyperfine split like the BES signal in **Fig. 1.9**. A nitrate based signal should have shown a tri-fold split. Therefore it is not clear what type of radical this is. Similar radicals are also observed under turnover conditions with regular substrate and additional techniques might be needed to assign this species and show it is relevant to the reaction.

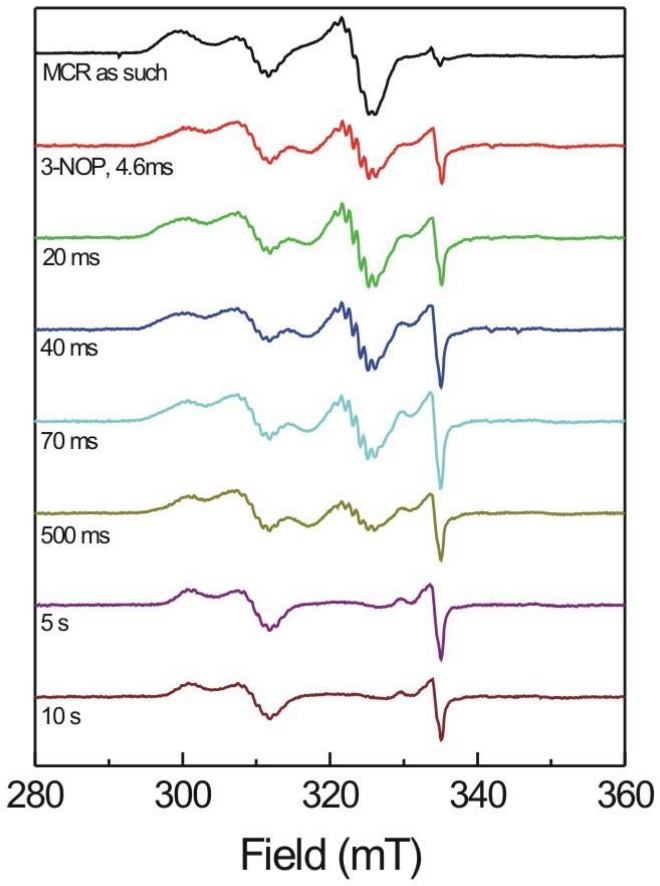

Figure 4.10: Freeze-quench experiment. 100 µM of MCR containing around 80% red1 form was incubated with 50 mM of 3-nitrooxypropanol.Samples were mixed and frozen 4.6ms, 20 ms, 40 ms, 70 ms, 500 ms, 5 S and 10 . The frozen samples were analyzed at 77K with micowave power 2mW.

4.3.6 Temperature study of radical EPR signal:

A Nitrite radical would show a three-fold splitting at higher temperatures because of the nuclear spin of nitrogen (150). Hence, to probe the origin of the radical species the EPR signal was measured at different temperatures. As depicted in **Fig. 4.11,** there was no trifold splitting at temperatures as high as 200 K. The signal appears to become broader and less intense at higher temperature, opposite to the behavior expected for a nitrite or nitrate based species. The radical species must have a different origin and labeling studies (^{13}C or ^{17}O) will be needed to solve this.

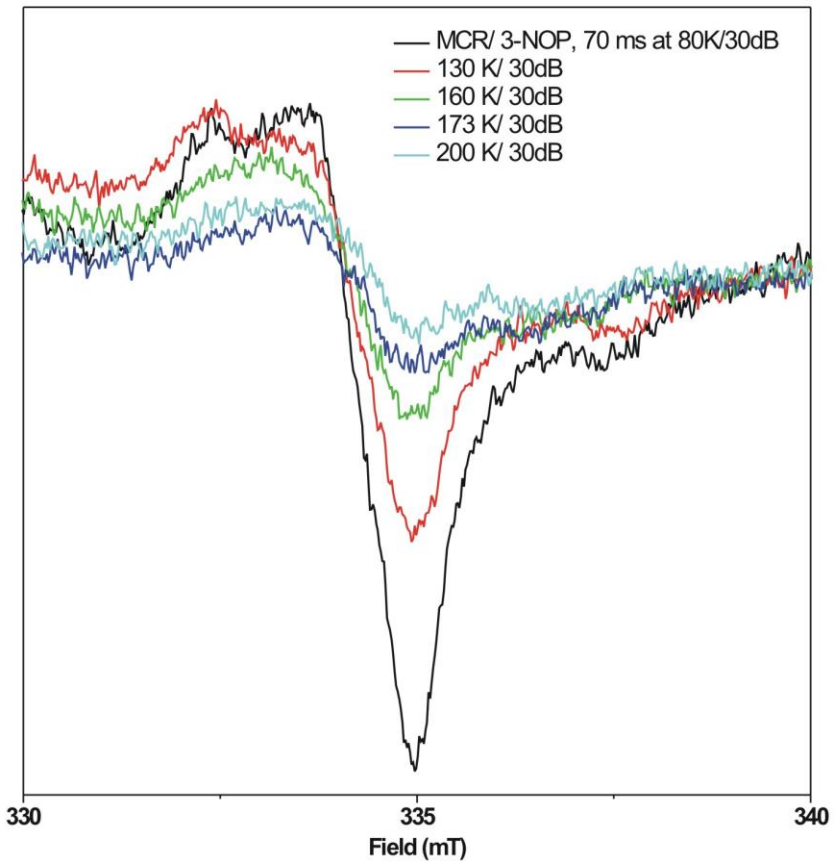

Figure 4.11: Temperature dependency of the radical species formed during time dependent experiment. The freeze quenching sample frozen at 70 ms was analyzed at 80, 130, 160, 173 and 200 K by EPR spectroscopy.

4.3.7 Nitrite determination with the Griess reagent:

In the presence of 3-NOP, The MCRred1-Ni(I) form converts into MCRsilent-Ni(II) and a possible radical species. This makes the inhibition by 3-NOP similar to that 2-bromoethanesulfonate (2-BES) where, SO_3^{2-} is released as a byproduct and there is the formation of free radical after incubating the active form of MCR in the presence of coenzyme B. Similar to 2-BES inhibition, it was possible that NO_2^-/NO_3^- is formed after incubating the MCRred1 form with 3-NOP. The Griess reagent was used to test the formation of nitrite. 105 µM of MCR was incubated with different concentration of 3-NOP for 15 min at RT and added to Griess reagent to measure the formation of NO_2^-.

As depicts in **Table 4.1**, the concentration of nitrite released increased with increasing concentration of inhibitor.

Table 4.1: Tabulation of Nitrite (NO_2^-) formation by active form of MCR in the presence of 3-Nitrooxypropanol.

Comments	Nitrite (μM)
MCR (105 μM) with Griess reagent	0
1 mM 3-Nitrooxyprpanol with Griess reagent	0
MCR with 50 uM 3-Nitrooxyprpanol with Griess reagent	26.043 ± 0.117
MCR with 100 uM 3-Nitrooxyprpanol with Griess reagent	60.025 ± 0.119
MCR with 200 uM 3-Nitrooxyprpanol with Griess reagent	131.487 ± 0.104

4.4 Discussion:

The active form of MCR, MCRred1, was queched in the presence of 3-NOP either in the cell extract or purified. No effect of 3-NOP was observed on MCRox1. This form was affected, however, when methyl-coenzyme M was present. Titration of MCR in the red1 form with 3-NOP revealed that it reacts with the MCRred form in almost 1:1 ratio.

To get an idea of how fast 3-NOP reacts with MCR, a freeze-quench study was performed. The second reason to do this experiment was to check if there are any radical species that are formed transiently during the reaction. The fact that the MCRred1-Ni(I) species is converted into the MCRsilent-Ni(II) form means that only one electron is transferred between MCR and 3-NOP. Dependent on the half-life of an inhibitor-based radical species it might be detectable in a freeze-quench experiment. The overall trend indicates that the reaction is fast: in 10 s almost all MCRred1 signal is lost (**Fig. 4.10**). At around 333 mT a radical-type signal can be detected which appears to reach its highest intensity at around 70 ms. Further, temperature EPR analysis of the 70 ms sample was conducted to further characterize the radical species. The observed signal does not show the typical three-fold split seen for other nitrate/nitrite radical species (**Fig. 4.11**) instead. Temperature broadening was observed at higher temperature. The radical species might be oxygen or carbon based and labelling studies in combination with EPR or ENDOR analysis will be needed.

Similar to the effects seen with 2-BES, the formation of free radical was even observed after incubating MCRred1 with 3-NOP in the presence of coenzyme B for 15 min. Coenzyme B binds at the entrance of active site channel in MCR and induces a confimational change (73,74). This is supposed to start the reaction cycle and in the presence of coenzyme B a much more intense radical species is induced by the additon of 2-BES than in the absence of coezyme B. The presence of coenzyme B at the entrance of the active site channel might also protect it from reacting with other

molecules, including water and the formed radical might stay in the active site cavity for longer time periods (15 min in our experiments).

3-NOP quenches the active form of MCR via a radical type mechanism in nitrite is released as a byproduct of this reaction. Based on the present data, the reaction mechanism of conversion of the red1 to the silent form in the presence of 3-NOP is not undertood. The radical species is not nitrite based and labelling studies (^{13}C or ^{17}O) will be needed to solve this. Product formation studies using NMR or HR-MASS are also required to come up with the mechanism of the inhibition of the active form of MCR.

References:

1. Zinder, S. H. (1993) Physiological ecology of methanogens. in *Methanogenesis*, Springer. pp 128-206
2. Sprott, G. D., and Beveridge, T. J. (1993) Microscopy. in *Methanogenesis*, Springer. pp 81-127
3. Kandler, O., and König, H. (1998) Cell wall polymers in Archaea (Archaebacteria). *Cellular and Molecular Life Sciences CMLS* **54**, 305-308
4. Boone, D. R., Whitman, W. B., and Rouvière, P. (1993) Diversity and taxonomy of methanogens. in *Methanogenesis*, Springer. pp 35-80
5. Saeki, K., and Kumagai, H. (1998) The rnf gene products in rhodobacter capsulatus play an essential role in nitrogen fixation during anaerobic DMSO-dependent growth in the dark. *Archives of Microbiology* **169**, 464-467
6. Hinrichs, K.-U., and Boetius, A. (2003) The anaerobic oxidation of methane: new insights in microbial ecology and biogeochemistry. in *Ocean margin systems*, Springer. pp 457-477
7. Hallam, S. J., Putnam, N., Preston, C. M., Detter, J. C., Rokhsar, D., Richardson, P. M., and DeLong, E. F. (2004) Reverse methanogenesis: testing the hypothesis with environmental genomics. *Science* **305**, 1457-1462
8. Meyerdierks, A., Kube, M., Kostadinov, I., Teeling, H., Glöckner, F. O., Reinhardt, R., and Amann, R. (2010) Metagenome and mRNA expression analyses of anaerobic methanotrophic archaea of the ANME-1 group. *Environmental Microbiology* **12**, 422-439
9. Knittel, K., and Boetius, A. (2009) Anaerobic oxidation of methane: progress with an unknown process. *Annual review of Microbiology* **63**, 311-334

10. Reeburgh, W. S. (2007) Oceanic methane Biogeochemistry. *Chemical Reviews* **107**, 486-513

11. Scheller, S., Goenrich, M., Boecher, R., Thauer, R. K., and Jaun, B. (2010) The key nickel enzyme of methanogenesis catalyses the anaerobic oxidation of methane. *Nature* **465**, 606-608

12. Krüger, M., Meyerdierks, A., Glöckner, F. O., Amann, R., Widdel, F., Kube, M., Reinhardt, R., Kahnt, J., Böcher, R., and Thauer, R. K. (2003) A conspicuous nickel protein in microbial mats that oxidize methane anaerobically. *Nature* **426**, 878-881

13. Orphan, V., Hinrichs, K.-U., Ussler, W., Paull, C. K., Taylor, L., Sylva, S. P., Hayes, J. M., and DeLong, E. F. (2001) Comparative analysis of methane-oxidizing archaea and sulfate-reducing bacteria in anoxic marine sediments. *Applied and Environmental Microbiology* **67**, 1922-1934

14. Knittel, K., Lösekann, T., Boetius, A., Kort, R., and Amann, R. (2005) Diversity and distribution of methanotrophic archaea at cold seeps. *Applied and Environmental Microbiology* **71**, 467-479

15. Thauer, R. K. (2010) Functionalization of methane in anaerobic microorganisms. *Angewandte Chemie International Edition* **49**, 6712-6713

16. Lollar, B. S., Westgate, T., Ward, J., Slater, G., and Lacrampe-Couloume, G. (2002) Abiogenic formation of alkanes in the Earth's crust as a minor source for global hydrocarbon reservoirs. *Nature* **416**, 522-524

17. Lelieveld, J., Crutzen, P. J., and Dentener, F. J. (1998) Changing concentration, lifetime and climate forcing of atmospheric methane. *Tellus B* **50**, 128-150

18. Conrad, R. (2009) The global methane cycle: recent advances in understanding the microbial processes involved. *Environmental Microbiology Reports* **1**, 285-292

19. Vaghjiani, G. L., and Ravishankara, A. (1991) New measurement of the rate coefficient for the reaction of OH with methane. *Nature* **350**, 406-409

20. Thauer, R. K., Kaster, A.-K., Seedorf, H., Buckel, W., and Hedderich, R. (2008) Methanogenic archaea: ecologically relevant differences in energy conservation. *Nature Reviews Microbiology* **6**, 579-591

21. Bertram, P. A., Karrasch, M., Schmitz, R. A., Bocher, R., Albracht, S. P., and Thauer, R. K. (1994) Formylmethanofuran dehydrogenases from methanogenic Archaea Substrate specificity, EPR properties and reversible inactivation by cyanide of the molybdenum or tungsten iron-sulfur proteins. *European Journal of Biochemistry* **220**, 477-484

22. Klein, A., Breitung, J., Linder, D., Stetter, K., and Thauer, R. (1993) N 5, N 10-Methenyltetrahydromethanopterin cyclohydrolase from the extremely thermophilic sulfate reducing Archaeoglobus fulgidus: comparison of its properties with those of the cyclohydrolase from the extremely thermophilic *Methanopyrus kandleri*. *Archives of Microbiology* **159**, 213-219

23. Schwörer, B., Breitung, J., Klein, A., Stetter, K., and Thauer, R. (1993) Formylmethanofuran: tetrahydromethanopterin formyltransferase and N 5, N 10-methylenetetrahydromethanopterin dehydrogenase from the sulfate-reducing Archaeoglobus fulgidus: similarities with the enzymes from methanogenic Archaea. *Archives of Microbiology* **159**, 225-232

24. Vaupel, M., and Thauer, R. K. (1995) Coenzyme F420-Dependent N5, N10-Methylenetetrahydromethanopterin Reductase (Mer) from *Methanobacterium Thermoautotrophicum* Strain Marburg. *European Journal of Biochemistry* **231**, 773-778

25. Stupperich, E., and Konle, R. (1993) Corrinoid-dependent methyl transfer reactions are involved in methanol and 3, 4-dimethoxybenzoate metabolism by *Sporomusa ovata*. *Applied and Environmental Microbiology* **59**, 3110-3116

26. BLAUT, M., and GOTTSCHALK, G. (1984) Coupling of ATP synthesis and methane formation from methanol and molecular hydrogen in *Methanosarcina barkeri*. *European Journal of Biochemistry* **141**, 217-222

27. Goenrich, M., Mahlert, F., Duin, E. C., Bauer, C., Jaun, B., and Thauer, R. K. (2004) Probing the reactivity of Ni in the active site of methyl-coenzyme M reductase with substrate analogues. *Journal of Biological Inorganic Chemistry* **9**, 691-705

28. Costa, K. C., Wong, P. M., Wang, T., Lie, T. J., Dodsworth, J. A., Swanson, I., Burn, J. A., Hackett, M., and Leigh, J. A. (2010) Protein complexing in a methanogen suggests electron bifurcation and electron delivery from formate to heterodisulfide reductase. *Proceedings of the National Academy of Sciences* **107**, 11050-11055

29. Kaster, A.-K., Moll, J., Parey, K., and Thauer, R. K. (2011) Coupling of ferredoxin and heterodisulfide reduction via electron bifurcation in hydrogenotrophic methanogenic archaea. *Proceedings of the National Academy of Sciences* **108**, 2981-2986

30. Lie, T. J., Costa, K. C., Lupa, B., Korpole, S., Whitman, W. B., and Leigh, J. A. (2012) Essential anaplerotic role for the energy-converting hydrogenase Eha in hydrogenotrophic methanogenesis. *Proceedings of the National Academy of Sciences* **109**, 15473-15478

31. Rouviere, P., and Wolfe, R. (1988) Novel biochemistry of methanogenesis. *Journal of Biological Chemistry* **263**, 7913-7916

32. Bonacker, L. G., Baudner, S., Morschel, E., Bocher, R., and Thauer, R. K. (1993) Properties of the two isoenzymes of methyl-coenzyme M reductase in *Methanobacterium thermoautotrophicum*. *European Journal of Biochemistry* **217**, 587-595

33. Duin, E. C. (2009) Role of coenzyme F430 in methanogenesis. in *Tetrapyrroles*, Springer. pp 352-374

34. Duin, E. C., Prakash, D., and Brungess, C. (2011) 9 Methyl-Coenzyme M Reductase from *Methanothermobacter marburgensis*. *Methods in Enzymology* **494**, 159

35. Thauer, R. K., and Shima, S. (2008) Methane as fuel for anaerobic microorganisms. *Annals of the New York Academy of Sciences* **1125**, 158-170

36. Ettwig, K. F., Shima, S., De Pas-Schoonen, V., Katinka, T., Kahnt, J., Medema, M. H., Op Den Camp, H. J., Jetten, M. S., and Strous, M. (2008) Denitrifying bacteria anaerobically oxidize methane in the absence of Archaea. *Environmental Microbiology* **10**, 3164-3173

37. Rospert, S., Linder, D., Ellermann, J., and Thauer, R. K. (1990) Two genetically distinct methyl-coenzyme M reductases in Methanobacterium thermoautotrophicum strain Marburg and ΔH. *European journal of Biochemistry* **194**, 871-877

38. Brenner, M. C., Zhang, H., and Scott, R. A. (1993) Nature of the low activity of S-methyl-coenzyme M reductase as determined by active site titrations. *Journal of Biological Chemistry* **268**, 18491-18495

39. Lehmacher, A. (1994) Cloning, sequencing and transcript analysis of the gene encoding formylmethanofuran: tetrahydromethanopterin formyltransferase from the

hyperthermophilic *Methanothermus fervidus*. *Molecular and General Genetics MGG* **242**, 73-80

40. Bult, C. J., White, O., Olsen, G. J., Zhou, L., Fleischmann, R. D., Sutton, G. G., Blake, J. A., FitzGerald, L. M., Clayton, R. A., and Gocayne, J. D. (1996) Complete genome sequence of the methanogenic archaeon, *Methanococcus jannaschii*. *Science* **273**, 1058-1073

41. Nölling, J., and Reeve, J. N. (1997) Growth-and substrate-dependent transcription of the formate dehydrogenase (fdhCAB) operon in *Methanobacterium thermoformicicum* Z-245. *Journal of Bacteriology* **179**, 899-908

42. Pihl, T. D., Sharma, S., and Reeve, J. N. (1994) Growth phase-dependent transcription of the genes that encode the two methyl coenzyme M reductase isoenzymes and N5-methyltetrahydromethanopterin: coenzyme M methyltransferase in *Methanobacterium thermoautotrophicum* delta H. *Journal of Bacteriology* **176**, 6384-6391

43. Reeve, J. N., Nölling, J., Morgan, R. M., and Smith, D. R. (1997) Methanogenesis: genes, genomes, and who's on first? *Journal of Bacteriology* **179**, 5975

44. Pennings, J. L., de Wijs, J. L., Keltjens, J. T., and van der Drift, C. (1997) Medium-reductant directed expression of methyl coenzymeM reductase isoenzymes in *Methanobacterium thermoautotrophicum* (strain ΔH). *FEBS letters* **410**, 235-237

45. Cram, D., Sherf, B., Libby, R., Mattaliano, R., Ramachandran, K., and Reeve, J. (1987) Structure and expression of the genes, mcrBDCGA, which encode the subunits of component C of methyl coenzyme M reductase in *Methanococcus vannielii*. *Proc. Natl. Acad. Sci. U. S. A.* **84**, 3992-3996

46. Bokranz, M., and Klein, A. (1987) Nucleotide sequence of the methyl coenzyme M reductase gene cluster from *Methanosarcina barkeri*. *Nucleic acids research* **15**, 4350

47. Prakash, D., Wu, Y., Suh, S.-J., and Duin, E. C. (2014) Elucidating the Process of Activation of Methyl-Coenzyme M Reductase. *Journal of Bacteriology* **196**, 2491-2498

48. Sherf, B. A., and Reeve, J. N. (1990) Identification of the mcrD gene product and its association with component C of methyl coenzyme M reductase in *Methanococcus vannielii*. *Journal of Bacteriology* **172**, 1828-1833

49. Ellermann, J., Rospert, S., Thauer, R. K., Bokranz, M., Klein, A., Voges, M., and Berkessel, A. (1989) Methyl-coenzyme-M reductase from *Methanobacterium thermoautotrophicum* (strain Marburg). *European Journal of Biochemistry* **184**, 63-68

50. Rospert, S., Böcher, R., Albracht, S., and Thauer, R. (1991) Methyl-coenzyme M reductase preparations with high specific activity from preincubated cells o *Methanobacterium thermoautotrophicum*. *FEBS letters* **291**, 371-375

51. Goubeaud, M., Schreiner, G., and Thauer, R. K. (1997) Purified Methyl-Coenzyme-M Reductase is Activated when the Enzyme-Bound Coenzyme F430 is Reduced to the Nickel (I) Oxidation State by Titanium (III) Citrate. *European Journal of Biochemistry* **243**, 110-114

52. Duin, E. C., Prakash, D., and Brungess, C. (2011) Methyl-coenzyme M reductase from *Methanothermobacter marburgensis*. *Meth. Enzymol.* **494**, 159-187

53. Ellefson, W. L., Whitman, W. B., and Wolfe, R. S. (1982) Nickel-containing factor F430: chromophore of the methylreductase of Methanobacterium. *Proceedings of the National Academy of Sciences* **79**, 3707-3710

54. Ermler, U. (2005) On the mechanism of methyl-coenzyme M reductase. *Dalton Transactions*, 3451-3458

55. Färber, G., Keller, W., Kratky, C., Jaun, B., Pfaltz, A., Spinner, C., Kobelt, A., and Eschenmoser, A. (1991) Coenzyme F430 from Methanogenic Bacteria: Complete Assignment of Configuration Based on an X-Ray Analysis of 12, 13-Diepi-F430 Pentamethyl Ester and on NMR Spectroscopy. *Helvetica chimica acta* **74**, 697-716

56. Holliger, C., Pierik, A. J., Reijerse, E. J., and Hagen, W. R. (1993) A spectroelectrochemical study of factor F430 nickel (II/I) from methanogenic bacteria in aqueous solution. *Journal of the American Chemical Society* **115**, 5651-5656

57. Jaun, B. (1990) Coenzyme F430 from methanogenic bacteria: oxidation of F430 pentamethyl ester to the Ni (III) form. *Helvetica chimica acta* **73**, 2209-2217

58. Jaun, B., and Pfaltz, A. (1986) Coenzyme F430 from methanogenic bacteria: reversible one-electron reduction of F430 pentamethyl ester to the nickel (I) form. *J. Chem. Soc., Chem. Commun.*, 1327-1329

59. Piskorski, R., and Jaun, B. (2003) Direct determination of the number of electrons needed to reduce coenzyme F430 pentamethyl ester to the Ni (I) species exhibiting the electron paramagnetic resonance and ultraviolet-visible spectra characteristic for the MCRred1 state of methyl-coenzyme M reductase. *Journal of the American Chemical Society* **125**, 13120-13125

60. Rospert, S., Bocher, R., Albracht, S. P., and Thauer, R. K. (1991) Methyl-coenzyme M reductase preparations with high specific activity from H2-preincubated cells of *Methanobacterium thermoautotrophicum*. *FEBS. Lett.* **291**, 371-375

61. Albracht, S., Ankel-Fuchs, D., Böcher, R., Ellermann, J., Moll, J., Van der Zwaan, J., and Thauer, R. (1988) Five new EPR signals assigned to nickel in methyl-coenzyme M reductase from *Methanobacterium thermoautotrophicum*, strain Marburg. *Biochim. Biophys. Acta.Protein Structure and Molecular Enzymology* **955**, 86-102

62. Goubeaud, M., Schreiner, G., and Thauer, R. K. (1997) Purified Methyl-Coenzyme M Reductase is Activated when the Enzyme Bound Coenzyme F430 is Reduced to the Nickel (I) Oxidation State by Titanium (III) Citrate. *Eur. J. Biochem.* **243**, 110-114

63. Becker, D. F., and Ragsdale, S. W. (1998) Activation of methyl-SCoM reductase to high specific activity after treatment of whole cells with sodium sulfide. *Biochemistry* **37**, 2639-2647

64. Ermler, U., Grabarse, W., Shima, S., Goubeaud, M., and Thauer, R. K. (1997) Crystal structure of methyl-coenzyme M reductase: the key enzyme of biological methane formation. *Science (New York, N.Y.)* **278**, 1457-1462

65. Cedervall, P. E., Dey, M., Li, X., Sarangi, R., Hedman, B., Ragsdale, S. W., and Wilmot, C. M. (2011) Structural analysis of a Ni-methyl species in methyl-coenzyme M reductase from *Methanothermobacter marburgensis*. *Journal of the American Chemical Society* **133**, 5626-5628

66. Färber, G., Keller, W., Kratky, C., Jaun, B., Pfaltz, A., Spinner, C., Kobelt, A., and Eschenmoser, A. (1991) Coenzyme F430 from Methanogenic Bacteria: Complete Assignment of Configuration Based on an X-Ray Analysis of 12, 13-Diepi-F430 Pentamethyl Ester and on NMR Spectroscopy. *Helv. Chim. Acta* **74**, 697-716

67. Livingston, D., Pfatz, A., Schreiber, J., and Eschenmoser, A. (1984) Factor F 430 from methanogenic bacteria: Structure of the protein-free factor. *Helv. Chim. Acta* **67**, 334-351

68. Pfaltz, A., Jaun, B., Fassler, A., Eschenmoser, A., Jaenchen, R., Gilles, H. H., Diekert, G., and Thauer, R. K. (1982) Factor F430 from methanogenic bacteria: structure of the porphinoid ligand system. *Helv. Chim. Acta* **65**, 828-865

69. Kahnt, J., Buchenau, B., Mahlert, F., Krüger, M., Shima, S., and Thauer, R. K. (2007) Post-translational modifications in the active site region of methyl-coenzyme M reductase from methanogenic and methanotrophic archaea. *FEBS journal* **274**, 4913-4921

70. Selmer, T., Kahnt, J., Goubeaud, M., Shima, S., Grabarse, W., Ermler, U., and Thauer, R. K. (2000) The biosynthesis of methylated amino acids in the active site region of methyl-coenzyme M reductase. *J. Biol. Chem.* **275**, 3755-3760

71. Pfeifer, T., Schierhorn, A., Friedemann, R., Jakob, M., Frank, R., Schutkowski, M., and Fischer, G. (1997) Specific fragmentation of thioxo peptides facilitates the assignment of the thioxylated amino acid. *Journal of mass spectrometry* **32**, 1064-1071

72. Artis, D. R., and Lipton, M. A. (1998) Conformations of thioamide-containing dipeptides: a computational study. *Journal of the American Chemical Society* **120**, 12200-12206

73. Grabarse, W., Mahlert, F., Duin, E. C., Goubeaud, M., Shima, S., Thauer, R. K., Lamzin, V., and Ermler, U. (2001) On the mechanism of biological methane formation: structural evidence for conformational changes in methyl-coenzyme M reductase upon substrate binding. *Journal of Molecular Biology* **309**, 315-330

74. Ebner, S., Jaun, B., Goenrich, M., Thauer, R. K., and Harmer, J. (2009) Binding of coenzyme B induces a major conformational change in the active site of methyl-coenzyme M reductase. *Journal of the American Chemical Society* **132**, 567-575

75. Atherton, N. M., Davies, M., and Gilbert, B. (1996) *Electron spin resonance*, Royal Society of Chemistry

76. Pilbrow, J. (1990) *Transition ion electron paramagnetic resonance*, Clarendon Press Oxford

77. Palmer, G., and Que, L., Jr. (2002) *Electron Paramagnetic Resonance of Metalloproteins ,, p 121,*. University Science Books, Sausalito, California

78. Mahlert, F., Grabarse, W., Kahnt, J., Thauer, R. K., and Duin, E. C. (2002) The nickel enzyme methyl-coenzyme M reductase from methanogenic archaea: in vitro interconversions among the EPR detectable MCR-red1 and MCR-red2 states. *Journal of Biological Inorganic Chemistry* **7**, 101-112

79. Kern, D. I., Goenrich, M., Jaun, B., Thauer, R. K., Harmer, J., and Hinderberger, D. (2007) Two sub-states of the red2 state of methyl-coenzyme M reductase revealed by high-field EPR spectroscopy. *Journal of Biological Inorganic Chemistry* **12**, 1097-1105

80. Finazzo, C., Harmer, J., Jaun, B., Duin, E. C., Mahlert, F., Thauer, R. K., Van Doorslaer, S., and Schweiger, A. (2003) Characterization of the MCRred2 form of methyl-coenzyme M reductase: a pulse EPR and ENDOR study. *Journal of Biological Inorganic Chemistry* **8**, 586-593

81. Mahlert, F., Bauer, C., Jaun, B., Thauer, R. K., and Duin, E. C. (2002) The nickel enzyme methyl-coenzyme M reductase from methanogenic archaea: In vitro induction of the nickel-based MCR-ox EPR signals from MCR-red2. *Journal of Biological Inorganic Chemistry* **7**, 500-513

82. Rospert, S., Voges, M., Berkessel, A., Albracht, S. P., and Thauer, R. K. (1992) Substrate-analogue-induced changes in the nickel-EPR spectrum of active methyl-coenzyme-M reductase from *Methanobacterium thermoautotrophicum*. *European Journal of Biochemistry* **210**, 101-107

83. Yang, N., Reiher, M., Wang, M., Harmer, J., and Duin, E. C. (2007) Formation of a nickel-methyl species in methyl-coenzyme M reductase, an enzyme catalyzing methane formation. *Journal of the American Chemical Society* **129**, 11028-11029

84. Dey, M., Li, X., Kunz, R. C., and Ragsdale, S. W. (2010) Detection of organometallic and radical intermediates in the catalytic mechanism of methyl-coenzyme M reductase using the natural substrate methyl-coenzyme M and a coenzyme B substrate analogue. *Biochemistry* **49**, 10902-10911

85. Sarangi, R., Dey, M., and Ragsdale, S. W. (2009) Geometric and Electronic Structures of the NiI and Methyl− NiIII Intermediates of Methyl-Coenzyme M Reductase†. *Biochemistry* **48**, 3146-3156

86. Dey, M., Telser, J., Kunz, R. C., Lees, N. S., Ragsdale, S. W., and Hoffman, B. M. (2007) Biochemical and spectroscopic studies of the electronic structure and reactivity of a methyl-Ni species formed on methyl-coenzyme M reductase. *J. Am. Chem. Soc.* **129**, 11030-11032

87. Pelmenschikov, V., and Siegbahn, P. E. (2003) Catalysis by methyl-coenzyme M reductase: a theoretical study for heterodisulfide product formation. *Journal of Biological Inorganic Chemistry* **8**, 653-662

88. Duin, E. C., and McKee, M. L. (2008) A new mechanism for methane production from methyl-coenzyme M reductase as derived from density functional calculations. *The Journal of Physical Chemistry B* **112**, 2466-2482

89. Chen, S.-l., Pelmenschikov, V., Blomberg, M. R., and Siegbahn, P. E. (2009) Is there a Ni-methyl intermediate in the mechanism of methyl-coenzyme M reductase? *Journal of the American Chemical Society* **131**, 9912-9913

90. Scheller, S., Goenrich, M., Mayr, S., Thauer, R. K., and Jaun, B. (2010) Intermediates in the Catalytic Cycle of Methyl Coenzyme M Reductase: Isotope Exchange is Consistent with Formation of a σ-Alkane–Nickel Complex. *Angewandte Chemie International Edition* **49**, 8112-8115

91. Richard, R. M., and Ball, D. W. (2008) Ab initio calculations on the thermodynamic properties of azaborospiropentanes. *J. Mol .Model.* **14**, 871-878

92. Scheller, S., Goenrich, M., Boecher, R., Thauer, R. K., and Jaun, B. (2010) The key nickel enzyme of methanogenesis catalyses the anaerobic oxidation of methane. *Nature* **465**, 606-608

93. Shima, S., Krueger, M., Weinert, T., Demmer, U., Kahnt, J., Thauer, R. K., and Ermler, U. (2012) Structure of a methyl-coenzyme M reductase from Black Sea mats that oxidize methane anaerobically. *Nature* **481**, 98-101

94. Ragsdale, S. W. (2003) Biochemistry of Methyl-CoM 67 Reductase and Coenzyme F430. *The Porphyrin Handbook: Elsevier Science, San Diego.* **11**, 205

95. Cedervall, P. E., Dey, M., Li, X., Sarangi, R., Hedman, B., Ragsdale, S. W., and Wilmot, C. M. (2011) Structural analysis of a Ni-methyl species in methyl-coenzyme M reductase from *Methanothermobacter marburgensis*. *J. Am. Chem. Soc.* **133**, 5626-5628

96. Yang, N., Reiher, M., Wang, M., Harmer, J., and Duin, E. C. (2007) Formation of a nickel-methyl species in methyl-coenzyme m reductase, an enzyme catalyzing methane formation. *J. Am. Chem. Soc.* **129**, 11028-11029

97. Zhou, Y., Dorchak, A. E., and Ragsdale, S. W. (2013) In vivo activation of methyl-coenzyme M reductase by carbon monoxide. *Front Microbiol* **4**

98. Holliger, C., Pierik, A. J., Reijerse, E. J., and Hagen, W. R. (1993) A spectroelectrochemical study of Factor F430 Nickel (II/I) from methanogenic bacteria in aqueous solution. *J. Am. Chem. Soc.* **115**, 5651-5656

99. Seefeldt, L. C., Hoffman, B. M., and Dean, D. R. (2009) Mechanism of Mo-dependent nitrogenase. *Annual review of Biochemistry* **78**, 701

100. Duval, S., Danyal, K., Shaw, S., Lytle, A. K., Dean, D. R., Hoffman, B. M., Antony, E., and Seefeldt, L. C. (2013) Electron transfer precedes ATP hydrolysis during nitrogenase catalysis. *Proceedings of the National Academy of Sciences* **110**, 16414-16419

101. Gunsalus, R., and Wolfe, R. (1980) Methyl coenzyme M reductase from *Methanobacterium thermoautotrophicum*. Resolution and properties of the components. *J. Biol. Chem.* **255**, 1891-1895

102. Rouvière, P. E., Bobik, T. A., and Wolfe, R. S. (1988) Reductive activation of the methyl coenzyme M methylreductase system of *Methanobacterium thermoautotrophicum* delta H. *J. Bacteriol.* **170**, 3946-3952

103. Brenner, M. C., Zhang, H., and Scott, R. A. (1993) Nature of the low activity of S-methyl-coenzyme M reductase as determined by active site titrations. *J. Biol. Chem.* **268**, 18491-18495

104. Sauer, K., and Thauer, R. K. (1999) Methanol: coenzyme M methyltransferase from *Methanosarcina barkeri*--substitution of the corrinoid harbouring subunit MtaC by free cob (I) alamin. *European Journal of Biochemistry* **261**, 674-681

105. Gunsalus, R. P., Romesser, J. A., and Wolfe, R. S. (1978) Preparation of coenzyme M analogs and their activity in the methyl coenzyme M reductase system of Methanobacterium thermoautotrophicum. *Biochemistry* **17**, 2374-2377

106. Noll, K., Donnelly, M., and Wolfe, R. (1987) Synthesis of 7-mercaptoheptanoylthreonine phosphate and its activity in the methylcoenzyme M methylreductase system. *Journal of Biological Chemistry* **262**, 513-515

107. Ellman, G. L., Courtney, K. D., and Featherstone, R. M. (1961) A new and rapid colorimetric determination of acetylcholinesterase activity. *Biochemical pharmacology* **7**, 88-95

108. Deakin, H., Ord, M. G., and Stocken, L. (1963) Glucose 6-phosphate-dehydrogenase'activity and thiol content of thymus nuclei from control and X-irradiated rats. *Biochemical Journal* **89**, 296

109. Bulaj, G., Kortemme, T., and Goldenberg, D. P. (1998) Ionization-reactivity relationships for cysteine thiols in polypeptides. *Biochemistry* **37**, 8965-8972

110. Schönheit, P., Moll, J., and Thauer, R. K. (1980) Growth parameters (K s, μmax, Y s) of *Methanobacterium thermoautotrophicum*. *Archives of Microbiology* **127**, 59-65

111. Bradford, M. M. (1976) A rapid and sensitive method for the quantitation of microgram quantities of protein utilizing the principle of protein-dye binding. *Analytical biochemistry* **72**, 248-254

112. Nagatomi, J., Wu, Y., and Gray, M. (2009) Proteomic Analysis of Bladder Smooth Muscle Cell Response to Cyclic Hydrostatic Pressure. *Cellular and Molecular Bioengineering* **2**, 166-173

113. Hagen, W. (2009) Biomolecular EPR spectroscopy. CRC. Taylor & Francis Group, Boca Raton

114. Mahlert, F., Grabarse, W., Kahnt, J., Thauer, R. K., and Duin, E. C. (2002) The nickel enzyme methyl-coenzyme M reductase from methanogenic archaea: in vitro

interconversions among the EPR detectable MCR-red1 and MCR-red2 states. *J. Biol. Inorg. Chem.* **7**, 101-112

115. Ellermann, J., Hedderich, R., Bocher, R., and Thauer, R. K. (1988) The final step in methane formation. *Eur. J. Biochem.* **172**, 669-677

116. Rouvière, P. E., and Wolfe, R. S. (1989) Component A3 of the methylcoenzyme M methylreductase system of *Methanobacterium thermoautotrophicum* delta H: resolution into two components. *J. Bacteriol.* **171**, 4556-4562

117. Kaster, A.-K., Moll, J., Parey, K., and Thauer, R. K. (2011) Coupling of ferredoxin and heterodisulfide reduction via electron bifurcation in hydrogenotrophic methanogenic archaea. *Proc. Natl. Acad. Sci. U.S.A.* **108**, 2981-2986

118. Costa, K. C., Wong, P. M., Wang, T., Lie, T. J., Dodsworth, J. A., Swanson, I., Burn, J. A., Hackett, M., and Leigh, J. A. (2010) Protein complexing in a methanogen suggests electron bifurcation and electron delivery from formate to heterodisulfide reductase. *Proc. Natl. Acad. Sci. U.S.A.* **107**, 11050-11055

119. Kuhner, C. H., Lindenbach, B. D., and Wolfe, R. S. (1993) Component A2 of methylcoenzyme M reductase system from *Methanobacterium thermoautotrophicum* delta H: nucleotide sequence and functional expression by Escherichia coli. *J. Bacteriol.* **175**, 3195-3203

120. Becker, D. F., Leartsakulpanich, U., Surerus, K. K., Ferry, J. G., and Ragsdale, S. W. (1998) Electrochemical and spectroscopic properties of the iron-sulfur flavoprotein from Methanosarcina thermophila. *J. Biol. Chem.* **273**, 26462-26469

121. Terlesky, K., and Ferry, J. (1988) Ferredoxin requirement for electron transport from the carbon monoxide dehydrogenase complex to a membrane-bound hydrogenase in acetate-grown Methanosarcina thermophila. *J. Biol. Chem.* **263**, 4075-4079

122. Clements, A. P., Kilpatrick, L., Lu, W. P., Ragsdale, S. W., and Ferry, J. G. (1994) Characterization of the iron-sulfur clusters in ferredoxin from acetate-grown Methanosarcina thermophila. *J. Bacteriol.* **176**, 2689-2693

123. Albracht, S. P. (1994) Nickel hydrogenases: in search of the active site. *Biochim. Biophys. Acta. Bioenergetics* **1188**, 167-204

124. Zhao, T., Cruz, F., and Ferry, J. G. (2001) Iron-Sulfur Flavoprotein (Isf) fromMethanosarcina thermophila Is the Prototype of a Widely Distributed Family. *Journal of Bacteriology* **183**, 6225-6233

125. Latimer, M. T., Painter, M. H., and Ferry, J. G. (1996) Characterization of an iron-sulfur flavoprotein from *Methanosarcina thermophila*. *Journal of Biological Chemistry* **271**, 24023-24028

126. Galagan, J. E., Nusbaum, C., Roy, A., Endrizzi, M. G., Macdonald, P., FitzHugh, W., Calvo, S., Engels, R., Smirnov, S., and Atnoor, D. (2002) The genome of M. acetivorans reveals extensive metabolic and physiological diversity. *Genome research* **12**, 532-542

127. Wang, S., Tiongson, J., and Rasche, M. E. (2014) Discovery and characterization of the first archaeal dihydromethanopterin reductase, an iron-sulfur flavoprotein from *Methanosarcina mazei*. *Journal of Bacteriology* **196**, 203-209

128. Ding, Y. H., and Ferry, J. G. (2004) Flavin mononucleotide-binding flavoprotein family in the domain Archaea. *Journal of Bacteriology* **186**, 90-97

129. Huth, J. R., Bewley, C. A., Clore, G. M., Gronenborn, A. M., Jackson, B. M., and Hinnebusch, A. G. (1997) Design of an expression system for detecting folded protein domains and mapping macromolecular interactions by NMR. *Protein science* **6**, 2359-2364

130. Lavallie, E. R., DiBlasio, E. A., Kovacic, S., Grant, K. L., Schendel, P. F., and McCoy, J. M. (1993) A thioredoxin gene fusion expression system that circumvents inclusion body formation in the E. coli cytoplasm. *Nature Biotechnology* **11**, 187-193

131. Andrade, S. L., Cruz, F., Drennan, C. L., Ramakrishnan, V., Rees, D. C., Ferry, J. G., and Einsle, O. (2005) Structures of the iron-sulfur flavoproteins from *Methanosarcina thermophila* and Archaeoglobus fulgidus. *Journal of Bacteriology* **187**, 3848-3854

132. Oprian, D., and Coon, M. (1982) Oxidation-reduction states of FMN and FAD in NADPH-cytochrome P-450 reductase during reduction by NADPH. *Journal of Biological Chemistry* **257**, 8935-8944

133. Langen, R., Jensen, G. M., Jacob, U., Stephens, P. J., and Warshel, A. (1992) Protein control of iron-sulfur cluster redox potentials. *Journal of Biological Chemistry* **267**, 25625-25627

134. Beauchemin, K., McAllister, T., and McGinn, S. (2009) Dietary mitigation of enteric methane from cattle. *CAB Reviews: Perspectives in Agriculture, Veterinary Science, Nutrition and Natural Resources* **4**, 1-18

135. Johnson, K. A., and Johnson, D. E. (1995) Methane emissions from cattle. *Journal of animal science* **73**, 2483-2492

136. Czerkawski, J., Blaxter, K., and Wainman, F. (1966) The metabolism of oleic, linoleic and linolenic acids by sheep with reference to their effects on methane production. *British Journal of Nutrition* **20**, 349-362

137. Mills, J., Dijkstra, J., Bannink, A., Cammell, S., Kebreab, E., and France, J. (2001) A mechanistic model of whole-tract digestion and methanogenesis in the lactating dairy cow: model development, evaluation, and application. *Journal of Animal Science* **79**, 1584-1597

138. Beauchemin, K., Kreuzer, M., O'mara, F., and McAllister, T. (2008) Nutritional management for enteric methane abatement: a review. *Animal Production Science* **48**, 21-27

139. Soliva, C. R., Amelchanka, S. L., Duval, S. M., and Kreuzer, M. (2011) Ruminal methane inhibition potential of various pure compounds in comparison with garlic oil as determined with a rumen simulation technique (Rusitec). *British Journal of Nutrition* **106**, 114-122

140. McAllister, T., and Newbold, C. J. (2008) Redirecting rumen fermentation to reduce methanogenesis. *Animal Production Science* **48**, 7-13

141. Martin, C., Morgavi, D., and Doreau, M. (2010) Methane mitigation in ruminants: from microbe to the farm scale. *animal* **4**, 351-365

142. Halgren, T. A., Murphy, R. B., Friesner, R. A., Beard, H. S., Frye, L. L., Pollard, W. T., and Banks, J. L. (2004) Glide: a new approach for rapid, accurate docking and scoring. 2. Enrichment factors in database screening. *Journal of Medicinal Chemistry* **47**, 1750-1759

143. Martínez-Fernández, G., Abecia, L., Arco, A., Cantalapiedra-Hijar, G., Martín-García, A., Molina-Alcaide, E., Kindermann, M., Duval, S., and Yáñez-Ruiz, D. (2014) Effects of ethyl-3-nitrooxy propionate and 3-nitrooxypropanol on ruminal fermentation, microbial abundance, and methane emissions in sheep. *Journal of dairy science* **97**, 3790-3799

144. Reynolds, C. K., Humphries, D. J., Kirton, P., Kindermann, M., Duval, S., and Steinberg, W. (2014) Effects of 3-nitrooxypropanol on methane emission, digestion, and energy and nitrogen balance of lactating dairy cows. *Journal of dairy science* **97**, 3777-3789

145. Haisan, J., Sun, Y., Guan, L., Beauchemin, K., Iwaasa, A., Duval, S., Barreda, D., and Oba, M. (2014) The effects of feeding 3-nitrooxypropanol on methane emissions and productivity of Holstein cows in mid lactation. *Journal of dairy science* **97**, 3110-3119

146. Romero-Perez, A., Okine, E., McGinn, S., Guan, L., Oba, M., Duval, S., Kindermann, M., and Beauchemin, K. (2014) The potential of 3-nitrooxypropanol to lower enteric methane emissions from beef cattle. *Journal of animal science* **92**, 4682-4693

147. Holliger, C., Schraa, G., Stupperich, E., Stams, A., and Zehnder, A. (1992) Evidence for the involvement of corrinoids and factor F430 in the reductive dechlorination of 1, 2-dichloroethane by *Methanosarcina barkeri*. *Journal of Bacteriology* **174**, 4427-4434

148. Stubbe, J., and van der Donk, W. A. (1998) Protein radicals in enzyme catalysis. *Chemical reviews* **98**, 705-762

149. Wagner, A., Frey, M., Neugebauer, F. A., Schäfer, W., and Knappe, J. (1992) The free radical in pyruvate formate-lyase is located on glycine-734. *Proceedings of the National Academy of Sciences* **89**, 996-1000

150. Damian, G., Cozar, O., Miclăus, V., Paizs, C., Znamirovschi, V., Chis, V., and David, L. (1998) ESR study of the dynamics of adsorbed nitroxide radicals on porous surfaces in the dehydration process. *Colloids and Surfaces A: Physicochemical and Engineering Aspects* **137**, 1-6